Design of Multi-Diagnostic POCT Devices for Early Diagnosis of NCDs at Low Resource Rural Settings

a thesis

submitted in partial fulfilment of the requirements for the degree of

Doctor of Philosophy

by

ANKIT CHOWDHURY

Centre for Nanotechnology

Indian Institute of Technology Guwahati

Guwahati, Assam-781039, India

May 2026

CENTRE FOR NANOTECHNOLOGY
INDIAN INSTITUTE OF TECHNOLOGY GUWAHATI
GUWAHATI , ASSAM-781039

DECLARATION

The thesis titled **"Design of Multi-Diagnostic POCT Devices for Early Diagnosis of NCDs at Low Resource Rural Settings"** represents my original research work carried out in the Centre for Nanotechnology, Indian Institute of Technology Guwahati, India, under the supervision of **Prof. Dipankar Bandyopadhyay** and **Dr. Pankaj Upadhyay**.

Sincere efforts have been made to acknowledge contributions from other investigators that helped in conceptualizing and executing the research work. Those who have provided suggestions and technical help have been duly acknowledged. All the research articles and resources used have been cited in the reference section.

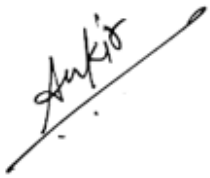

30 May 2026

Mr. Ankit Chowdhury
Roll number: 196153002
Centre for Nanotechnology
Indian Institute of Technology Guwahati

CENTRE FOR NANOTECHNOLOGY
INDIAN INSTITUTE OF TECHNOLOGY GUWAHATI
GUWAHATI, ASSAM-781039

CERTIFICATE

This is to certify that the work described in the thesis titled, **"Design of Multi-Diagnostic POCT Devices for Early Diagnosis of NCDs at Low Resource Rural Settings"** submitted by **Ankit Chowdhury** (Roll No. 196153002) to the Indian Institute of Technology Guwahati, India, for the award of the degree of Doctor of Philosophy is an authentic record of the research work carried out under our supervision in the Centre for Nanotechnology, Indian Institute of Technology Guwahati, India.

This thesis or any part thereof has not been submitted elsewhere for the award of any other degree or diploma.

30 May 2026

Prof. Dipankar Bandyopadhyay
Professor, Department of Chemical Engineering &
Centre for Nanotechnology,
IIT Guwahati, Guwahati-39

30 May 2026

Dr. Pankaj Upadhyay
Assistant Professor, Design Department
IIT Guwahati, Guwahati-39

To my beloved family

Acknowledgements

I wish to begin by expressing my profound and sincere gratitude to my supervisors, ***Prof. Dipankar Bandyopadhyay*** *and* ***Dr. Pankaj Upadhyay****, whose guidance has shaped every stage of this journey. Prof. Bandyopadhyay's unwavering faith in my abilities, his clarity of thought, and his compassionate mentorship have been instrumental in my growth as both a researcher and an individual. Dr. Upadhyay's steady encouragement, insightful suggestions, and continuous support have equally enriched my work and strengthened my scientific perspective. I am deeply grateful to both of them for their time, dedication, and the immense learning I have gained under their mentorship. I extend my heartfelt thanks to my doctoral committee members,* ***Dr. Amaresh Dalal, Dr. Sharmistha Banerjee,*** *and* ***Dr. Harshal B. Nemade****, for their valuable comments, thoughtful inputs, and continuous guidance, all of which greatly strengthened my work.*

My sincere appreciation goes to ***Dr. Akshai Kumar A. S.,*** *Head of the Centre for Nanotechnology, for providing access to essential facilities and for cultivating an atmosphere conducive to research and innovation.*

A special note of appreciation is due to ***Dr. Sangita Semwal****, Scientist 'E' and Additional Director, and* ***Dr. Sunita Verma****, Scientist 'G' and Group Coordinator, R&D Division, MeitY, Government of India, for their valuable guidance and encouragement. I also extend my sincere thanks to* ***Dr. Suchita Markan****, Scientist 'E', Division of Development Research, and* ***Mr. Rajesh Sagar****, Scientist 'C', ICMR, Government of India, for their support throughout this work. I remain grateful to* ***Dr. Nihar Ranjan Dash****, Professor, GI Surgery & Liver Transplant, AIIMS New Delhi;* ***Dr. Sudip Kr. Datta****, Professor, Laboratory Medicine, AIIMS New Delhi; and* ***Dr. Madhumita Das****, Head, Biochemistry Lab, GNRC Hospital, for their valuable guidance and support during the clinical trials.*

Mr. Sahil Jagnani*, whose camaraderie, collaborative spirit, and encouragement have brought warmth and meaning to my research life. I am highly grateful to him.*

I also wish to thank my ***lab mates*** *for their camaraderie, meaningful discussions, and encouragement, which have enriched my research journey and added joy to the everyday rhythm of lab life.*

My deepest gratitude is reserved for ***my family****, whose boundless love, patience, and sacrifices have been my strongest source of strength. Their unwavering belief in me has carried me through the most challenging moments.*

Finally, I offer my humble thanks to the ***Almighty,*** *whose blessings and quiet guidance have sustained me throughout this endeavour and brought me to this milestone.*

Ankit Chowdhury

Table of Contents

List of Figures

List of Table

Synopsis

Introduction

Non-communicable diseases (NCDs) such as diabetes mellitus, cardiovascular disorders, and chronic kidney disease (CKD) account for more than 70% of global mortality and represent one of the most critical public health challenges of the present century [1]. Low- and middle-income countries bear the greatest burden due to delayed diagnosis, limited access to healthcare infrastructure, and high out-of-pocket medical expenditure. In India alone, over 77 million individuals are affected by diabetes, with a large proportion remaining undiagnosed, thereby significantly increasing their risk of renal and cardiovascular complications [2]. Early biochemical screening using serum biomarkers such as creatinine, uric acid, cholesterol, triglycerides, and glucose is therefore essential for timely intervention and disease management.

Despite this need, conventional centralized laboratory analyzers—both semi-automated and fully automated systems—remain largely inaccessible to rural and semi-urban populations due to their high capital cost, infrastructure dependency, skilled manpower requirement, and regulated laboratory conditions [3-5]. Primary Health Centres (PHCs), Sub-Centres (SCs), and Community Health Centres (CHCs), which form the backbone of rural healthcare delivery, often lack advanced diagnostic facilities, leading to delayed referrals and poor clinical outcomes.

Point-of-care testing (POCT) offers a viable alternative by enabling near-patient diagnostics outside conventional laboratory environments. The World Health Organization (WHO) defines ideal POCT systems through the ASSURED framework-Affordable, Sensitive, Specific, User-friendly, Rapid and robust, Equipment-free, and Deliverable to end users [6]. However, most currently available POCT devices are limited to single-parameter

testing, show restricted analytical precision, require manual handling, and lack seamless digital integration [7–10]. Multi-parameter, quantitative POCT platforms with laboratory-comparable performance remain scarce, especially for kidney and cardiovascular biomarkers.

The present research addresses these gaps through the design, development, and clinical validation of a low-cost, modular, multi-parameter point-of-care testing (POCT) platform intended for rural and resource-limited healthcare settings. The system integrates a portable spectrophotometric detection module based on Beer–Lambert's law, a PID-controlled incubation unit for temperature-dependent enzymatic reactions, smartphone-based connectivity for real-time reporting and cloud storage, and a frugal centrifugal microfluidic multiplexer fabricated using 3D printing for low-cost multiplexing.

Objectives of the Study

[1] To design, develop, and optimize a low-cost, modular, multi-parameter POCT platform with portable spectrophotometric detection, closed-loop illumination control, and PID-regulated incubation for accurate quantitative analysis of kidney and cardiovascular serum biomarkers in resource-limited settings.

[2] To clinically validate the developed POCT system against a fully automated gold-standard analyzer using retained patient serum samples and standard statistical comparison methods.

[3] To design and evaluate a frugal centrifugal microfluidic multiplexer with smartphone-based colorimetric detection for low-cost, automated, multiplexed biochemical testing in decentralized settings.

Chapter-wise Description of the Study:

Chapter 1: Introduction

This chapter establishes the scientific and clinical background of the study by reviewing the global and Indian burden of NCDs, with particular emphasis on diabetes, CKD, and

cardiovascular disorders [1,2]. It highlights the diagnostic challenges faced by rural healthcare systems due to limited laboratory infrastructure and skilled manpower [3].

The chapter clearly defines the aim, objectives, and research hypothesis, proposing that a low-cost, multi-parameter POCT device integrating optical detection, thermal control, and simplified fluid handling can achieve laboratory-comparable diagnostic performance in resource-limited settings.

Chapter 2: Design and Development of a portable optical system for multi-parameter serum analysis for early diagnosis of NCDs.

This chapter presents the complete engineering design and development of the POCT platform. Based on field-derived requirements, three successive design iterations are described:

(i) a paper-based modular diagnostic prototype,

(ii) a hybrid electrochemical–spectrophotometric prototype ("Analyte"), and

(iii) the final four-slot modular spectrophotometric architecture.

The development of a portable optical system based on Beer–Lambert's law is detailed, including optimization of source–sensor alignment, optical path geometry, and mechanical tolerances using extensive CAD modelling and FDM prototyping. The chapter further describes the resolution of illumination instability through a closed-loop source control circuit (SCC) operating in constant-current mode. Integration of a PID-controlled ceramic heating core enabled precise incubation at 37 °C for enzymatic reactions. Validation across multiple test levels demonstrated a reduction in reinsertion CV from ~10–13% to <1.5%, blank CV <0.1%, and incubation CV <0.8%, establishing the analytical robustness of the system.

Chapter 3: Clinical evaluation of heart and kidney profiles

This chapter focuses on the clinical performance validation of the developed POCT platform using retained patient serum samples from an NABL-accredited hospital laboratory.

Five clinically significant biomarkers, cholesterol (CHOL), triglycerides (TGL), LDL-cholesterol (LDL-C), creatinine (CRE), and uric acid (UA), were evaluated. The Siemens Dimension EXL 200 analyzer was used as the reference gold-standard system. Method comparison was performed using Passing–Bablok regression, Bland–Altman analysis, paired t-tests, and evaluation of analytical sensitivity (LOB, LOD), linearity, intra-day precision, and diagnostic performance metrics in accordance with CLSI EP09-A3 guidelines [11–13]. The results demonstrated strong correlation ($R^2 \geq 0.94$), intra-day CV < 5%, sensitivity and specificity > 90%, and high overall diagnostic accuracy, thereby confirming the clinical reliability and translational potential of the device for primary healthcare screening.

Chapter 4: Design and Development of centrifugal multiplexer for targeting frugal POCT

This chapter describes the design and fabrication of a 3D-printed centrifugal microfluidic (CM) platform intended for low-cost multiplexed biochemical testing. The CM chip integrates microchannels, collection chambers, and sensing zones fabricated using fused deposition modelling. A portable centrifuge and smartphone-based optical detection module were developed to automate reagent–sample mixing and colorimetric sensing. Image processing using RGB channel extraction and clustering algorithms enabled quantification of serum albumin and total protein. Proof-of-concept experiments yielded linearity up to $R^2 = 0.97$ with acceptable intra-chip CV, validating the feasibility of frugal microfluidic multiplexing. Limitations associated with FDM print resolution and smartphone imaging were analyzed, and future improvements using SLA printing and integrated CMOS (Complementary Metal-Oxide-Semiconductor) detection were proposed.

Chapter 5: Conclusion

This chapter integrates the engineering, clinical, and microfluidic outcomes into a unified discussion. It establishes that the proposed POCT platform satisfies WHO ASSURED

principles while achieving laboratory-comparable analytical performance [4–7]. The synergistic integration of stable optical detection, PID-controlled incubation, centrifugal microfluidics, and smartphone connectivity is shown to significantly reduce pre-analytical and analytical variability. The chapter further discusses scalability, digital interoperability, and field deployability of the platform. Future research directions—including expanded analyte panels, multi-site clinical trials, AI-assisted calibration, and HL7/FHIR-based interoperability—are outlined. The study concludes that the developed POCT ecosystem represents a clinically reliable, economically viable, and socially impactful solution for decentralized NCD screening.

CHAPTER 1

INTRODUCTION

1.1 Background and Motivation

Non-communicable diseases (NCDs) have emerged as the leading cause of morbidity and mortality worldwide, accounting for more than 70% of all global deaths [15]. The burden of diseases such as diabetes mellitus, chronic kidney disease, cardiovascular disorders, and liver dysfunction is rising rapidly in low- and middle-income countries, particularly in India, where demographic transitions, lifestyle changes, and urbanization have intensified long-term health risks [16]. Unlike infectious diseases, NCDs progress silently over long periods, often remaining undiagnosed until irreversible organ damage has occurred [17]. Early detection is therefore central to preventing complications, reducing healthcare expenditure, and improving long-term patient outcomes [18].

In India, healthcare delivery in rural and semi-urban regions is primarily anchored around Sub-Centres (SCs), Primary Health Centres (PHCs), and Community Health Centres (CHCs) [19]. While these facilities form the backbone of the public health system, their diagnostic capabilities are limited due to inadequate infrastructure, lack of skilled laboratory personnel, and dependence on centralized laboratories for biochemical investigations [20]. This diagnostic gap delays clinical decision-making and significantly reduces the effectiveness of early intervention programs for NCDs [21]. The situation is further aggravated by the logistical challenges of sample transport, reagent storage, power instability, and equipment maintenance in resource-constrained environments [22].

Conventional clinical biochemistry analyzers used in centralized laboratories offer high analytical accuracy and throughput but are inherently unsuitable for deployment in peripheral healthcare settings [23]. These systems are expensive, require uninterrupted power supply, climate-controlled environments, trained technicians, and regular calibration and maintenance [24]. As a result, rural healthcare facilities often rely on symptom-based diagnosis or referral-driven testing, which limits proactive disease management and continuity of care [25].

1.2 Research Rationale and Proposed Technological Solution

Non-communicable diseases such as diabetes mellitus, chronic kidney disease, and cardiovascular disorders constitute a rapidly growing public health challenge in India and other low- and middle-income countries [26]. These conditions often progress asymptomatically and require periodic biochemical testing for early diagnosis, risk stratification, and long-term management [27]. However, in rural and semi-urban healthcare settings, access to reliable laboratory diagnostics remains limited due to high equipment costs, infrastructure requirements, dependence on skilled technicians, and delays associated with centralized testing facilities [28]. This diagnostic gap significantly undermines early intervention efforts and leads to late-stage disease detection [29].

While point-of-care testing (POCT) has emerged as a promising strategy to decentralize diagnostics, most commercially available POCT solutions are limited to single-analyte or semi-quantitative measurements [30]. Such systems are insufficient for comprehensive screening of kidney and cardiovascular disorders, which require simultaneous evaluation of multiple interrelated biochemical markers [31]. Existing multi-analyte POCT platforms reported in the literature often compromise analytical accuracy, robustness, or affordability, restricting their practical deployment in resource-limited environments [32].

The rationale of the present research is therefore to bridge the gap between laboratory-grade clinical chemistry analyzers and field-deployable POCT systems by developing a low-cost, quantitative, and multi-parameter diagnostic platform tailored for decentralized healthcare settings [33]. The study is grounded in the hypothesis that stable optical sensing, precise thermal regulation, and simplified fluid handling, when systematically integrated, can deliver laboratory-comparable performance without the infrastructural burden of centralized laboratories [34].

To address this challenge, the research proposes a modular POCT platform based on portable spectrophotometric detection using Beer–Lambert's law [35]. A closed-loop illumination control mechanism operating in constant-current mode is implemented to mitigate source drift and ensure optical signal stability across repeated measurements [36]. Enzymatic assay requirements are met through a PID-controlled ceramic heating system capable of maintaining precise incubation at physiological temperatures, thereby minimizing reaction variability under field conditions [37].

Further, to reduce user dependency and enable affordable multiplexing, a frugal centrifugal microfluidic multiplexer fabricated using low-cost additive manufacturing is developed and evaluated [38]. Automated fluid actuation combined with smartphone-based colorimetric detection provides an accessible and scalable approach to multiplexed biochemical testing [39]. The integration of smartphone-based interfaces also facilitates data visualization, storage, and future digital interoperability [40].

Through this integrated technological framework, the proposed solution aims to deliver a clinically reliable, economically feasible, and operationally robust POCT ecosystem [41]. The research seeks to demonstrate that multi-parameter biochemical diagnostics for kidney and cardiovascular disease screening can be effectively decentralized, thereby strengthening primary healthcare diagnostics and enabling timely management of non-communicable diseases [42].

1.3 Emergence of Point-of-Care Testing (POCT)

Point-of-care testing (POCT) has emerged as a transformative approach to address diagnostic inequities by enabling rapid, near-patient testing with minimal infrastructure [43]. The World Health Organization (WHO) formalized the requirements for effective POCT systems through the ASSURED criteria—Affordable, Sensitive, Specific, User-friendly, Rapid and robust, Equipment-free, and Deliverable to end users [44]. These principles

emphasize usability and accessibility while maintaining sufficient analytical reliability for clinical decision-making.

Over the past two decades, POCT solutions have demonstrated remarkable success in infectious disease screening, glucose monitoring, and pregnancy testing [45]. However, most commercially available POCT devices remain limited to single-parameter or semi-quantitative measurements [46]. While devices such as glucometers have become widespread, their diagnostic scope is narrow and insufficient for comprehensive NCD screening, which typically requires multiple biochemical markers evaluated together to form clinically meaningful profiles [47].

For example, diabetes management requires not only glucose estimation but also lipid profiling and kidney function assessment to monitor complications [48]. Similarly, cardiovascular risk stratification relies on a combination of lipid parameters rather than a single biomarker [49]. The lack of integrated multi-analyte POCT platforms therefore restricts the clinical utility of existing solutions and necessitates repeated testing across different devices or centralized labs, undermining the very purpose of decentralized diagnostics [50].

1.4 Need for Multi-Parameter POCT Platforms

To effectively support early diagnosis and monitoring of NCDs in low-resource settings, POCT systems must evolve from single-parameter tools to multi-diagnostic platforms capable of performing quantitative biochemical analysis comparable to laboratory analyzers [51]. A multi-parameter POCT device offers several critical advantages: reduced sample volume requirement, consolidated testing workflow, faster turnaround time, lower operational costs, and improved clinical interpretation through integrated disease profiling [52].

Recent advances in microfluidics, low-power electronics, optical sensing, and additive manufacturing have enabled the development of compact diagnostic systems with enhanced analytical capabilities [53]. Multiplexed POCT platforms integrating spectrophotometric,

electrochemical, or colorimetric detection methods have been reported, demonstrating potential for decentralized diagnostics [54]. However, many of these systems remain either prohibitively expensive, mechanically complex, or poorly suited for field deployment due to sensitivity to environmental conditions [55].

Moreover, the translation of laboratory-scale diagnostic principles into robust field-ready POCT devices presents several challenges. Enzymatic biochemical assays require precise temperature control, stable optical paths, reproducible fluid handling, and accurate signal processing [56]. Variations in ambient temperature, illumination stability, reagent quality, and user handling can significantly impact analytical accuracy [57]. Therefore, engineering a multi-diagnostic POCT system demands a careful balance between performance, robustness, cost, and usability [58].

1.5 Technological Challenges in Low-Resource Diagnostics

One of the major challenges in developing POCT devices for rural healthcare is achieving laboratory-grade analytical performance within extreme design constraints [59]. Advanced diagnostic techniques such as high-performance liquid chromatography (HPLC) and mass spectrometry offer exceptional precision and sensitivity but are incompatible with decentralized deployment due to their high cost, bulkiness, and operational complexity [60,61]. Translating comparable analytical reliability into a portable, battery-operated platform requires innovative system-level optimization [62].

Optical spectrophotometry remains a widely accepted method for quantitative biochemical analysis due to its simplicity, robustness, and compatibility with established clinical assays [63]. However, miniaturizing spectrophotometric systems introduces challenges related to optical alignment, stray light, illumination stability, and detector sensitivity [64]. In addition, enzymatic reactions used in common assays (e.g., glucose

oxidase-peroxidase, alkaline picrate, uricase-PAP) are temperature-dependent, necessitating accurate incubation control typically unavailable in handheld devices [65].

Fluid handling presents another critical bottleneck. Conventional laboratory workflows rely on centrifugation, pipetting, and controlled mixing steps that are difficult to replicate reliably in low-cost POCT systems [66]. Improper mixing or inconsistent incubation can lead to significant analytical errors [67]. Recent approaches employing centrifugal microfluidics and disposable cartridges have shown promise in reducing user dependence and improving repeatability, but scalability and manufacturing consistency remain concerns [68–70].

1.6 Integration of Digital Health and Connectivity

In parallel with diagnostic innovation, digital health infrastructure has undergone rapid expansion [71]. Smartphone penetration, mobile data networks, and cloud-based health platforms have transformed how diagnostic data can be captured, transmitted, and utilized for patient care [72]. Integrating POCT devices with smartphones enables intuitive user interfaces, automated data logging, and remote clinical oversight, thereby extending the diagnostic value beyond individual test results [73].

Connected diagnostics also enable longitudinal monitoring, population-level disease surveillance, and integration with electronic medical records (EMRs) [74]. For rural healthcare systems, such connectivity facilitates referral linkage, telemedicine support, and centralized decision-making [75]. However, digital integration must be designed carefully to ensure data security, offline operability, and minimal cognitive load on frontline healthcare workers [76].

1.7 Motivation for the Present Work

Despite significant progress in POCT research, there remains a clear gap between laboratory-validated diagnostic systems and field-deployable, multi-parameter POCT platforms suitable for low-resource rural settings [77]. Many existing solutions compromise

either analytical performance or affordability, limiting their adoption in real-world healthcare delivery systems [78].

The present research is motivated by the need to bridge this gap through the design, development, and validation of a low-cost, multi-diagnostic POCT platform capable of performing quantitative biochemical analysis relevant to major non-communicable diseases [79]. By focusing on modular design, stable optical detection, precise thermal control, simplified user workflows, and smartphone-based data integration, this work aims to demonstrate that high-quality diagnostics can be delivered at the point of care without sacrificing affordability or robustness [80].

1.8 Clinical and Biochemical Mapping of Selected NCD-Related Parameters

Early diagnosis and effective management of non-communicable diseases (NCDs) require the integrated interpretation of multiple biochemical parameters rather than reliance on isolated biomarkers [81]. Disorders such as diabetes mellitus, chronic kidney disease, and cardiovascular disease are pathophysiologically interlinked, and their clinical progression is often reflected through characteristic changes in serum biochemical profiles [82]. Accordingly, the present study focuses on a selected panel of clinically relevant biomarkers mapped to kidney and cardiovascular function, enabling meaningful risk stratification and screening at the point of care [83]. Table 1 provides an integrated clinical and biochemical mapping of key biomarkers used in the assessment of cardiovascular and renal health. The selected parameters—total cholesterol (CHOL), triglycerides (TGL), creatinine (CRE), and uric acid (UA), represent essential indicators of lipid metabolism, kidney function, and metabolic stress. The table summarizes their typical adult reference ranges, interprets the clinical significance of abnormal values, and outlines associated pathophysiological risks. This mapping highlights the interconnected nature of heart and kidney disorders and

underscores the importance of multi-parameter biochemical screening for early detection and risk stratification of non-communicable diseases.

Table 1. Clinical and Biochemical Mapping of Selected Heart and Kidney Profile Parameters

Profile	Biomarker	Normal Clinical Range	Clinical Interpretation	Associated Pathophysiology / Risk
Heart Profile	Total Cholesterol (CHOL)	< 200 mg/dL	Elevated levels indicate dyslipidaemia and increased cardiovascular risk [102]	Endothelial dysfunction, LDL oxidation, atherosclerotic plaque formation, coronary artery disease [103, 104]
	Triglycerides (TGL)	< 150 mg/dL	High levels reflect altered lipid metabolism and metabolic risk [105]	Insulin resistance, increased VLDL production, small dense LDL formation, pancreatitis risk at severe elevation [106, 107]
Kidney Profile	Creatinine (CRE)	0.6–1.2 mg/dL	Elevated levels suggest reduced glomerular filtration and renal impairment [108]	Nephron loss, reduced renal clearance, progression of CKD, cardio-renal complications [109, 110]
	Uric Acid (UA)	3.5–7.2 mg/dL (M), 2.6–6.0 mg/dL (F)	Hyperuricaemia indicates impaired purine metabolism or renal excretion [111]	Oxidative stress, endothelial dysfunction, gout, CKD progression, cardiovascular risk [112, 113]

1.8.1 Cardiovascular Risk Markers

Serum lipid parameters are central to cardiovascular disease screening and prognostication [84]. Total cholesterol (CHOL) provides an initial estimate of circulating cholesterol levels, while triglycerides (TGL) reflect lipid metabolism and are strongly associated with atherogenic risk [85]. Low-density lipoprotein cholesterol (LDL-C) is clinically recognized as the primary contributor to atherosclerotic plaque formation and remains a key target for cardiovascular risk management [86]. Collectively, these lipid markers offer a comprehensive assessment of dyslipidemia, which is a major risk factor for

coronary artery disease and stroke [87]. In the context of decentralized diagnostics, their simultaneous estimation enables rapid cardiovascular risk screening and follow-up [88].

1.8.1.1 Total Cholesterol (CHOL)

Total cholesterol is a fundamental biomarker of lipid metabolism and cardiovascular risk, widely used in dyslipidaemia screening and atherosclerotic cardiovascular disease (ASCVD) risk assessment [89, 90]. Clinically, serum total cholesterol levels <200 mg/dL are considered desirable, 200–239 mg/dL borderline high, and ≥240 mg/dL high, with increasing concentrations strongly associated with elevated risk of coronary artery disease and stroke [89, 91]. These thresholds reflect progressive disturbances in hepatic cholesterol synthesis, lipoprotein transport, and receptor-mediated clearance [90].

Cholesterol is an essential cellular component and precursor for steroid hormones, bile acids, and vitamin D, and circulates in plasma bound to lipoproteins, primarily LDL and HDL [92]. Elevated total cholesterol, driven largely by excess LDL, promotes endothelial dysfunction, oxidative stress, and subendothelial lipid deposition, leading to macrophage-driven inflammation and atheromatous plaque formation [93, 94]. In contrast, abnormally low cholesterol may indicate underlying metabolic or inflammatory disorders [95].

Given its central role in atherogenesis, measurement of total cholesterol remains critical for early cardiovascular risk stratification and preventive intervention, particularly in decentralized and point-of-care screening settings [89, 91].

1.8.1.2 Triglycerides (TGL)

Triglycerides are a key biomarker of lipid metabolism and cardiometabolic risk, reflecting circulating energy storage and postprandial lipid handling [96, 97]. Clinically, fasting serum triglyceride levels <150 mg/dL are considered normal, 150–199 mg/dL borderline high, 200–499 mg/dL high, and ≥500 mg/dL very high, with progressively increasing risk of atherosclerotic cardiovascular disease (ASCVD) and acute pancreatitis at extreme elevations

[96, 98]. Elevated triglycerides arise from insulin resistance, enhanced hepatic very-low-density lipoprotein (VLDL) production, impaired lipoprotein lipase activity, and defective clearance of triglyceride-rich lipoproteins [97, 99].

Pathophysiologically, hypertriglyceridaemia contributes to endothelial dysfunction, oxidative stress, and chronic low-grade inflammation, promoting atherogenesis through accumulation of remnant lipoproteins and small dense LDL particles [98, 100]. It is frequently associated with metabolic syndrome, type 2 diabetes mellitus, obesity, non-alcoholic fatty liver disease, and chronic kidney disease [97, 101]. Severe elevations in triglycerides (>500 mg/dL) increase blood viscosity and pancreatic lipase activation, predisposing to acute pancreatitis [96, 99]. Given its strong association with metabolic dysregulation and cardiovascular risk, triglyceride measurement is an essential component of comprehensive lipid profiling, enabling early identification of high-risk individuals and guiding therapeutic and lifestyle interventions in both centralized and point-of-care settings [98, 100].

1.8.2 Kidney Function Markers

Chronic kidney disease (CKD) frequently coexists with diabetes and cardiovascular disorders, necessitating routine biochemical monitoring for early detection and assessment of disease progression [114]. Serum creatinine (CRE) is widely used as a primary indicator of renal filtration efficiency, while uric acid (UA) serves as an additional biomarker associated with impaired renal clearance and metabolic dysfunction [115]. Elevation of these parameters often precedes overt clinical symptoms, making them particularly valuable for early-stage CKD screening [116]. Mapping creatinine and uric acid measurements within a point-of-care testing (POCT) framework allows timely identification of renal compromise in high-risk populations [117].

1.8.2.1 Creatinine (CRE)

Creatinine is a key biomarker of renal function, widely used to assess glomerular filtration efficiency and detect kidney impairment [118, 119]. Clinically, serum creatinine levels typically range from 0.6–1.2 mg/dL in adults, with elevated values indicating reduced renal clearance and potential progression of chronic kidney disease (CKD) [118]. Creatinine is generated at a relatively constant rate from muscle creatine metabolism and is freely filtered by the glomeruli, with minimal tubular reabsorption, making it a reliable indicator of kidney function under steady-state conditions [119, 120].

Pathophysiologically, elevated creatinine reflects declining nephron function due to glomerular damage, reduced renal perfusion, or tubular dysfunction. Persistent creatinine elevation is associated with progressive CKD, hypertension, diabetic nephropathy, and increased cardiovascular risk [121, 122]. Even mild increases in serum creatinine may correspond to significant reductions in estimated glomerular filtration rate (eGFR), underscoring its importance in early renal impairment detection [120].

Given its clinical significance and routine use in kidney function assessment, quantitative measurement of creatinine is essential for early CKD screening, disease staging, and monitoring therapeutic response. Incorporation of creatinine estimation into POCT platforms enables timely identification of renal dysfunction in high-risk populations, particularly in resource-limited settings [118, 122].

1.8.2.2 Uric Acid (UA)

Uric acid is a clinically important biomarker of purine metabolism and renal excretory function, commonly used in the assessment of metabolic, renal, and cardiovascular disorders [123, 124]. In adults, normal serum uric acid levels typically range from 3.5–7.2 mg/dL in men and 2.6–6.0 mg/dL in women. Persistent elevations beyond these ranges indicate

hyperuricaemia and are associated with gout, renal dysfunction, and increased cardiometabolic risk [123, 125].

Biochemically, uric acid is the end product of purine catabolism and is primarily eliminated through renal filtration and tubular handling. Elevated uric acid levels result from increased production, reduced renal excretion, or a combination of both, often influenced by insulin resistance, high fructose intake, hypertension, and chronic kidney disease [124, 126]. Hyperuricaemia promotes oxidative stress, endothelial dysfunction, and activation of inflammatory pathways, contributing to renal microvascular injury and acceleration of atherosclerotic processes [125, 127].

Clinically, elevated uric acid levels frequently precede overt renal dysfunction and are increasingly recognized as an independent risk factor for chronic kidney disease progression and cardiovascular morbidity [126, 128]. Therefore, quantitative assessment of uric acid provides valuable insight into metabolic and renal health. Its inclusion in POCT platforms enables early identification of high-risk individuals and supports timely clinical intervention in decentralized healthcare settings [123, 128].

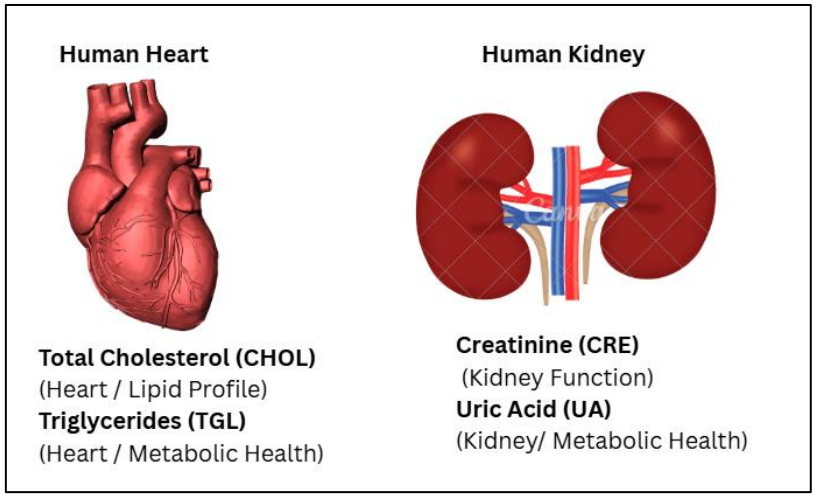

Figure 1: Clinical Mapping of Heart and Kidney Biomarkers for Non-Communicable Disease Screening

The Figure 1 illustrates the anatomical representation of the human heart and kidneys alongside the key biochemical biomarkers employed for cardiovascular and renal health

assessment in the present study. The heart panel highlights lipid-related markers—total cholesterol (CHOL) and triglycerides (TGL), used for evaluating dyslipidaemia, metabolic status, and cardiovascular risk. The kidney panel depicts renal function markers—serum creatinine (CRE) and uric acid (UA), which reflect glomerular filtration efficiency, renal excretory capacity, and metabolic health. Together, these parameters enable integrated cardiorenal risk stratification and support early detection of non-communicable diseases at the point of care.

Table 2. Biochemical Parameters Selected for the Assessment of Heart and Kidney Disorders: Adult Reference Ranges with Clinical Consequences of Abnormally High and Low Results

Test (Profile)	**Typical Adult Reference Range**	**If High (Possible Meaning & Consequences)**	**If Low (Possible Meaning & Consequences)**
Total Cholesterol (CHOL) (Heart / Lipid Profile)	<200 mg/dL desirable; 200–239 borderline; ≥240 high [129, 130]	Hypercholesterolaemia → atherosclerosis, coronary artery disease, ischemic stroke, peripheral vascular disease; long-term risk of myocardial infarction and cardiovascular mortality [131, 132–134].	Hypocholesterolaemia → malnutrition, chronic liver disease, hyperthyroidism, inflammatory states; may be associated with frailty and increased all-cause mortality in elderly [135].
Triglycerides (TGL) (Heart / Metabolic Health)	<150 mg/dL normal; 150–199 borderline; 200–499 high; ≥500 very high [136, 137]	Hypertriglyceridemia → insulin resistance, metabolic syndrome, NAFLD/NASH, atherogenic dyslipidaemia; severe elevation (>500) increases risk of acute pancreatitis [138–140].	Low triglycerides → malnutrition, malabsorption syndromes, hyperthyroidism, chronic illness; usually less clinically significant when isolated [141, 137].
Creatinine (Serum) (Kidney Function)	Men: ~0.74–1.35 mg/dL; Women: ~0.59–1.04 mg/dL [142]	Elevated creatinine → reduced GFR, AKI/CKD, dehydration, urinary obstruction, nephrotoxic drugs; consequences include uremia, electrolyte	Low creatinine → low muscle mass, malnutrition, pregnancy, overhydration; typically, not pathologic when isolated [147, 143].

		imbalance, hypertension, fluid overload, and progression to renal failure if persistent [142–146].	
Uric Acid (UA) (Kidney / Metabolic Health)	Men: 3.5–7.2 mg/dL; Women: 2.6–6.0 mg/dL [148, 149]	Hyperuricaemia → gout, urate nephropathy, CKD progression, hypertension, endothelial dysfunction, increased cardiovascular risk [150–154].	Low uric acid → malnutrition, SIADH (Syndrome of Inappropriate Antidiuretic Hormone Secretion), severe liver disease, xanthine oxidase deficiency, or drug effects; usually low clinical concern unless symptomatic [148].

Table 2 summarizes the key biochemical parameters selected for the assessment of cardiovascular and renal disorders, presenting their typical adult reference ranges alongside the clinical implications of abnormally high or low values. The included biomarkers—total cholesterol, triglycerides, serum creatinine, and uric acid, represent essential indicators of lipid metabolism, kidney function, and metabolic health. Elevated or reduced levels of these analytes are associated with well-established pathophysiological mechanisms, ranging from atherosclerosis and metabolic dysfunction to impaired renal filtration and systemic inflammatory responses. By outlining both upper and lower deviation consequences, the table provides a comprehensive framework for interpreting biomarker alterations in the context of non-communicable disease screening and clinical decision-making.

1.9 Objectives of the Study

The overarching goal of this research is to develop and clinically validate a frugal, robust, and multi-parameter point-of-care testing (POCT) ecosystem capable of delivering laboratory-comparable biochemical diagnostics in decentralized and resource-limited

healthcare settings. To achieve this goal, the specific objectives of the study are defined as follows:

[1] To design, develop, and optimize a low-cost, modular multi-parameter POCT platform incorporating portable spectrophotometric detection based on Beer–Lambert's law, closed-loop illumination control for optical signal stability, and PID-regulated thermal incubation to enable accurate quantitative estimation of kidney and cardiovascular serum biomarkers under field conditions.

[2] To clinically validate the analytical and diagnostic performance of the developed POCT system against a fully automated, gold-standard clinical chemistry analyzer using retained patient serum samples, employing internationally accepted statistical comparison methodologies to establish accuracy, precision, sensitivity, specificity, and diagnostic agreement.

[3] To design, fabricate, and evaluate a frugal centrifugal microfluidic multiplexing platform, integrating low-cost additive manufacturing and smartphone-based colorimetric detection, aimed at automated, low-volume, multiplexed biochemical testing to further enhance affordability and scalability of decentralized diagnostics.

Chapter 1: Introduction

This chapter establishes the scientific, clinical, and technological motivation for the present research. It begins by reviewing the global and Indian burden of non-communicable diseases (NCDs), with particular emphasis on diabetes mellitus, chronic kidney disease, and cardiovascular disorders, which collectively account for a significant proportion of morbidity and mortality [1,2]. The chapter highlights systemic diagnostic challenges in rural and semi-urban healthcare delivery, including inadequate laboratory infrastructure, limited skilled manpower, and delayed access to biochemical testing [3].

The chapter articulates the core research hypothesis that a low-cost, multi-parameter POCT device integrating stable optical detection, precise thermal control, and simplified fluid handling can achieve laboratory-comparable diagnostic performance even in resource-limited settings. The chapter concludes by clearly defining the aim, objectives, and scope of the study.

Chapter 2: Design and Development of a portable optical system for multi-parameter serum analysis for early diagnosis of NCDs.

This chapter presents the complete engineering development lifecycle of the proposed POCT platform, guided by field-derived clinical and operational requirements. Three successive design iterations are detailed:

(a) a paper-based modular diagnostic prototype for early feasibility,

(b) a hybrid electrochemical–spectrophotometric prototype ("Analyte") for functional validation, and

(c) the final four-slot modular spectrophotometric architecture optimized for clinical deployment.

The development of a portable optical system based on Beer–Lambert's law is discussed, including optimization of source–sensor alignment, optical path geometry, stray light reduction, and mechanical tolerances using extensive CAD modeling and fused deposition modeling (FDM) prototyping. The chapter further details the mitigation of illumination instability through the development of a closed-loop source control circuit (SCC) operating in constant-current mode. Integration of a PID-controlled ceramic heating core enabled precise enzymatic incubation at 37 °C. Validation studies demonstrated a significant reduction in reinsertion CV (~10–13% to <1.5%), blank CV (<0.1%), and incubation CV (<0.8%), establishing high analytical robustness of the platform.

Chapter 3: Clinical evaluation of heart and kidney profile

This chapter focuses on clinical performance validation of the developed POCT system using retained patient serum samples obtained from an NABL-accredited hospital laboratory. Five clinically relevant biomarkers, total cholesterol (CHOL), triglycerides (TGL), LDL-cholesterol (LDL-C), creatinine (CRE), and uric acid (UA), were evaluated. The Siemens Dimension EXL 200 fully automated analyzer served as the reference gold-standard system.

Method comparison was conducted using Passing–Bablok regression, Bland–Altman analysis, paired t-tests, and evaluation of analytical sensitivity parameters (LOB, LOD), linearity, and intra-day precision in accordance with CLSI EP09-A3 guidelines [11–13]. The results demonstrated strong correlation ($R^2 \geq 0.94$), intra-day CV < 5%, sensitivity and specificity exceeding 90%, and high diagnostic accuracy, confirming the clinical reliability and translational suitability of the developed POCT platform for primary healthcare screening.

Chapter 4: Design and Development of centrifugal multiplexer for targeting frugal POCT

This chapter describes the design and experimental evaluation of a centrifugal microfluidic (CM) platform aimed at low-cost, multiplexed biochemical testing. A 3D-printed CM chip fabricated using fused deposition modeling integrates microchannels, reagent chambers, and optical sensing zones. A portable centrifuge was developed to automate fluid actuation, while smartphone-based imaging was used for colorimetric signal acquisition.

Quantitative analysis was performed using RGB channel extraction and clustering-based image processing algorithms. Proof-of-concept experiments for serum albumin and total protein demonstrated acceptable linearity (up to $R^2 = 0.97$) and intra-chip reproducibility, validating the feasibility of frugal microfluidic multiplexing. The chapter critically analyzes limitations arising from FDM print resolution and smartphone camera variability and proposes future enhancements using SLA-based microfabrication and integrated CMOS detectors.

Chapter 5: Conclusions

This chapter synthesizes the engineering, clinical, and microfluidic contributions of the thesis into a unified discussion. It establishes that the proposed POCT ecosystem adheres closely to WHO ASSURED principles while delivering laboratory-comparable analytical performance [4–7]. The synergistic integration of stable optical detection, PID-controlled incubation, centrifugal microfluidics, and smartphone-based connectivity is shown to significantly reduce both pre-analytical and analytical variability.

The chapter further discusses system scalability, digital interoperability, and field deployability within national healthcare frameworks. Future research directions, including expanded analyte panels, multi-site clinical trials, AI-assisted calibration, and HL7/FHIR-based data interoperability—are outlined. The thesis concludes that the developed POCT ecosystem represents a clinically reliable, economically viable, and socially impactful solution for decentralized screening and monitoring of non-communicable diseases.

1.10 Scope of the Thesis

This thesis presents a comprehensive engineering and clinical validation framework for a multi-parameter POCT device targeting early diagnosis of diabetes, kidney disease, cardiovascular disorders, and liver dysfunction. The research encompasses system design, optical and thermal optimization, disposable cartridge development, centrifugal microfluidics, and clinical performance evaluation against gold-standard laboratory analyzers. By addressing both technological and translational challenges, this work contributes to the broader goal of democratizing diagnostics and strengthening primary healthcare systems in resource-constrained settings.

CHAPTER 2

DESIGN AND DEVELOPMENT OF A PORTABLE OPTICAL SYSTEM FOR MULTI-PARAMETER SERUM ANALYSIS FOR EARLY DIAGNOSIS OF NCDs

Abstract

This chapter presents the design, development, and validation of a compact, low-cost, and modular spectrophotometric point-of-care testing (POCT) system engineered for multi-parameter biochemical analysis relevant to non-communicable disease (NCD) screening. Guided by field requirements from primary healthcare settings, the system was built around four independent optical modules coupled to a central core, enabling rapid quantitative testing using disposable reagent–sample cartridges. The optical system incorporates a CMOS–LED detection architecture optimized through more than 200 CAD iterations to minimize mechanical misalignment, illumination drift, and optical noise. A closed-loop constant-current source control circuit was developed to ensure illumination stability, achieving blank and water coefficients of variation below 0.1%. Recognizing the high temperature sensitivity of glucose and creatinine assays, a CNC (Computer Numerical Control)-machined heating core with PID regulation was integrated, along with a predictive temperature profile (T1) capable of raising reagents from 8–30 °C to the target 37 °C with thermal CV <0.8%. Experimental validation demonstrated that creatinine measurements performed without incubation exhibited ~19% error, whereas implementation of the optimized incubation system reduced error to ~1.5%, confirming more than a twelve-fold improvement in analytical accuracy. The platform is battery-powered, smartphone-connected, and cloud-enabled, supporting decentralized digital diagnostics. Collectively, the chapter establishes the feasibility of a portable, robust, and scalable spectrophotometric POCT device capable of achieving laboratory-comparable precision for multi-parameter biochemical testing in resource-limited settings.

2.1 Introduction

Non-communicable diseases (NCDs) constitute one of the most critical public health challenges of the twenty-first century, accounting for a substantial proportion of global morbidity, mortality, and healthcare expenditure. Unlike communicable diseases, NCDs—including cardiovascular disorders, diabetes mellitus, chronic kidney disease (CKD), and liver dysfunction—progress insidiously over extended periods and often remain clinically silent until advanced organ damage has occurred [155, 156]. The World Health Organization estimates that NCDs are responsible for more than 70% of all global deaths, with a disproportionate burden borne by low- and middle-income countries (LMICs), where access to advanced diagnostic and treatment facilities is limited [157].

The escalating prevalence of NCDs is driven by a complex interplay of demographic transitions, sedentary lifestyles, unhealthy dietary patterns, population ageing, urbanization, and environmental exposures [158]. Beyond their clinical consequences, NCDs impose a significant socio-economic burden due to lifelong treatment requirements, recurrent hospitalizations, productivity loss, and long-term disability [159]. In resource-constrained settings, delayed diagnosis further exacerbates disease severity and contributes to avoidable complications and premature mortality.

Early diagnosis and continuous monitoring of disease-specific biochemical markers are fundamental to effective NCD management. Biomarkers such as blood glucose for diabetes mellitus, serum creatinine and urea for renal function, and bilirubin for hepatic health provide objective indicators of underlying pathophysiology and disease progression [160, 161]. Regular biochemical assessment enables timely clinical intervention, therapeutic monitoring, and risk stratification, ultimately improving patient outcomes and reducing healthcare costs.

However, conventional laboratory-based diagnostic testing relies on centralized facilities equipped with sophisticated analyzers, uninterrupted power supply, climate-controlled environments, and skilled laboratory personnel. These infrastructural requirements pose

substantial barriers in rural and remote settings, resulting in delayed sample transport, prolonged turnaround times, and limited testing frequency [162]. Consequently, many patients in underserved regions experience delayed diagnosis and suboptimal disease monitoring, undermining the effectiveness of early intervention strategies.

Point-of-Care Testing (POCT) has emerged as a viable solution to overcome these constraints by enabling decentralized diagnostic testing at or near the patient site. POCT systems significantly reduce turnaround time—from hours or days to minutes—thereby facilitating rapid clinical decision-making and improving workflow efficiency [163]. Additionally, POCT minimizes sample handling errors, reduces dependency on specialized personnel, and enhances access to essential diagnostics in primary healthcare settings [164].

Despite substantial technological progress, currently available commercial POCT systems remain limited in their applicability to comprehensive NCD management. Two major gaps are consistently reported in the literature. First, most POCT devices are parameter-specific, designed primarily for single biomarker measurements such as glucose or hemoglobin, thereby failing to provide integrated disease profiling required for complex NCDs [166]. Second, analytical accuracy and precision in many POCT systems deviate from laboratory gold standards, particularly under variable environmental conditions, limiting their clinical reliability for quantitative biochemical analysis [167].

Table 3. Major Gaps in Existing Point-of-Care Testing (POCT) Systems.

Gap in POCT Systems	Limitation
Parameter-specific design	Most systems measure only a single biomarker, typically glucose or hemoglobin
Compromised analytical accuracy	Performance frequently deviates from laboratory gold standards, limiting clinical reliability

This Table 3 summarizes the key limitations of currently available POCT technologies, highlighting two critical gaps that restrict their clinical applicability in non-communicable disease (NCD) management: (1) parameter-specific design, where devices are limited to

single-analyte measurements, and (2) compromised analytical accuracy, characterized by deviations from laboratory reference standards. These constraints underscore the need for a multi-parameter, laboratory-comparable POCT platform suitable for decentralized healthcare settings.

These limitations highlight the urgent need for a next-generation POCT platform capable of delivering multi-parameter biochemical analysis with laboratory-comparable accuracy, while retaining portability, affordability, and operational simplicity. Addressing this unmet need, the present work focuses on the development of a compact, battery-operated, spectrophotometric point-of-care device for quantitative measurement of multiple serum biomarkers relevant to NCD screening and monitoring.

The proposed system integrates modular optical and electronic components optimized for stable signal acquisition, minimal sample volume requirement, and robust performance under field conditions. While the current study primarily emphasizes glucose and creatinine detection as representative biomarkers for metabolic and renal assessment, the system architecture is inherently extensible to additional assays, including urea and bilirubin. This modular approach lays the foundation for a comprehensive, multi-parameter diagnostic solution tailored for decentralized healthcare delivery.

This chapter presents a detailed account of the scientific rationale and engineering strategy underlying the portable optical diagnostic system. It describes the conceptual framework, design methodology, performance optimization, and experimental validation undertaken to establish the feasibility of the proposed device as a reliable and quantitative point-of-care platform for non-communicable disease biomarker analysis.

2.2 Fundamentals of Spectrophotometric POCT Systems

Spectrophotometry is one of the most widely used analytical techniques in clinical chemistry because of its robustness, affordability, and compatibility with a broad range of biochemical assays. Its principles have been employed in centralized laboratories for decades,

forming the backbone of quantitative diagnostic testing for analytes such as glucose, urea, creatinine, bilirubin, and lipid biomarkers [168]. When adapted into portable, low-power point-of-care testing (POCT) platforms, spectrophotometry provides an attractive pathway for decentralized biochemical analysis, especially in resource-limited settings.

2.2.1 Optical Components and Signal Pathway

A spectrophotometric POCT device typically comprises four essential components:

(a) Light Source: Light-emitting diodes (LEDs) offer narrowband emission, low power consumption, and thermal stability. Their tunability allows alignment with assay-specific wavelengths (e.g., 520–550 nm for peroxidase complexes), making them ideal for portable systems [171].

(b) Sample Holder / Cuvette: Disposable cuvettes or microfluidic chambers maintain a fixed optical path length and minimize contamination. Path-length consistency is critical for reliable absorbance measurements [172].

(c) Optical Detector: Photodiodes convert transmitted light into measurable electrical signals. Their sensitivity, low noise characteristics, and fast response times make them suited for real-time POCT applications [173].

(d) Signal Processing Unit: Microcontrollers or embedded processors digitize signals, apply calibration curves, correct for drift, and compute final concentration values. Modern POCT devices increasingly incorporate wireless communication and automated quality checks [174].

2.2.2 Engineering Challenges in Miniaturized Spectrophotometry

Translating laboratory-grade spectrophotometry into portable POCT devices introduces several challenges:

(a) Optical Alignment & Stray Light: Compact form factors increase susceptibility to misalignment and ambient light interference, reducing measurement accuracy [175].

(b) Illumination Instability: LED intensity drift caused by temperature fluctuations or aging can distort absorbance measurements unless mitigated through constant-current drivers or feedback-controlled illumination [176].

(c) Temperature Dependence of Enzymatic Reactions: Many colorimetric assays require stable incubation at 37°C. Fluctuations significantly impact reaction kinetics and reproducibility, necessitating precise PID-based thermal regulation [177].

(d) Short Optical Path Length Effects: Portable devices often employ micro-cuvettes or microfluidic channels, reducing optical path length and increasing noise-to-signal ratio, demanding careful calibration and compensation [178].

2.2.3 Advantages of Spectrophotometric Methods for POCT

Despite these engineering constraints, spectrophotometry remains the most practical and scalable detection method for multi-analyte POCT due to:

(a) High Versatility: Compatible with enzymatic, end-point, kinetic, and colorimetric assays across a broad biomarker panel [168, 170].

(b) High Sensitivity & Selectivity: Capable of detecting analyte concentrations relevant to diagnosis of diabetes, CKD, liver disease, and cardiovascular disorders [171].

(c) Low Cost and Component Availability: LEDs, photodiodes, and plastic cuvettes are inexpensive, enabling large-scale production of portable devices [174].

(d) Integration Capability: Easily interfaced with microfluidic platforms for automated reagent mixing and sample handling, supporting multi-parameter testing [178].

2.3 Principle of UV-Visible Spectrophotometry

UV–Visible spectrophotometry is a widely used analytical technique in clinical biochemistry for quantitative measurement of chemical species based on light absorption in the ultraviolet (200–400 nm) and visible (400–700 nm) regions. Many biologically relevant analytes or their chromogenic reaction products exhibit characteristic absorption peaks in this spectral range, making the technique well suited for biochemical diagnostics [179, 180].

When monochromatic light passes through a colored solution, part of the incident radiation is absorbed as molecules undergo electronic transitions, while the remaining light is transmitted to the detector. The extent of absorption depends on the concentration of the absorbing species, the optical path length, and the intrinsic absorptivity of the analyte or reaction product [169, 170, 181].

This quantitative relationship is governed by the Beer–Lambert law:

$$A=\varepsilon\times l\times C$$

Where,

A is absorbance,

ε is the molar absorptivity ($L\cdot mol^{-1}\cdot cm^{-1}$),

l is the optical path length (cm), and

C is the concentration of the absorbing species ($mol\cdot L^{-1}$).

Under ideal conditions, absorbance varies linearly with concentration, forming the analytical basis for quantitative biochemical testing [182].

In clinical diagnostics, UV–Visible spectrophotometry is commonly employed in enzymatic and colorimetric assays such as glucose oxidase–peroxidase, creatinine picrate, and bilirubin diazo reactions, where measurement at the wavelength of maximum absorbance improves sensitivity and specificity [183–185]. Although deviations from Beer–Lambert behavior may arise due to turbidity, stray light, or temperature effects, these limitations can be mitigated through proper optical design, calibration, and thermal control—particularly important in point-of-care devices [186].

Owing to its simplicity, robustness, and compatibility with established clinical assays, UV–Visible spectrophotometry remains a core detection principle for quantitative point-of-care testing systems aimed at delivering laboratory-comparable performance in decentralized healthcare settings [187, 188].

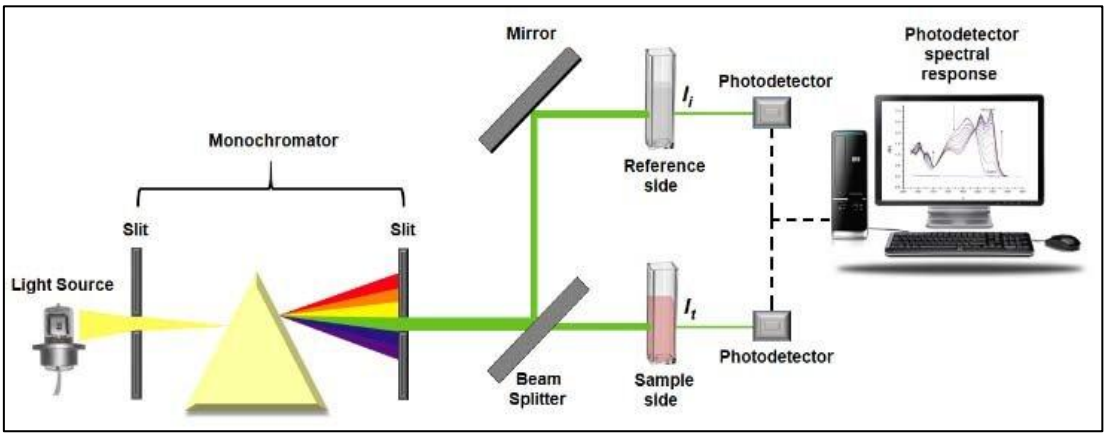

Figure 2: Schematic of a Conventional UV–Visible Double-Beam Spectrophotometric System.

This schematic (Figure 2) depicts the operating principle of a laboratory-grade UV–Visible double-beam spectrophotometer used in quantitative chemical and biochemical analysis. Light emitted from the source is first collimated and wavelength-selected by a monochromator, which disperses the incident radiation and isolates a narrow spectral band using adjustable slits. The monochromatic beam is then divided by a beam splitter into two parallel optical paths: one directed through a reference cuvette containing a blank solution, and the other through a sample cuvette containing the analyte.

Mirrors guide the beams toward independent photodetectors, where the transmitted intensities (I_r for the reference and I_t for the sample) are converted into electrical signals. The ratio of these signals is processed by the detector electronics and computer interface to calculate absorbance based on the Beer–Lambert law. By continuously monitoring both reference and sample paths, the double-beam configuration minimizes errors due to source drift, optical alignment changes, and detector fluctuations. This architecture serves as the analytical foundation for high-precision spectrophotometric measurements and provides a benchmark for the design and miniaturization of point-of-care spectrophotometric diagnostic systems.

2.3.1 Spectrophotometric Techniques in Clinical Chemistry

Spectrophotometry is a foundational analytical tool in clinical chemistry and remains one of the most commonly employed methods for quantifying biochemical analytes in both

centralized laboratories and point-of-care (POC) systems. Its widespread adoption is primarily due to its precision, rapidity, versatility, and compatibility with a broad range of colorimetric and enzymatic assays used in clinical diagnostics [189]. Many clinically relevant biomarkers—including glucose, creatinine, bilirubin, urea, and lipid components, produce chromogenic products through well-established biochemical reactions, making spectrophotometric detection indispensable for routine laboratory workflows [190].

In clinical practice, spectrophotometric assays typically operate in either end-point or kinetic modes. End-point assays quantify the concentration of an analyte after the reaction has reached completion, whereas kinetic assays monitor reaction rates to measure enzyme activity or analyte conversion over time. This dual capability enables spectrophotometry to accommodate diverse biochemical processes ranging from oxidation–reduction reactions to enzyme-mediated chromogenic transformations [191]. Table 3 summarizes two major categories of spectrophotometric assays commonly used in clinical biochemistry: kinetic and end-point assays. Kinetic assays measure the rate of change in absorbance over time, enabling the evaluation of dynamic biochemical reactions such as enzyme activities or rapid chemical transformations (e.g., the Jaffe reaction for creatinine). In contrast, end-point assays quantify the final color intensity once the reaction has reached completion, making them widely applicable for stable chromogenic assays such as the glucose GOD-POD method. This comparison highlights how different biochemical processes are matched with appropriate spectrophotometric strategies to ensure reliable quantitative measurement in both laboratory and POCT settings. [192].

Table 4. Types of Spectrophotometric Assays and Their Analytical Principles in Clinical Chemistry

Type	Principle	Example
Kinetic Assay	Time-dependent change in absorbance	Creatinine (Jaffe reaction)
End-Point Assay	Final color intensity measurement	Glucose (GOD-POD reaction)

Modern clinical spectrophotometric systems also incorporate enhanced optical components, including narrow-band LEDs, photodiodes, and silicon detectors, to improve sensitivity and reduce noise in absorbance measurements. Advances in miniaturized cuvette design, microfluidics, and temperature-controlled incubation have further expanded the applicability of spectrophotometry to decentralized diagnostic environments. These improvements allow compact POCT devices to achieve analytical performance approaching that of high-throughput benchtop analyzers, even when working with small sample volumes and varying environmental conditions [193].

As a result, spectrophotometric techniques have become essential for developing portable multi-parameter diagnostic systems aimed at addressing the rising burden of non-communicable diseases. Their analytical robustness, compatibility with standard clinical reagents, and adaptability to automated and miniaturized formats make them central to the design of next-generation POCT platforms that deliver accurate biochemical assessment in resource-limited settings [194].

2.3.2 CMOS Sensors vs Photodiodes vs Spectrometers

The choice of optical detection hardware is a critical design consideration in any spectrophotometric point-of-care testing (POCT) system. The detector directly influences analytical sensitivity, measurement stability, spectral resolution, power consumption, and overall device cost. Among the commonly employed detectors, CMOS sensors, photodiodes, and miniaturized spectrometers each offer distinct advantages and limitations that must be evaluated in the context of portable biochemical analysis.

Table 5. Comparative Characteristics of CMOS Sensors, Photodiodes, and Miniaturized Spectrometers Used in Spectrophotometric Point-of-Care Testing (POCT)

Detector Type	Key Principle	Advantages	Limitations	Typical POCT Use Cases
CMOS Sensors	Pixel arrays measure light	Low cost, compact, low	Lower sensitivity,	Colorimetric strip reading,

	intensity using integrated photodiodes and color filters	power, compatible with smartphone-based diagnostics	higher noise, limited wavelength specificity [195]	smartphone POC imaging
Photodiodes	Convert incident photons into electrical current with high linearity	High sensitivity, low noise, fast response, excellent for absorbance quantification [196]	Single-wavelength detection unless multiple detectors used	Creatinine, glucose, uric acid assays; kinetic and endpoint spectrophotometry
Miniaturized Spectrometers	Disperse light into full spectrum using diffraction gratings and CCD/CMOS arrays	High spectral resolution, multiplexing capability, laboratory-grade precision [197]	High cost, higher power consumption, sensitive to mechanical alignment [198]	Multi-analyte POCT, spectral fingerprinting, research-grade quantitative diagnostics

The **Table 5** outlines the operational principles, strengths, limitations, and diagnostic suitability of three major detector technologies used in portable POCT optical systems. Their performance and practicality vary significantly depending on assay requirements, sensitivity needs, cost constraints, and environmental robustness.

This table provides a comparative evaluation of detector technologies relevant to spectrophotometric POCT systems. CMOS sensors, widely used in consumer electronics, offer low-cost imaging suitable for qualitative or semi-quantitative colorimetric assays but lack the spectral selectivity and sensitivity required for precise biochemical quantification. Photodiodes, by contrast, provide excellent sensitivity, linearity, and stability for single- or dual-wavelength absorbance measurements, making them the preferred choice for quantitative POCT devices measuring biomarkers such as glucose, creatinine, and uric acid. Miniaturized spectrometers deliver full spectral information and laboratory-grade analytical performance but are limited in POCT deployment due to higher cost, power requirements, and mechanical fragility. These comparisons underscore why photodiode-based detection

remains the most practical and reliable technology for portable, field-ready biochemical analyzers.

In the present work, a CMOS detector coupled with an LED light source was selected as the core optical sensing module due to several advantages essential for point-of-care implementation. CMOS sensors offer low power consumption, a compact physical footprint, and direct digital output, enabling seamless integration with embedded microcontrollers and smartphone interfaces. When appropriately optimized, the CMOS architecture also provides a high signal-to-noise ratio, supporting reliable quantitative absorbance measurements suitable for NCD biomarker detection. However, adopting a CMOS-LED configuration introduces critical engineering challenges that must be meticulously managed to achieve laboratory-comparable analytical precision. These include maintaining consistent light path geometry, ensuring accurate sensor–source alignment, stabilizing LED intensity over time and temperature, and achieving high reproducibility of disposable test cartridges. Each of these challenges is systematically analyzed and addressed in subsequent sections of this chapter through optical design refinement, electronic feedback control, and structured cartridge engineering. This integrated approach ensures that the chosen CMOS-LED detection architecture delivers both the robustness and performance required for practical field-ready POCT applications.

For example, the optical sensing modules are fabricated using a combination of 3D-printed polymeric components and CNC-machined metallic support structures designed to maintain fixed optical alignment and minimize stray light interference. The outer optical housing and cartridge alignment chamber are fabricated using black polylactic acid (PLA) and acrylonitrile butadiene styrene (ABS) materials due to: low manufacturing cost, ease of rapid prototyping, dimensional stability, and reduced internal optical reflection. The optical detection system utilizes a TSL2591 CMOS-based light sensor for measuring transmitted light intensity through the reaction mixture, enabling quantitative absorbance analysis.

Illumination control has been achieved using an MCP4725 12-bit Digital-to-Analog Converter (DAC), which regulates the constant-current LED driving circuit to ensure stable light output, minimize intensity fluctuations, and improve measurement reproducibility during spectrophotometric analysis.

2.4 Literature Review

Modern diagnostic technologies used in healthcare, environmental monitoring, and food analysis rely heavily on advanced analytical methods such as UV–Visible spectroscopy, high-performance liquid chromatography (HPLC), and mass spectrometry. While HPLC offers excellent chemical separation and quantification capabilities, it remains expensive and requires trained personnel and laboratory infrastructure, limiting its applicability in decentralized settings. Similarly, mass spectrometry provides unmatched molecular specificity but is unsuitable for field deployment due to instrument complexity, maintenance requirements, and high operational costs [199].

To overcome these limitations, point-of-care testing (POCT) technologies have evolved considerably over the past two decades. Three major biochemical detection approaches dominate POCT development: paper-based microfluidics, electrochemical biosensing, and optical spectrophotometric systems. Paper-based microfluidic devices are low-cost and simple but are typically qualitative or semi-quantitative due to inconsistent illumination and signal variability [200]. Electrochemical biosensors offer strong analytical sensitivity but depend on precisely engineered electrodes, surface chemistry stability, and regular calibration, which complicate field use in low-resource settings [201–202]. Optical POCT platforms, particularly those based on spectrophotometry, provide a promising balance between quantitative accuracy, robustness, and compatibility with established clinical assays [203]. However, miniaturizing spectrophotometric systems introduces engineering challenges such as optical drift, stray light suppression, and maintaining precise cartridge geometry. These issues become particularly critical for analytes like creatinine, where the Jaffe reaction

produces very small absorbance changes at normal physiological levels and is prone to chemical interferences, making commercial POCT creatinine meters less reliable [204–205].

Conventional double-beam spectrophotometers (Figure 1) address many of these limitations by splitting monochromatic light into reference and sample paths, allowing real-time correction for lamp instability and detector drift according to Beer–Lambert's law [206–207]. However, such instruments remain bulky and power-intensive, reinforcing the need for compact, portable POCT devices engineered for optical stability, temperature control, and consistent fluid handling. A thorough literature study reveals three major approaches in POCT biochemical detection**.** Table 6 summarizes the three dominant technological approaches used in point-of-care biochemical detection systems – paper-based microfluidics, electrochemical biosensing, and optical spectrophotometric methods. Each method is evaluated based on its inherent strengths and practical limitations when applied to decentralized diagnostic settings.

Table 6. Major Technological Approaches in POCT Biochemical Detection

Method	Benefits	Limitations
Paper-based microfluidics	Very low cost	Mostly qualitative
Electrochemical biosensing	Good sensitivity	Requires electrode stabilization
Optical POCT (spectrophotometric)	Quantitative & robust	Requires optical alignment

The **Figure 3** presents the WHO-endorsed ASSURED criteria [208], which outline the essential characteristics required for effective point-of-care diagnostic technologies. The acronym represents Affordable, Sensitive, Specific, User-friendly, Rapid and Robust, Equipment-free, and Delivered, collectively emphasizing both analytical reliability and practical usability in resource-limited settings. These seven principles highlight the need for diagnostic tools that are economically accessible, capable of accurate detection with minimal false outcomes, simple to operate with limited training, fast and stable under varying environmental conditions, independent of complex instrumentation, and easily deployable to

end users. The ASSURED framework serves as a global benchmark for evaluating and designing POCT systems, particularly for rural and decentralized healthcare environments.

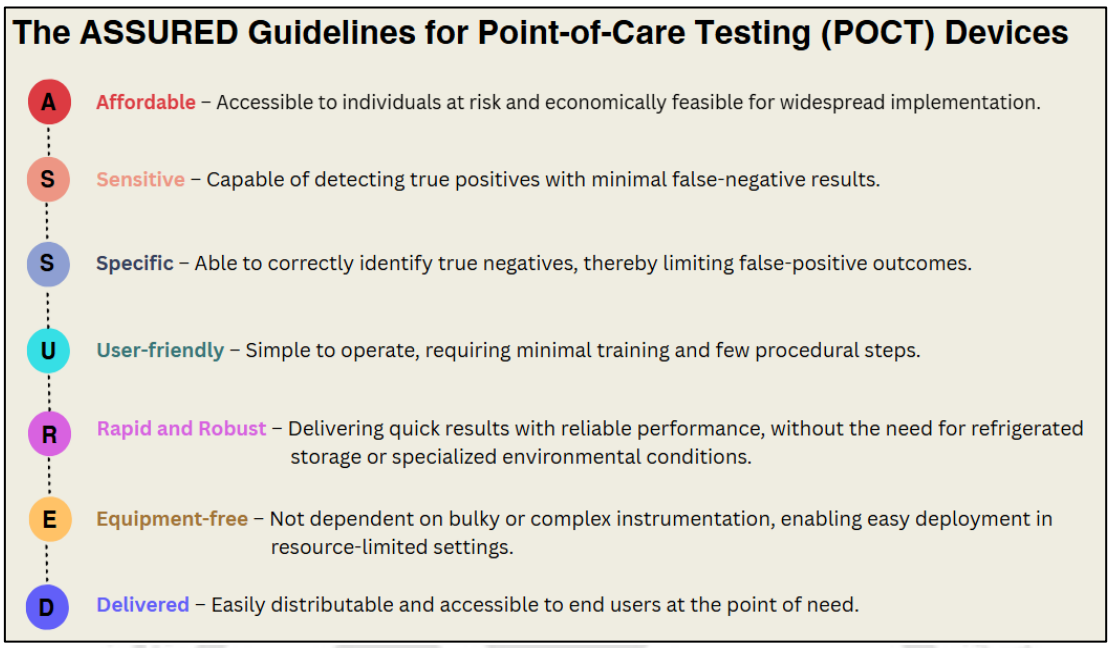

Figure 3: The WHO ASSURED Guidelines for Point-of-Care Testing (POCT) Devices

2.4.1 Field Requirement Analysis

A comprehensive field study, including interviews and contextual observations at rural healthcare facilities, revealed several critical gaps in existing diagnostic workflows. Physicians consistently expressed the need for multi-parameter biochemical testing, particularly for profiles such as the Liver Function Test (LFT) and Kidney Function Test (KFT), which are essential for early detection and monitoring of non-communicable diseases. However, most Primary Health Centres (PHCs) and Community Health Centres (CHCs) lack trained laboratory technicians capable of operating conventional semi-automated analyzers.

Moreover, the high cost of semi-auto analyzers, along with their dependence on stable electricity and maintenance-intensive components, makes them unsuitable for widespread deployment in resource-limited rural environments. Additional challenges included the absence of digital record-keeping, resulting in poor continuity of care and difficulty tracking long-term patient outcomes. Based on these field insights, an effective point-of-care diagnostic device must satisfy the following requirements:

(a) Affordable per-test cost (ideally < INR 50) to ensure accessibility in low-resource populations

(b) Battery-powered operation enabling use in remote or intermittent-power settings

(c) Programmable, allowing expansion to multiple biochemical assays

(d) Robust and simple to operate, requiring minimal operator training

(e) Digitally connected, enabling automated storage and retrieval of patient history and test records

These user-centered observations directly informed the context-driven design strategy adopted in this work, ensuring that the developed POCT system aligns with real-world needs and constraints of rural healthcare ecosystems.

2.5 Methodology

2.5.1 Conceptualization of Proof of Concept

Based on the field-driven requirements and functional specifications, the conceptualization phase involved developing a series of modular diagnostic device prototypes using fused deposition modeling (FDM). Two initial concepts were fabricated to explore the feasibility of multi-parameter POCT integration.

Figure 4: Mutli-Diagnostic device for paper-based sensors

Figure 4 illustrates the first concept, a modular platform designed for paper-based POCT sensors. This version demonstrated the potential for integrating multiple disposable test strips into a single diagnostic unit.

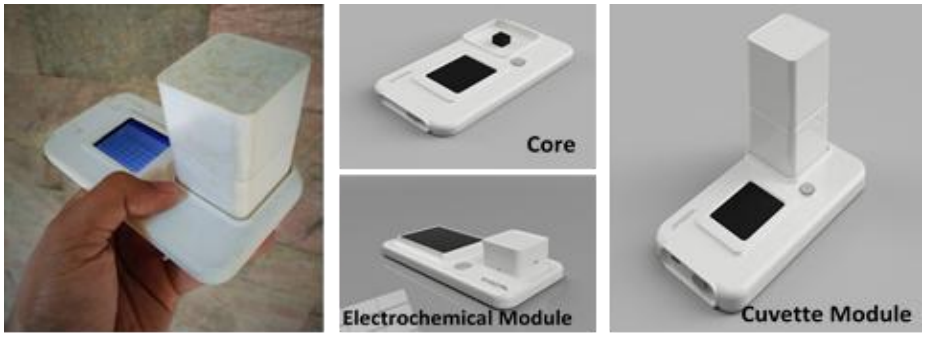

Figure 5: Representation of Analyte

Figure 5 presents Analyte, the second design iteration, which expanded the functionality to support both spectrophotometric and electrochemical analysis within a modular framework. Although this iteration successfully established the practicality of modularity, the Analyte system exhibited limitations in sensitivity, precision, and analytical accuracy, preventing it from meeting clinical-grade performance standards.

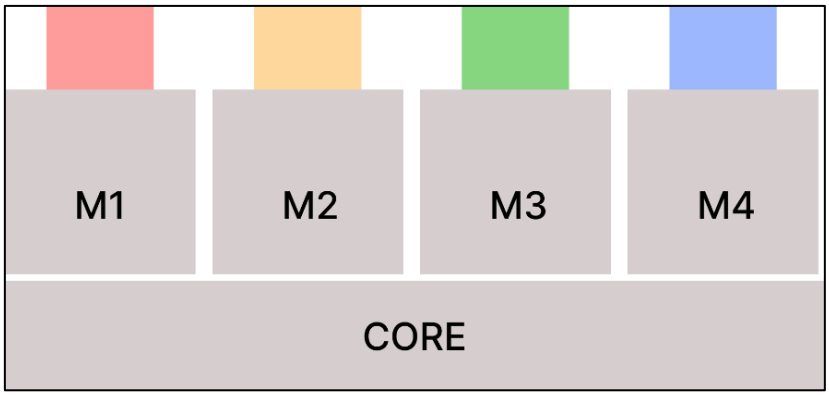

Figure 6: Schematic of a multislot multi parameter POCT device, M1, M2, M3 and M4 are the modules that consists the optical system for spectrophotometric analysis.

The third and final conceptual prototype, shown in Figure 6, represents a significant advancement in functionality. This design incorporates a multi-slot, multi-parameter POCT architecture capable of simultaneously analysing four biochemical parameters, thereby reducing the average test time to 2–3 minutes per sample. Each module operates independently while being electronically coupled to the central Core Module, which manages power, communication, and test processing. Dedicated cartridge insertion slots within each module facilitate streamlined workflow and improved usability.

(a) The development of this novel multi-parameter POCT device was structured into five major stages, as outlined below:

(b) Development of a portable optical system capable of spectrophotometric quantification of Creatinine and Glucose, with stable illumination and optimized detection pathways.

(c) Fabrication of proof-of-concept modules, followed by iterative prototype refinement to achieve acceptable levels of repeatability, sensitivity, specificity, and accuracy, benchmarked against semi-automated analyzers and established guidelines.

(d) Evaluation and validation of multiple prototype versions using standard calibration sera, followed by preliminary clinical testing to assess diagnostic performance.

(e) Establishment of communication protocols between the Core Module and individual test modules to ensure synchronized operation and data transfer.

(f) Final development, including refined prototyping, algorithm development, integrated device testing, and full-scale clinical validation of the complete multi-parameter POCT system.

This systematic, staged approach ensured that each engineering and analytical challenge was addressed progressively, resulting in a functional, modular diagnostic platform suitable for decentralized NCD screening.

2.5.2 Development of portable optical system

As a first stage of development, the focus was on determination of concentration creatinine and glucose in human blood serum, as per our prior study conducted. The goal here is to develop a portable low powered inexpensive optical system for spectrophotometric analysis in order to determine absorbance by virtue of Beer Lamberts Law. Initially the idea is to develop and validate, only one module and then couple four of them with a single core. As discussed earlier this inexpensive portable optical system for spectrophotometric analysis has

been fabricated using Fusion Deposition Modelling (FDM), that is capable of multiple analysis viz Glucose and Creatinine at this stage with possibility of Urea analysis in future.

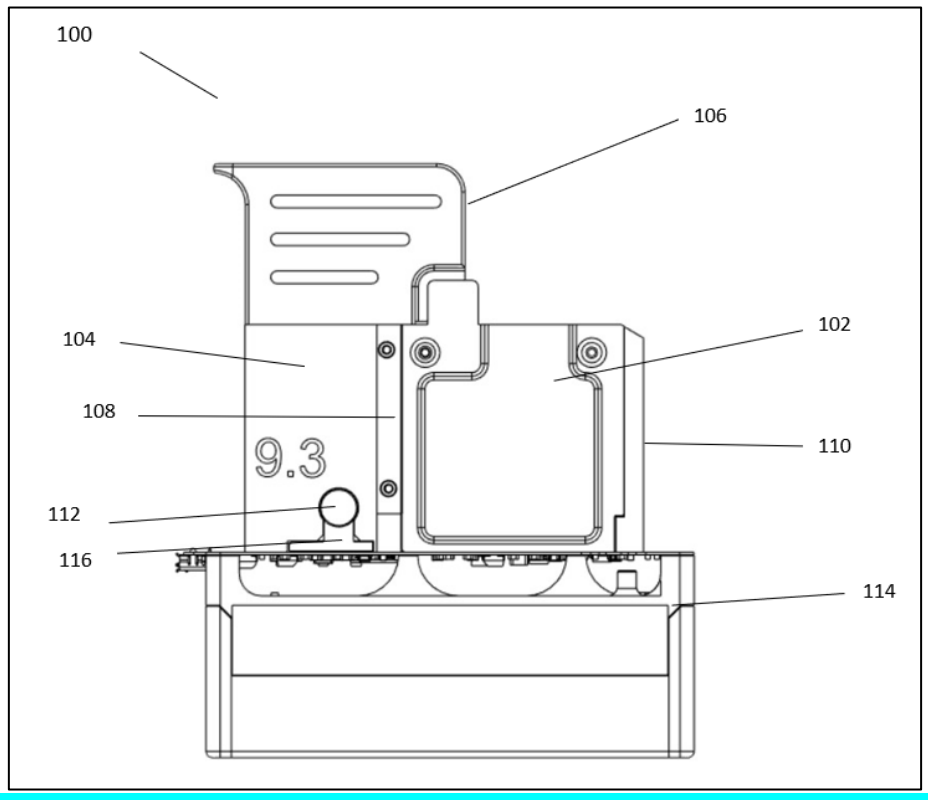

Figure 7: Engineering Design of the Portable Optical System for Spectrophotometric Analysis

Figure 7, shows engineering design of the potable optical system for spectrophotometric analysis (100). A cartridge filled with specific chemical and sample is inserted by opening the Lid (106), the source present at the front part (102) is illuminated momentarily based on a specific algorithm and the transmitted light through the cartridge is registered in the CMOS sensor present at the back (104). Both the front (102) and back part of the optical system is fastened at (108) by fastening means and is coupled with a control circuit at the bottom. Bottom unit (114) consists the Lithium-Ion batteries for back up, the control circuit further communicates with a computing device through a USB B port to any computing device that can be a PC or a Smartphone via UART protocol.

Figure 7 illustrates the schematic layout of the portable optical system designed for spectrophotometric analysis (100). A pre-filled test cartridge containing the reagent–sample mixture is inserted into the device by opening the top Lid (106). During measurement, the

optical source located at the front section of the system (102) is activated momentarily according to a programmed illumination algorithm. The transmitted light passing through the cartridge is subsequently detected by the CMOS sensor positioned at the rear side of the optical assembly (104).

The front (102) and back (104) optical modules are mechanically secured onto the central mounting frame (108) using fastening elements and are coupled to the primary control electronics situated in the lower section. The bottom unit (114) houses the Lithium-ion battery pack, providing portable power for field deployment. The control circuit interfaces with external computing devices, such as a PC or smartphone, via a USB-B port using UART communication protocol, enabling data acquisition, processing, and display.

After receiving the intensity data, the absorbance is calculated for a fixed wavelength using Beer Lamberts Law and corelated with the concentration of the biomarker under observation. But, this system had to be optimized in terms of repeatability, sensitivity and accuracy with a significant number of challenges that needs to be overcome as discussed in the next section.

2.5.3 Progress and Challenges

During the initial development phase, the emphasis was placed on quantifying serum creatinine and glucose, two clinically significant biomarkers for early detection of chronic kidney disease (CKD) and diabetes. The iterative engineering process revealed several critical challenges that shaped subsequent design decisions.

2.5.3.1 Optical System Challenges

(a) Collimation of the Light Source

One of the foremost challenges was achieving proper collimation of the illumination source. The high radiation angle of commonly available LEDs resulted in a wide beam spread, limiting the number of parallel rays reaching the CMOS detector. Controlled collimation was essential to improve signal strength and minimize optical noise.

(b) Low Analyte Concentration and High Noise

Given the physiological concentration of serum creatinine (~0.5–1.2 mg/dL), with clinically observed lower limits reaching ~0.2 mg/dL, the chromophoric compounds produced during the Jaffe reaction were minimal. Consequently, the sensor exhibited significant noise in kinetic absorbance signals, complicating detection at the lower range.

(c) 1.3 Illumination Stability

Both rising and declining illumination drift were observed from several LED sources, influenced by their electrical driving conditions. The variation was further amplified by sensor gain settings, affecting reproducibility and reducing signal fidelity.

(d) 1.4 Mechanical Alignment Constraints

Reliable spectrophotometric detection required consistent alignment between the cartridge, light source, and detector. Even slight misalignment introduced unacceptable variation in baseline readings, affecting repeatability across tests.

2.5.3.2 Temperature Sensitivity in Biochemical Reactions

The kinetic behavior of glucose (GOD-POD) and creatinine (Jaffe reaction) assays demonstrated noticeable variability due to ambient temperature fluctuations. To ensure reaction stability, maintaining the cartridge temperature at 37 °C became essential. Key temperature-related challenges included:

(a) Optical System Redesign for Incubation

An integrated incubation mechanism needed to be incorporated without compromising optical performance.

(b) Cartridge Temperature Profiling

Repeated temperature mapping was required to understand heat transfer characteristics and stabilize reagent temperature inside the slot.

(c) Development of a Low-Power Heating System

A PID-controlled heating module was required to maintain precise temperature regulation using minimal power—critical for portable and battery-operated POCT devices.

2.5.4 Methods

To systematically address the challenges identified, several experimental, mechanical, and electronic optimization strategies were implemented.

A. Optical Path and Illumination Optimization

To address collimation issues (challenge 1.1), multiple low-power LEDs with varying beam angles were evaluated. Pure optical collimation would ideally require lasers or lens arrays; however, for low-cost, field-deployable applications, a 3D-printed optical ray-guiding system was developed. This system integrated an illumination chamber, light tunnel, refractive lens, and CMOS detector.

(a) Extensive experiments were performed to optimize:

(b) Light tunnel dimensions (diameter, length)

(c) Internal wall reflectivity

(d) Source–lens–cartridge–detector alignment

(e) Minimization of stray light and internal reflections

B. Stabilization of the Illumination Source

Addressing challenge (a) and (b), experiments were designed to compare LED behaviour under constant-voltage vs. constant-current driving. Five sources were evaluated to understand intensity drift patterns. Based on observations, programmable constant-current drivers were developed to ensure illumination uniformity suitable for precise kinetic assays.

C. Integration of Incubation Mechanism

The optical system was redesigned to accommodate a compact incubation chamber. A CNC-machined aluminium heating core was fabricated to ensure uniform heat distribution. Cartridge insertion tolerances (0.10–0.30 mm) were fine-tuned to maximize thermal transfer without damaging the cartridge surface.

D. Signal Processing and Noise Reduction

For accurate measurement at low analyte concentrations, digital filtering was essential. Initially, an Exponential Moving Average (EMA) filter was applied to smooth raw kinetic curves. Polynomial regression and alternative curve-fitting models were evaluated using eight datasets spanning low and high concentration ranges to select the optimal signal-processing algorithm.

E. Temperature Regulation Using PID Control

To achieve precise incubation at 37 °C, a PID-based control strategy was implemented. Extensive experiment sets were conducted to fine-tune PID coefficients for stability and minimal overshoot. Temperature response studies involved varying the heating core from 37 °C up to 60 °C and evaluating reagent temperature transitions from ~8 °C to ~30 °C to finalize the optimal heating profile.

2.6 Results and Discussion

2.6.1 Development of the Portable Optical System

The development of the portable optical system underwent multiple design iterations to address key engineering challenges related to optical alignment, signal stability, thermal control, and repeatability of measurements. **Figure 8** presents the CAD models of various stages of optical system evolution, demonstrating the progressive refinement of geometry, component placement, and structural robustness. Each iteration was evaluated with respect to mechanical tolerances, material behavior, internal fit, and component alignment to achieve consistent optical performance with a coefficient of variation (CV) of <0.1%.

The first stage of optimization involved extensive experimentation with **3D-printed prototypes**, systematically adjusting tolerances, layer heights, and interface geometries to ensure reproducibility in base and sample readings. These refinements were essential to overcoming the reinsertion error of cuvettes, a common challenge in compact spectrophotometric systems.

Subsequent iterations focused on improvements in optical performance. This included precise alignment of the **light source, cuvette slot, and CMOS sensor**, optimization of the light path, and reduction of stray reflections. CAD-based simulations and empirical testing guided refinements in source placement, beam direction, tunnel geometry, and detector positioning.

To address temperature-dependent variability in biochemical assays—particularly for glucose and creatinine—a dedicated **ceramic metal heating core** was integrated into the system. This modification enabled maintenance of a constant incubation temperature at **37°C**, significantly improving reaction consistency. Mechanical tolerances between the cartridge, heating core, and surrounding components were adjusted (0.10–0.30 mm) to ensure efficient thermal transfer without damaging the cartridge.

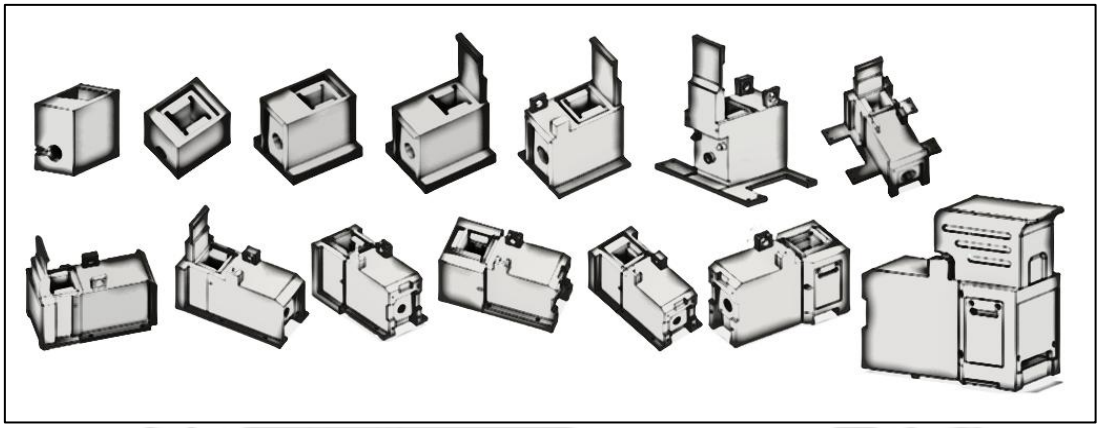

Figure 8: CAD models representing multiple design iterations of the portable optical spectrophotometric system.

Figure 8 shows the progression of CAD models representing multiple design iterations of the portable optical spectrophotometric system. Each iteration builds upon previous learnings, incorporating improvements in mechanical stability, optical alignment, lens placement, cartridge fit, and thermal integration. The iterative approach enabled systematic refinement of structural and optical performance factors critical to achieving reliable point-of-care biochemical measurements.

The development process progressed through several structured phases:

1. Optimization of Mechanical Constraints

Initial experiments focused on understanding and refining design constraints, including component tolerances, 3D printing layer height, material selection, and interface detailing. These adjustments were critical for ensuring mechanical stability and repeatable cuvette positioning. Through systematic iteration, the coefficient of variation (CV) was reduced to below 0.1%, demonstrating high reproducibility in optical measurements.

2. Optical Path Refinement and Alignment

Subsequent modifications targeted the optimization of the optical pathway. This included fine-tuning the alignment of the light source and CMOS sensor, redefining the angle of illumination, adjusting component positioning, and minimizing internal reflections. Both CAD-based optical modelling and experimental prototypes were used to arrive at the final configuration that ensured maximal transmission efficiency and signal stability.

3. Integration of Controlled Thermal Environment

Given the temperature sensitivity of enzymatic and colorimetric assays, a constant incubation temperature of **37 °C** was required for reliable biochemical reactions. A ceramic-metal heating core was designed and incorporated into the optical housing. This heater provided uniform thermal distribution, enabling rapid heat transfer to the cartridge and stabilizing reaction kinetics. Together, these iterative improvements resulted in a compact, robust, and highly stable optical module suitable for point-of-care spectrophotometric analysis.

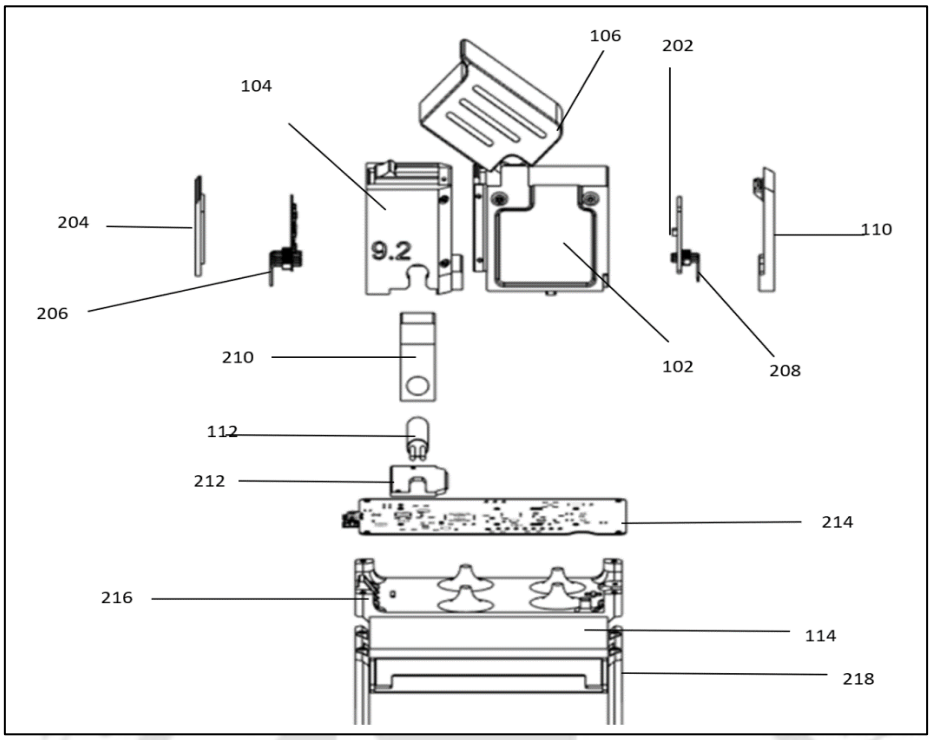

Figure 9: Exploded View of the Modified Optical System

Figure 9 illustrates the exploded view of the finalized optical system architecture. Key components include the front illumination housing (102), the rear CMOS sensor enclosure (104), the hinged lid for cartridge insertion (106), fastening elements (108), the cuvette/cartridge (210), the LED source (112), sensor mounting block (212), the heating core assembly (214), battery compartment (114), PCB support (216), and the structural base (218), The diagram highlights modularity, ease of assembly, and precise alignment of optical and thermal components.

This exploded view highlights how individual subcomponents integrate to form the complete optical system. The layout demonstrates a clean separation of the illumination path, detection unit, and control electronics. The design allows efficient assembly, maintenance, and troubleshooting, while ensuring a robust optical pathway. The placement of the heating core directly below the cartridge slot ensures uniform temperature distribution. The bottom unit houses the lithium-ion battery pack and control circuitry, enabling portable, battery-powered operation. Communication through a USB-B port (not shown) allows real-time data acquisition via PC or smartphone.

A number FDM fabrication prototypes has been developed and experimentations were carried out in order to determine the CV at various levels.

Table 7. Overview of test levels and corresponding experimental conditions used to evaluate optical system stability, repeatability, and incubation performance.

Levels	Meaning	No. of repeats	Time (min)
L1	Continuous Blank Test without incubation	5	15
L2	Continuous Water Test without incubation	5	15
L3	Reinsertion test with water	3	Not specified
L4	Reinsertion test with 4 different dye concentrations	3	Not specified
L5	Continuous Blank test with incubation	3	15
L6	Continuous Water test with incubation	3	15

Table 7 summarizes the different test levels and corresponding experimental conditions designed to evaluate the stability, repeatability, and operational robustness of the portable optical system. Each level (L1–L6) represents a specific diagnostic scenario intended to isolate and assess performance factors such as baseline drift, sensor consistency, mechanical reinsertion errors, incubation effects, and dye-based signal variability.

Levels L1 and L2 involve continuous blank and water tests without incubation, repeated five times to examine inherent optical noise, baseline stability, and the influence of repeated measurements under identical non-incubated conditions. Levels L3 and L4 introduce reinsertion-based testing—first with water and then with four different dye concentrations—to assess alignment sensitivity, mechanical reproducibility, and optical path consistency when cartridges are removed and reinserted. Levels L5 and L6 repeat the blank and water experiments under incubated conditions at 37 °C, providing insight into thermal effects on signal stability and device performance during biochemical reactions.

Table 8. Device-wise Coefficient of Variance (CV) Measurements Obtained for the Six Experimental Levels (L1: Blank, L2: Water, L3–L4: Reinsertion, L5–L6: Incubation)

Device	L1	L2	L3	L4	L5	L6

VB4GRD2	0.02	0.01	0.34	0.43	0.02	0.04
VB4GRD3	0.04	0.07	0.63	0.61	0.02	0.03
VB4GRD4	0.03	0.03	0.35	0.51	0.04	0.06
VB4GRD5	0.04	0.04	0.33	1.34	0.05	0.15
VB4GRD7	0.02	0.03	0.49	0.59	0.02	0.07
VB4GRD8	0.03	0.40	0.38	0.32	0.05	0.02
VB4GRD9	0.02	0.05	0.93	0.59	0.05	0.15
VB4GRD11	0.02	0.05	0.44	0.62	0.03	0.05
VB4GRD12	0.02	0.03	0.59	1.37	0.05	0.05
VB4GRD13	0.02	0.04	0.37	0.23	0.02	0.03
VB4GRD14	0.03	0.19	1.25	0.88	0.03	0.03
VB5GRD1	0.02	0.04	1.16	1.11	0.03	0.03
VB5GRD6	0.02	0.07	0.27	0.71	0.03	0.03
VB5GRD7	0.02	0.05	1.19	1.08	0.05	0.03
VB5GRD8	0.04	0.06	0.31	0.26	0.08	0.04
VB5GRD9	0.03	0.03	0.86	1.07	0.03	0.03
VB5GRD10	0.02	0.04	0.19	0.43	0.04	0.08
VB5GRD11	0.05	0.05	1.34	1.11	0.07	0.07
VB5GRD12	0.04	0.07	1.71	1.11	0.04	0.05

Following the execution of the six defined experimental test levels (L1–L6), multiple devices—labelled VB4GRD2 through VB5GRD12—were evaluated to quantify variability, signal response, and overall system stability. The table above presents the numerical outputs recorded for each device under each test condition.

Understanding the Meaning of Each Level

- L1 – Continuous blank test (no incubation): Assesses baseline optical noise and system drift in the absence of sample or reagent.
- L2 – Continuous water test (no incubation): Evaluates optical consistency during repeated measurements with a neutral reference fluid.
- L3 – Reinsertion test with water: Measures mechanical repeatability by analysing signal variation caused by removing and reinserting the cuvette.

- L4 – Reinsertion test with four dye concentrations: Assesses system linearity, sensitivity, and the effect of user-handling variability under colored samples.
- L5 – Continuous blank test with incubation: Determines baseline stability under controlled thermal conditions.
- L6 – Continuous water test with incubation: Evaluates combined optical and thermal stability.

Summary of Observed Trends

1. Baseline Stability (L1 and L5)

Across devices, signal values in L1 and L5 remain mostly low (0.02–0.08), indicating:

- Minimal baseline noise
- Good consistency of the optical path
- Improved stability with incubation in L5, as reflected by slightly more uniform values

This consistency is crucial for detecting low-concentration analytes such as creatinine at physiological levels.

2. Water Baseline Consistency (L2 and L6)

Values in L2 show slightly higher variability (0.03–0.40), suggesting:

- Minor differences in cuvette alignment
- Sensitivity of the optical path to small variations in refractive index or cartridge placement
- L6, with incubation, shows improved uniformity, confirming:
- Temperature regulation mitigates drift
- The heating architecture enhances repeatability

3. Reinsertion Repeatability (L3)

The L3 column displays moderate variability across devices (0.27–1.34). This reflects the mechanical sensitivity of the reinsertion process, indicating:

- Small angular or lateral misalignments introduce measurable deviations
- The optical system is highly responsive to positional accuracy

This reinforces the importance of:

- Tight tolerance control
- Well-defined cuvette seating geometry
- Minimizing user-dependent variation

4. Dye Concentration Sensitivity (L4)

Values in L4 show the largest spread (0.23–1.37), representing:

- Strong responsiveness to different dye concentrations
- Higher absorbance values due to colored solutions
- Expected variability due to reinsertion plus concentration differences

This level is crucial because it demonstrates:

- The system can successfully detect changes corresponding to analyte concentration
- Linear response behaviour is observable in most units
- A few outliers indicate the need for enhanced stray-light suppression or video-signal smoothing

5. Impact of Thermal Control (L5 and L6)

The relatively consistent output values in L5 and L6 confirm that:

- PID-controlled heating stabilizes reaction conditions
- Temperature uniformity reduces optical noise
- Incubated measurements are more repeatable

This supports the design decision to integrate a ceramic heating core for assays requiring 37 °C.

In summary, the dataset demonstrates that: Blank and water tests (L1, L2, L5, L6) show low variation, confirming baseline optical stability. Reinsertion tests (L3, L4) reveal sensitivity to mechanical handling, emphasizing the need for precise fixture design. Dye tests

(L4) validate the system's ability to differentiate concentration-dependent absorbance levels, a key requirement for spectrophotometric biochemical assays. Temperature-controlled tests (L5, L6) highlight improved reproducibility, supporting the integration of thermal regulation in the final device architecture. These observations collectively validate the iterative improvements made in the optical, mechanical, and thermal subsystems of the portable spectrophotometric POCT device.

2.6.2 Stability of the Illumination Source

During the initial blank testing of the optical system—performed without inserting any cartridge—significant instability was observed in the illumination source. These instabilities manifested as sudden fluctuations, as well as gradual elevations or degradations in light intensity over time. Such variations directly affected the transmitted-light signal captured by the CMOS sensor, introducing noise that compromised the accuracy and repeatability of spectrophotometric measurements.

To systematically investigate the root cause of this instability, two controlled experiments were conducted:

(a) Constant Voltage Operation

(b) Constant Current Operation (via Source Control Circuit, SCC)

Two different light sources (Source A and Source B) were evaluated under both electrical driving conditions.

Figure 10 presents the comparative signal plots from these experiments. The graphs clearly demonstrate that constant-voltage operation produced large oscillations and transient spikes, resulting in a high coefficient of variation (CV). In contrast, constant-current operation markedly reduced intensity drift and noise, thereby stabilizing the baseline and improving the CV values significantly.

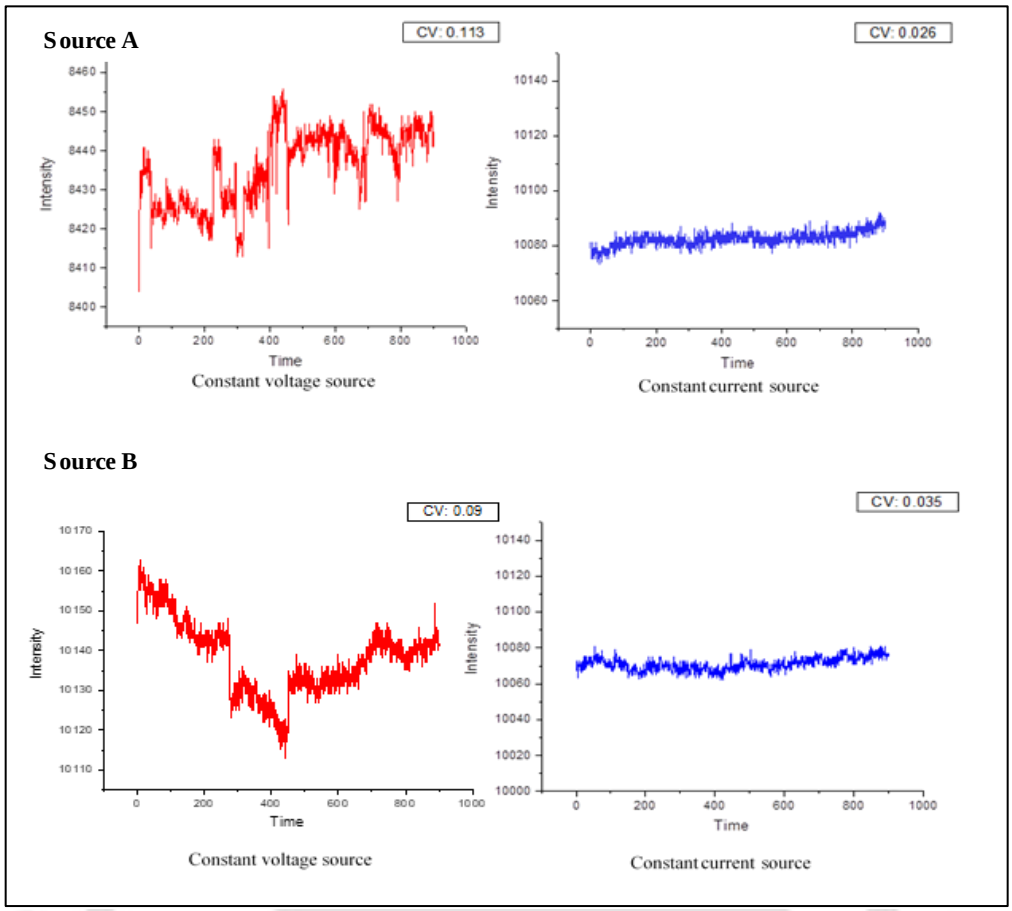

Figure 10: Stability Analysis of Illumination Sources Under Constant Voltage and Constant Current Operation

This comparative study confirms that illumination stability is critically dependent on current regulation. The findings strongly justify the implementation of a Source Control Circuit (SCC) in the final optical module to ensure consistent illumination, minimize noise propagation into reaction kinetics data, and enhance analytical accuracy—particularly important when measuring low-concentration analytes such as creatinine in the physiological range. Figure 11 illustrates the block diagram of the closed-loop analog–digital control system designed to regulate the illumination source used in the spectrophotometric POCT device. The system operates by allowing the microcontroller to send a predefined control signal to the Source Control Circuit (SCC), which functions as a constant-current driver for the illumination source. By maintaining a stable current, the SCC ensures that the LED emits light at a consistent and precise intensity, minimizing fluctuations that could otherwise introduce

noise into the optical measurement. The emitted light passes through the test cartridge, and the transmitted light is detected by the sensor.

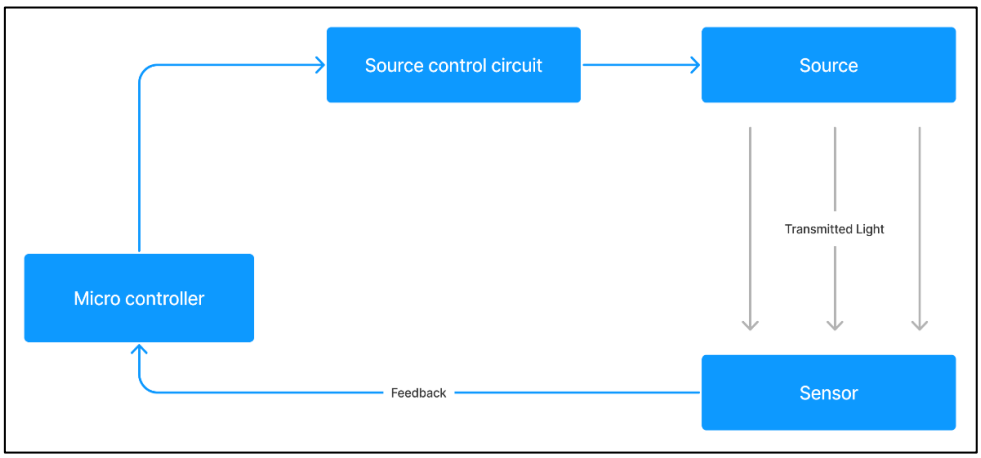

Figure 11: Closed-Loop Source Control Architecture for Illumination Stability

The sensor output is then fed back to the microcontroller, enabling continuous monitoring of illumination stability. Based on this feedback loop, the microcontroller dynamically adjusts the SCC's control signal to compensate for variations due to temperature changes, source aging, or external disturbances.

This closed-loop regulation is essential for achieving high measurement accuracy, especially when detecting low-absorbance biochemical reactions such as the Jaffe method for creatinine. By ensuring tightly controlled illumination, the system significantly improves signal reliability, repeatability, and overall analytical performance.

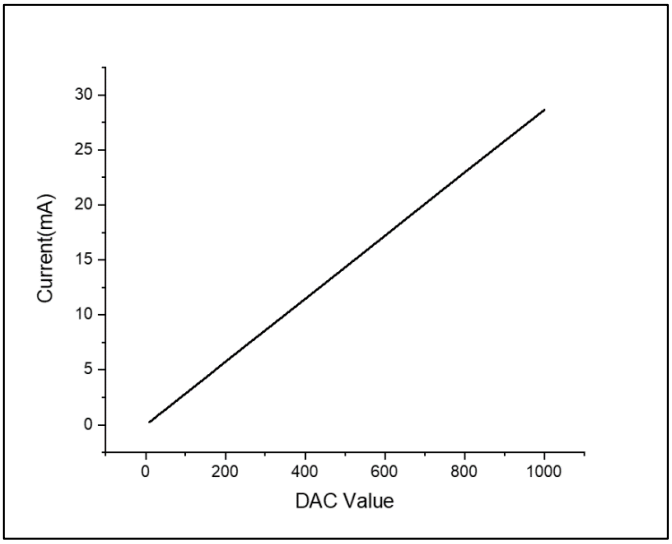

Figure 12: Linearity Plot Between DAC Input Value and Output Drive Current

Figure 12 illustrates the linear relationship between the digital input value supplied to the DAC (Digital-to-Analog Converter) and the corresponding output current delivered by the source control circuit. The measured current values were obtained using a 6½-digit precision digital multimeter, ensuring high-resolution and low-noise characterization of the circuit response. The plot demonstrates excellent linearity across the full input range (0–1023 DAC units), indicating that the current driver accurately translates digital control signals into stable, predictable output currents. This linear behavior is essential for regulating LED intensity in the optical system, allowing fine-tuned illumination control for spectrophotometric measurements.

The strong proportionality between DAC input and output current further validates the effectiveness of the constant-current design used in the Source Control Circuit (SCC), ensuring reproducible illumination conditions critical for minimizing variability in absorbance readings. Table 9 presents the repeatability data for five different DAC input values (200, 400, 600, 800, and 1000 units) and their corresponding output currents, measured over five repeated trials for each input level. The measurements were obtained using a high-precision 6½-digit digital multimeter to ensure reliable characterization of the current source performance.

Table 9. Repeatability Analysis of Source Control Circuit: Output Current Stability Across Multiple Input Values

Repeat 1			**Repeat 2**		
Input Value	**Test**	**Current(mA)**	**Input Value**	**Test**	**Current(mA)**
200	**Test 1**	**5.73**	**400**	**Test 1**	**11.45**
	Test 2	5.73		Test 2	11.45
	Test 3	5.73		Test 3	11.45
	Test 4	5.73		Test 4	11.45
	Test 5	5.73		Test 5	11.45
SD		**0.001**	SD		**0.001**
CV		**0.031**	CV		**0.014**
Repeat 3			**Repeat 4**		
Input Value	**Test**	**Current(mA)**	**Input Value**	**Test**	**Current(mA)**
600	Test 1	17.19	**800**	Test 1	22.95
	Test 2	17.19		Test 2	22.95
	Test 3	17.19		Test 3	22.95
	Test 4	17.19		Test 4	22.95
	Test 5	17.19		Test 5	22.95
SD		**0.003**	SD		**0.002**
CV		**0.019**	CV		**0.012**
Repeat 5					
Input Value	**Test**	**Current(mA)**			
600	Test 1	17.19			
	Test 2	17.19			
	Test 3	17.19			
	Test 4	17.19			
	Test 5	17.19			
SD		**0.003**			
CV		**0.019**			

Across all input levels, the coefficient of variation (CV) for the output current remains exceptionally low—typically below 0.020%—demonstrating excellent stability and

reproducibility of the Source Control Circuit (SCC). This high degree of consistency indicates that the SCC reliably regulates current with minimal drift or fluctuation, which is critical for maintaining uniform illumination intensity in the spectrophotometric optical system. Such stability directly contributes to reducing noise in absorbance measurements and improving analytical accuracy in POCT applications.

2.6.3 Incubation and Temperature Control

The third phase of system development focused on integrating a reliable incubation mechanism into the optical detection module. During preliminary experiments, it was observed that the calculated concentration of analytes—particularly creatinine and glucose—varied significantly with changes in ambient temperature. This temperature dependency led to noticeable fluctuations in accuracy during long-term, inter-day testing.

Further analysis of reaction kinetics revealed that the enzymatic and colorimetric reactions occurring within the cuvette were highly sensitive to temperature variations inside the optical chamber. Even small deviations from the optimal reaction temperature resulted in altered absorbance rates, thereby impacting the calculated concentration. Such sensitivity necessitated the incorporation of an in-built incubation system capable of maintaining a constant temperature of 37 °C**,** ensuring consistent reaction conditions across tests.

To determine the heating efficiency and establish an appropriate temperature control profile, a series of reagent temperature studies were conducted. Reagents R1–R4 were evaluated across a broad range of initial temperatures (approximately 8–30 °C). The rise in reagent temperature after 2 minutes, the stabilized reagent temperature at a heating core set to 37 °C, and the maximum temperature attained were recorded. Results demonstrated that even when reagents began at low temperatures (8–10 °C), they approached near-physiological temperatures (~35–36 °C) within 2 minutes and achieved the target incubation range (~36–38 °C) once equilibrated with the metal heating core. These findings underscore the necessity

of integrating PID-controlled heating in the cartridge slot to ensure thermal uniformity and reaction repeatability, especially under variable field conditions.

Table 10. Temperature Study of Reagents Across Low, Medium, and High Initial Temperatures

Reagent	Initial Temp. (Reagent) (in °C)	Reagent Temp after 2 mins (in °C)	Reagent Temp (Metal Temp:37) (in °C)	Maximum Reagent Temp (in °C)
R1	10.0	31.6	36.0	-
	21.5	35.5	37.0	-
	29.0	37.3	38.6	39.0
R2	10.0	31.8	36.3	-
	21.3	35.1	37.8	-
	29.1	37.7	39	39.2
R3	8.1	31.2	35.6	-
	22	35.5	38.1	-
	29	37.8	39.2	39.3
R4	9.4	32.4	36.3	-
	22.1	35.1	37.7	-
	28.9	37.9	38.9	39.1

Table 10 presents the temperature response of four reagents (R1–R4) evaluated across different initial temperature conditions (8–30 °C). For each reagent, the temperature was recorded: (i) at the starting condition, (ii) after two minutes of heating, (iii) upon equilibration with the metal heating core set to 37 °C, and (iv) at the maximum temperature attained during the heating cycle.

This temperature characterization clearly indicates that all reagents rapidly approach the desired incubation temperature, demonstrating the efficiency of the heating system. Even at low initial temperatures, the heating mechanism elevates the reagent to ~31–32 °C within two minutes and subsequently stabilizes near the physiological reaction temperature. This confirms that the integrated incubation system can effectively compensate for environmental

temperature fluctuations, thereby enabling accurate and repeatable biochemical measurements in point-of-care settings.

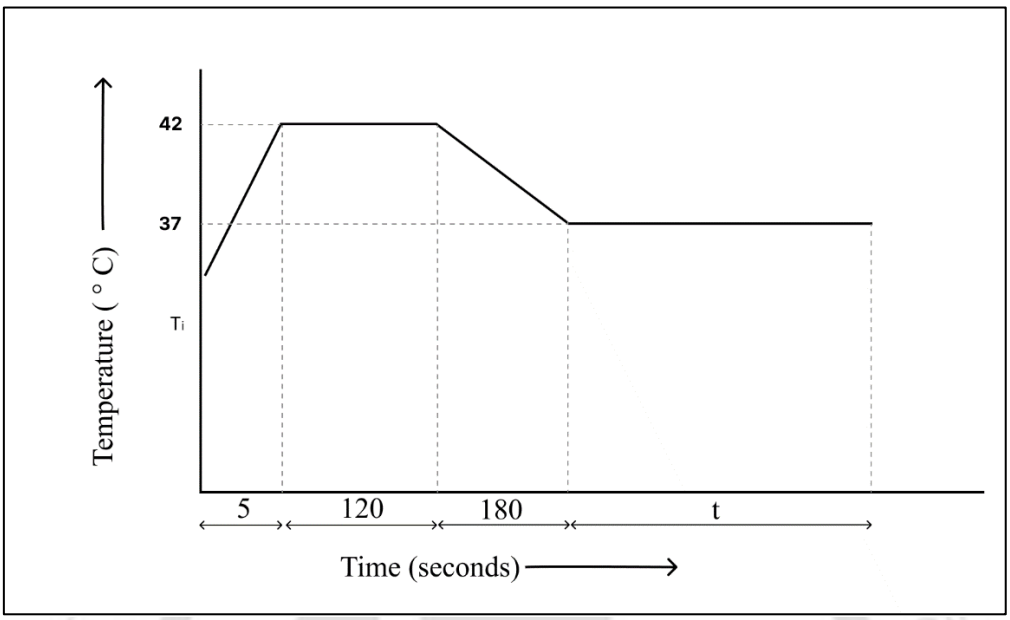

Figure 13: Finalised temperature profile T1 used for controlled reagent incubation.

The Figure 13 illustrates the finalized temperature control profile (T1) developed for the integrated incubation system within the optical module. The profile begins with a rapid ramp from ambient temperature to ~42 °C within approximately 5 seconds, followed by a short high-temperature hold to accelerate thermal equilibration of the reagent. After this stabilization phase, the temperature is gradually reduced to 37 °C by ~180 seconds and maintained for the remainder of the reaction cycle. This structured heating profile ensures that reagents of varying initial temperatures rapidly approach the optimal reaction temperature while minimizing overshoot and thermal instability.

This Figure 14 presents the empirically measured temperature response inside the optical heating chamber when executing the programmed T1 temperature profile. The red trace shows the real-time reagent metal-contact temperature, while the black line represents the theoretical programmed profile. The results demonstrate close alignment during the initial high-temperature stabilization period, followed by a controlled cooling phase that settles near 37 °C. Minor fluctuations reflect realistic thermal inertia and heat transfer dynamics between the

metal core and the reagent-filled cartridge. Overall, the actual profile confirms effective PID-based temperature regulation with sufficient accuracy for temperature-sensitive biochemical assays.

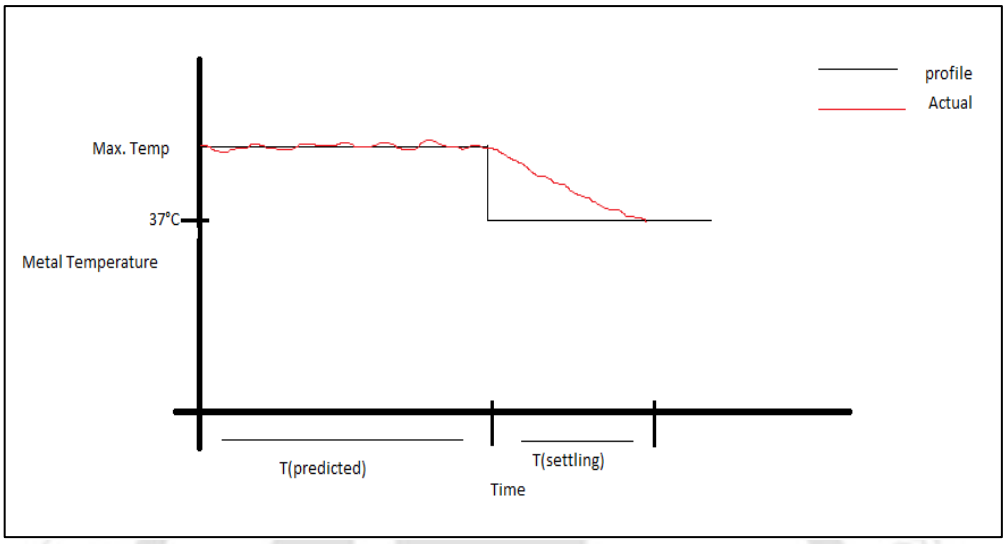

Figure 14: Actual temperature profile obtained after implementing temperature profile T1 in the device.

Table 11. Measured values, CV, and error percentage for 2 mg/dL creatinine samples tested without incubation

2mg/dl Creatinine_ without incubation				
Test	T6, T12		T9, T15	
	RM	Normal 1	RM	Normal 2
0	2.27	2.27	2.33	2.33
1	2.37	2.37	2.37	2.37
2	2.38	2.38	2.48	2.48
3	2.34	2.34	2.42	2.42
4	2.37	2.37	2.38	2.38
5	2.36	2.36	2.41	2.41
6	2.29	2.29	2.38	2.38
7	2.43	2.43	2.39	2.39
8	2.40	2.40	2.37	2.37
mean	2.37	2.37	2.39	2.39
Error %	**18.98**	**18.98**	**19.62**	**19.62**

Table 11 presents the raw absorbance-derived creatinine readings for eight consecutive tests performed at a target concentration of 2 mg/dL using two reagent modes (T6_T12 and T9_T15) under non-incubated conditions. Both reagent modes were tested in duplicate (RM and Normal). The results show substantial variability across runs, with the mean values deviating significantly from the expected concentration. The calculated error percentage for all four conditions is approximately 19%, indicating a high level of temperature-induced analytical inconsistency. This table highlights the strong dependence of the Jaffe reaction kinetics on temperature and demonstrates the limitations of performing creatinine estimation without incubation in a portable POCT system.

Table 12. Measured values, CV, and error percentage for 2 mg/dL creatinine samples tested with incubation.

2mg/dl Creatinine_ with incubation				
Test	T6, T12		T9, T15	
	RM	Normal 1	RM	Normal 2
0	1.94	1.94	1.98	1.98
1	1.95	1.95	1.98	1.98
2	1.95	1.95	1.96	1.96
3	1.92	1.92	1.93	1.93
4	1.89	1.89	1.86	1.86
5	2.04	2.04	2.04	2.04
6	2.02	2.02	2.02	2.02
7	2.01	2.01	2.03	2.03
8	1.96	1.96	1.94	1.94
mean	1.97	1.97	1.97	1.97
Error%	**1.47**	**1.47**	**1.16**	**1.16**

Table 12 summarizes the creatinine readings obtained from eight consecutive tests at the same target concentration of 2 mg/dL, performed using the optimized incubation profile (T1) integrated into the optical system. Both reagent modes (T6_T12 and T9_T15) show highly

consistent values across the RM and Normal conditions. The mean values closely match the expected concentration, and the calculated error percentages drop dramatically to approximately 1.47% and 1.16%, respectively. This table clearly demonstrates the effectiveness of controlled incubation in stabilizing reaction kinetics, reducing analytical variability, and improving assay accuracy. The results confirm that temperature regulation is essential for reliable spectrophotometric creatinine measurement in point-of-care settings.

2.7 Conclusions

In this work, a novel, low-cost, portable, and modular spectrophotometric point-of-care testing (POCT) device was conceptualized, engineered, and experimentally validated for multi-parameter biochemical analysis. The developed architecture integrates four independent optical modules connected to a central core, enabling simultaneous or sequential testing with a total assay time of under 15 minutes. Each module incorporates a compact, solid-state spectrophotometric system with no moving parts, ensuring mechanical robustness and suitability for field deployment.

Core engineering challenges—including optical alignment, illumination drift, reinsertion variability, and temperature-dependent reaction kinetics—were systematically investigated and resolved through more than 200 CAD iterations and 50 optical prototypes. Implementation of a closed-loop, constant-current source control circuit reduced blank and water CV values to <0.1%, confirming excellent illumination stability. Similarly, integration of a CNC-machined heating core with PID temperature control enabled highly reproducible incubation at 37 °C. The finalized predictive temperature profile (T1) demonstrated consistent reagent heating from a wide range of initial temperatures (8–30 °C), with overall thermal CV values <0.8%.

The impact of incubation on biochemical performance was validated using 2 mg/dL creatinine assays. Without incubation, measurements exhibited substantial variability with an average error of ~19%. When performed with the optimized heating profile, the error

decreased dramatically to ~1.5%, demonstrating more than a twelve-fold improvement in analytical accuracy. These results confirm that precise illumination regulation, optical alignment, and thermal stabilization are critical to enabling laboratory-comparable quantitative analysis in portable POCT systems.

The complete device is low-power, battery-operated, smartphone-connected, and cloud-enabled, allowing seamless data recording, remote monitoring, and digital health integration. More than 20 standardized prototypes are currently undergoing extended validation for creatinine and glucose analysis, establishing a strong foundation for scalable multi-parameter POCT diagnostics aimed at decentralized healthcare environments. Although the present study primarily focuses on maintaining stable incubation at 37°C for enzymatic biochemical reactions, operation under high ambient temperatures in rural settings may introduce challenges related to reagent stability, enzyme degradation, and thermal drift. Therefore, future versions of the developed POCT platform may incorporate active cooling mechanisms, thermal insulation strategies, or adaptive temperature control systems to improve performance under extreme environmental conditions.

CHAPTER 3

CLINICAL EVALUATION OF HEART AND KIDNEY PROFILES

Abstract

Non-communicable diseases pose a serious threat to the world population. In this direction, point-of-care testing (POCT) devices can expedite the delivery of rapid and timely results, offering a clinically significant advantage in patient management even at low resource settings. To address these issues, this study has been performed to make a comparison between a portable blood testing analyzer device named "Mobilab" as a POCT device with a clinical laboratory fully automated analyzer (Siemens Dimension EXL 200) to evaluate the device performance. Mobilab is a portable, Internet of Things (IoT) enabled, battery operated, and smartphone-app-operated device that provides digital patient data in real-time at an affordable cost. Present study evaluated the efficacy of Mobilab by analyzing five biochemical parameters, viz., Cholesterol (CHOL), Triglyceride (TGL), Low-Density Lipoprotein-Cholesterol (LDL-C), Creatinine (CRE), and Uric acid (UA), as crucial parameters that are indicative of normal functionality in healthy individuals. Validation of Mobilab was performed by comparing results from 50-52 human serum samples assessing analytical sensitivity, linearity, precision, and performance matrices. In terms of statistical analysis, all the tested parameters showed consistency and accuracy, indicating reliable and consistent performance by Mobilab. As a POCT device, Mobilab delivers digital, rapid, and direct results from patient' blood sample, eliminating the need for manual result analysis. Utilizing Mobilab to monitor health parameters could promote a healthy lifestyle with cost-effectiveness and time efficiency, potentially preventing the development of critical health conditions in resource-constrained areas of both developed and developing countries.

This chapter is submitted in ***IEEE Sensors Journal,*** 2025 (Under review)

3.1 Introduction

The healthcare delivery system constitutes an extensive network of institutions responsible for providing diagnostic, therapeutic, and preventive services to diverse populations across urban and rural settings. In low- and middle-income countries (LMICs), Primary Healthcare Centres (PHCs) function as the backbone of this system, serving as the first point of contact for early disease detection, routine diagnostics, and long-term management of chronic illnesses [209]. Their decentralized nature makes PHCs pivotal for improving public health coverage, reducing disease burden, and lowering overall healthcare expenditure by ensuring that individuals receive timely and appropriate care close to their communities [210, 211].

Despite their critical role, PHCs frequently operate under significant infrastructural and resource constraints. Limited diagnostic equipment, inadequate laboratory infrastructure, shortage of trained personnel, and inconsistent electricity supply hinder their ability to provide accurate and timely biochemical testing [212]. Traditional high-throughput analyzers used in tertiary hospitals, while highly reliable, require stable power, substantial sample volumes, regular calibration, and skilled technicians for operation and maintenance. These factors contribute to increased diagnostic costs and make the deployment of such analyzers across PHCs logistically and economically challenging [213].

To bridge this gap, Point-of-Care Testing (POCT) has emerged as an effective and scalable solution for decentralized diagnostics. POCT devices enable rapid acquisition of clinically actionable information at or near the patient site, significantly reducing result turnaround time and improving clinical decision-making in acute and chronic conditions [214]. When deployed in remote and resource-constrained areas (RCAs), POCT enables frequent monitoring of biochemical parameters, early detection of disease progression, and improved continuity of care, particularly for the rising burden of non-communicable diseases (NCDs) [216, 217].

However, currently available POCT devices often fall short of meeting field requirements. Many instruments are limited to single-parameter testing, require manual intervention by trained operators, and lack integration with digital health systems for storing and transmitting electronic medical records [218]. These limitations restrict their utility in PHCs, where multi-parameter testing, automated workflows, and digital record management are essential for longitudinal patient follow-up.

Mobilab, a portable, battery-operated spectrophotometric analyzer, has been developed to address these unmet needs. Designed to function seamlessly with a smartphone-based Android application, Mobilab facilitates automated data acquisition, analysis, report generation, and cloud-based transmission to remote clinicians or laboratory experts. Its modular architecture supports the quantification of multiple serum biomarkers with minimal maintenance, low sample volume, and substantially reduced turnaround time compared with conventional laboratory analyzers. These features make Mobilab particularly suited for deployment in rural PHCs and other RCAs where reliability, portability, and operational simplicity are essential. The portable optical system developed in Chapter 2 formed the analytical core of the Mobilab POCT platform evaluated in Chapter 3. The optimized optical, thermal, and mechanical modules were integrated with sample handling, digital connectivity, cloud reporting, and user-interface components to create a clinically deployable multi-parameter point-of-care diagnostic system.

This study evaluates the analytical performance of Mobilab by focusing on five key biochemical markers widely used in routine diagnostics and early detection of NCDs. Serum creatinine (CRE) and uric acid (UA) serve as crucial indicators of kidney function, reflecting glomerular filtration efficacy and renal metabolic processes [219, 220, 221]. Dyslipidemia-related markers—total cholesterol (CHOL), triglycerides (TGL), and low-density lipoprotein cholesterol (LDL-C)—are essential for assessing cardiovascular risk, with elevated levels

strongly associated with atherosclerosis, coronary artery disease, and stroke [222, 223, 224, 225]. Early and accurate quantification of these parameters can substantially reduce morbidity and mortality associated with chronic kidney disease (CKD) and cardiovascular disorders. To determine clinical reliability, results obtained from Mobilab were compared against a gold-standard, fully automated analyzer, Siemens Dimension EXL™ 200, -across all selected parameters. This comparative assessment serves as an important validation step in establishing Mobilab as a robust, field-deployable diagnostic solution capable of strengthening PHC capabilities and contributing to improved NCD management in underserved regions.

Cholesterol (Heart profile):

Total cholesterol is a major lipid component of blood and cell membranes and plays an essential role in membrane integrity, bile acid synthesis, and steroid hormone production. It circulates in the bloodstream bound to lipoproteins and is a key biomarker in the assessment of cardiovascular health. Clinically, elevated total cholesterol levels are strongly associated with atherosclerosis and an increased risk of coronary artery disease.

Total cholesterol estimation is commonly performed using the CHOD–PAP (Cholesterol Oxidase–Phenol Aminophenazone) enzymatic method. In this assay, cholesterol esters present in the sample are first hydrolyzed by cholesterol esterase to free cholesterol and fatty acids. The liberated cholesterol is then oxidized by cholesterol oxidase in the presence of oxygen to form 4-cholesten-3-one and hydrogen peroxide (H_2O_2). In the final chromogenic step, hydrogen peroxide reacts with phenol and 4-aminoantipyrine in the presence of peroxidase to form a red-colored quinoneimine complex. The intensity of the color produced is directly proportional to the total cholesterol concentration and is measured spectrophotometrically.

Physiologically, cholesterol is synthesized primarily in the liver and obtained from dietary sources, with circulating levels regulated by hepatic metabolism and lipoprotein transport. Elevated cholesterol levels are associated with dyslipidaemia, obesity, diabetes mellitus, and

cardiovascular disease, whereas abnormally low levels may be observed in malnutrition or chronic liver disorders. Due to its specificity, reproducibility, and compatibility with automated and point-of-care platforms, the CHOD–PAP method is widely used for routine clinical and decentralized cholesterol testing.

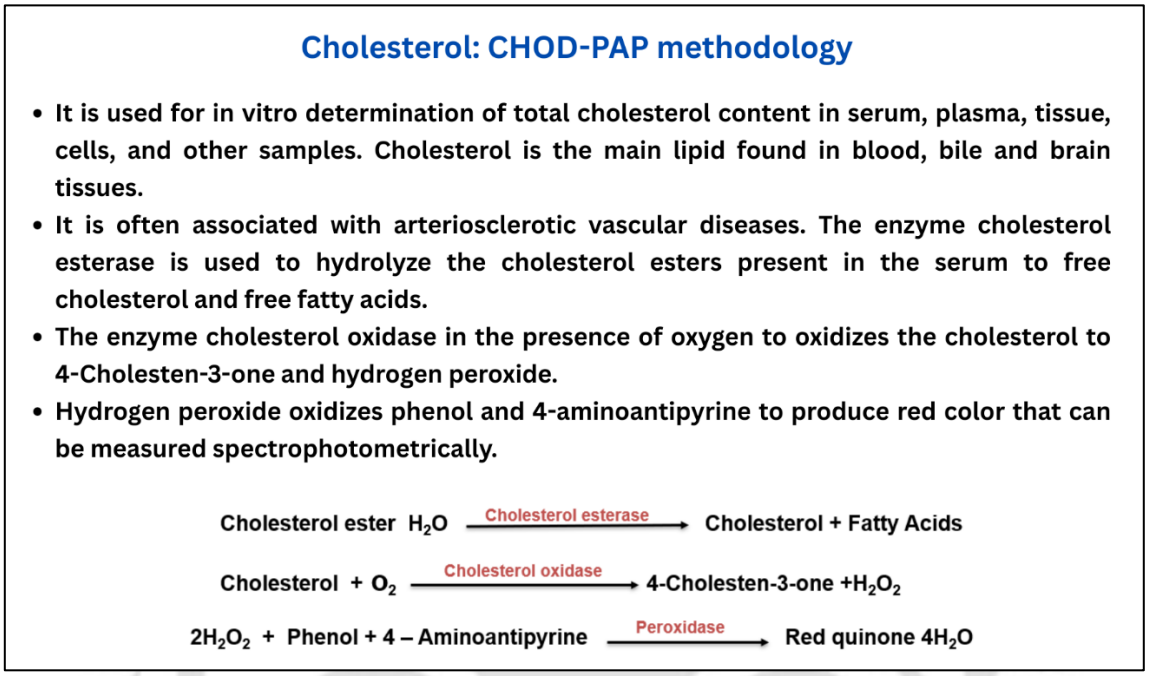

Figure 15: Total cholesterol estimation by the CHOD–PAP enzymatic method. The figure illustrates the enzymatic sequence used for in-vitro determination of total cholesterol in serum or plasma. Cholesterol esters are hydrolyzed by cholesterol esterase to free cholesterol, which is subsequently oxidized by cholesterol oxidase to form 4-cholesten-3-one and hydrogen peroxide. The generated hydrogen peroxide participates in a peroxidase-catalyzed chromogenic reaction to produce a red quinoneimine dye measured spectrophotometrically.

Figure 15 shows the CHOD–PAP method, total cholesterol is enzymatically converted to hydrogen peroxide, which reacts with phenol and 4-aminoantipyrine in the presence of peroxidase to form a colored complex. The color intensity is directly proportional to the cholesterol concentration in the sample.

Triglycerides (Heart profile)

Triglycerides (TGs) are a key component of the lipid profile and an important biomarker for assessing metabolic status and cardiovascular risk. Structurally, they are esters of glycerol and

three fatty acids and serve as the primary energy storage form in adipose tissue. Clinically, serum triglyceride levels reflect lipid metabolism and are routinely evaluated in the diagnosis and management of cardiometabolic disorders.

Triglyceride estimation is commonly performed using the GPO–PAP (Glycerol-3-Phosphate Oxidase–Phenol Aminophenazone) enzymatic method. In this method, serum triglycerides are hydrolyzed by lipoprotein lipase (LPL) to glycerol and free fatty acids. Glycerol is phosphorylated by glycerol kinase (GK) to glycerol-3-phosphate, which is subsequently oxidized by glycerol-3-phosphate oxidase (GPO) to produce dihydroxyacetone phosphate and hydrogen peroxide (H_2O_2). In the final chromogenic step, H_2O_2 reacts with 4-aminoantipyrine and TOOS in the presence of peroxidase (POD) to form a stable violet-colored quinoneimine complex. The color intensity is directly proportional to the triglyceride concentration and is measured spectrophotometrically.

Physiologically, triglycerides are synthesized in the liver and intestine and circulate in the blood mainly as chylomicrons and very low-density lipoproteins (VLDL). Elevated triglyceride levels are strongly associated with obesity, type 2 diabetes mellitus, metabolic syndrome, and cardiovascular disease, while very low levels may indicate malnutrition or impaired fat absorption.

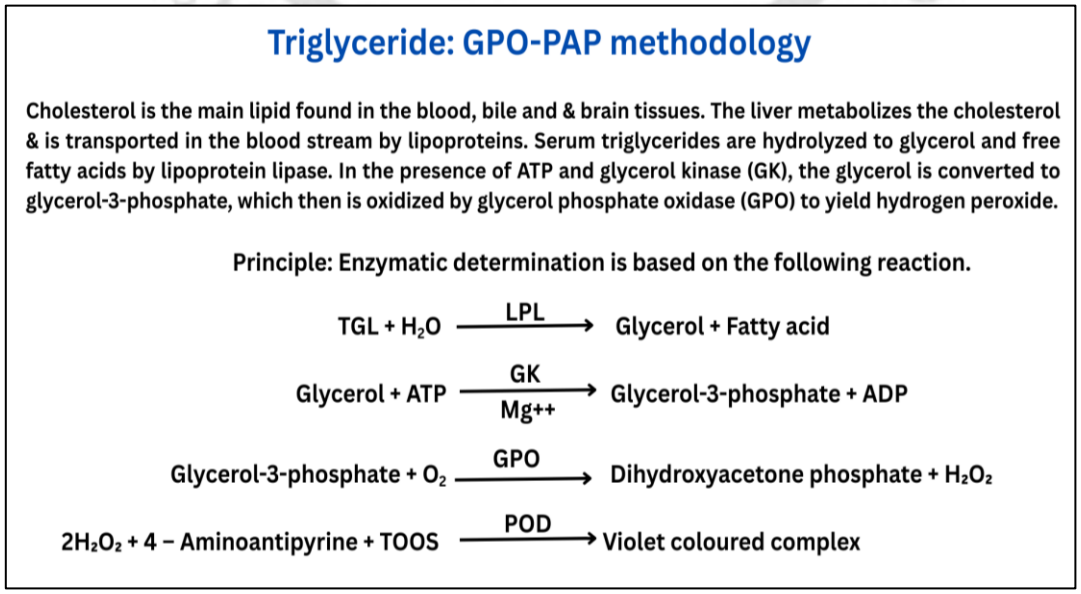

Figure 16: Triglyceride estimation by GPO–PAP method. The figure illustrates the enzymatic cascade used for serum triglyceride measurement, where triglycerides are hydrolyzed to glycerol and fatty acids by lipoprotein lipase, followed by sequential reactions involving glycerol kinase, glycerol phosphate oxidase, and peroxidase to form a violet-colored complex measured photometrically. (*The method and data optimization for the triglyceride parameter were adopted from the PhD thesis study of Sahil Jagnani).*

In Figure 16 shows the GPO–PAP method, triglycerides are enzymatically converted to hydrogen peroxide, which reacts with chromogenic substrates to produce a violet color. The color intensity is directly proportional to the triglyceride concentration in the sample.

Low-Density Lipoprotein Cholesterol (LDL-C) (Heart profile):

Low-density lipoprotein cholesterol (LDL-C) is a major component of the lipid profile and a critical biomarker for assessing cardiovascular risk. LDL particles are rich in cholesterol esters and contain apolipoprotein B-100, which facilitates the transport of cholesterol from the liver to peripheral tissues for membrane synthesis and hormone production. Clinically, LDL-C levels reflect cholesterol homeostasis and are widely used in the diagnosis, risk stratification, and management of atherosclerotic cardiovascular disease.

LDL-cholesterol estimation is commonly performed using a direct enzymatic method that selectively measures LDL-associated cholesterol without the need for prior lipoprotein separation. In this method, non-LDL lipoproteins such as HDL, VLDL, and chylomicrons are masked or solubilized using specific surfactants. Cholesterol esters present in LDL are hydrolyzed by cholesterol esterase to free cholesterol and fatty acids. The liberated cholesterol is then oxidized by cholesterol oxidase to cholest-4-en-3-one with the generation of hydrogen peroxide (H_2O_2). In the final chromogenic reaction, H_2O_2 reacts with 4-aminoantipyrine and a phenolic compound in the presence of peroxidase to form a colored quinoneimine complex. The intensity of the color produced is directly proportional to the LDL-cholesterol concentration and is measured spectrophotometrically.

Physiologically, LDL is formed from the metabolic conversion of very low-density lipoproteins (VLDL) in the circulation. Elevated LDL-cholesterol levels promote cholesterol deposition in arterial walls, leading to plaque formation, atherosclerosis, and an increased risk of coronary artery disease and stroke. Conversely, lower LDL-C levels are associated with reduced cardiovascular risk, making LDL-cholesterol a primary target in lipid-lowering therapy and preventive cardiology.

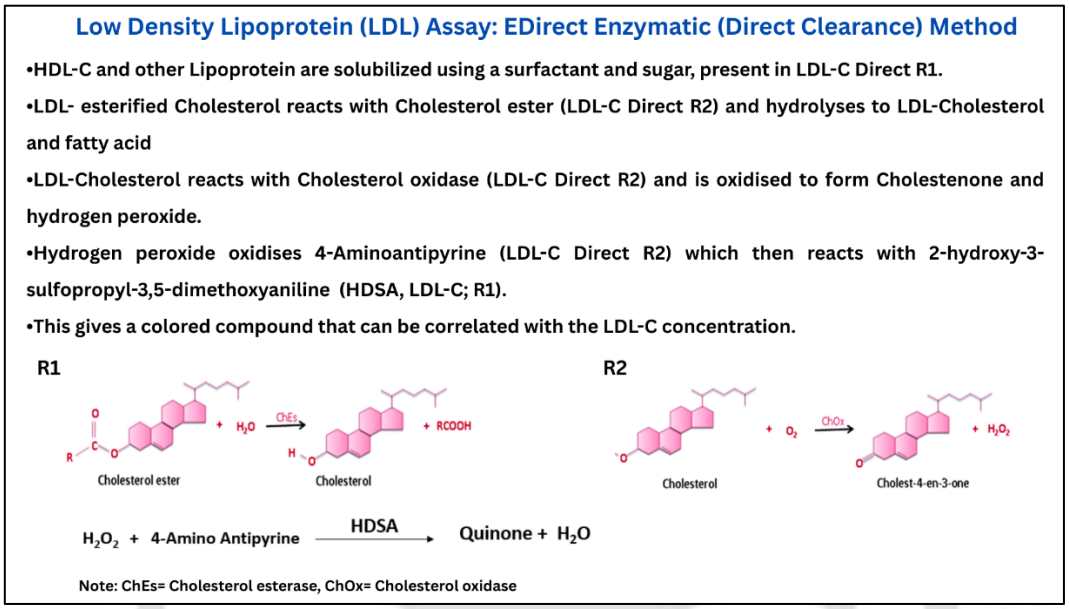

Figure 17: Direct LDL-Cholesterol (LDL-C) enzymatic methodology. The figure depicts the selective enzymatic reactions used for direct LDL-C estimation. LDL-cholesterol esters are hydrolyzed by cholesterol esterase (ChEs) to free cholesterol and fatty acids. The liberated cholesterol is oxidized by cholesterol oxidase (ChOx) to cholest-4-en-3-one with generation of hydrogen peroxide, which participates in a chromogenic reaction to form a measurable colored complex.

In the Figure 17 direct LDL-C method, non-LDL lipoproteins are masked using selective surfactants. LDL-cholesterol undergoes esterase- and oxidase-mediated reactions, producing hydrogen peroxide that reacts with chromogens to generate a colored product proportional to LDL-C concentration.

Creatinine (Kidney Function Test – KFT)

Cretinine is a key biochemical marker used to assess renal function and estimate glomerular filtration rate (GFR). It is produced at a relatively constant rate from the non-enzymatic degradation of creatine and phosphocreatine in skeletal muscle and is eliminated primarily

through glomerular filtration. Because its production is stable and minimally influenced by diet or hepatic function, serum creatinine serves as a reliable indicator of kidney function.

Creatinine estimation in Mobilab-Uni is performed using an enzymatic colorimetric (Trinder-based) method. In this multi-enzyme cascade, creatinine is sequentially converted to creatine, sarcosine, and finally hydrogen peroxide. The generated hydrogen peroxide reacts with chromogenic substrates in the presence of peroxidase to form a quinoneimine dye, the intensity of which is directly proportional to the creatinine concentration and is measured spectrophotometrically. Elevated creatinine levels indicate impaired renal filtration and are associated with chronic kidney disease, a growing global health concern. Compared to the conventional Jaffe method, the enzymatic assay offers superior specificity with minimal interference from glucose, bilirubin, ketones, and proteins, making it well suited for low-volume samples in point-of-care settings.

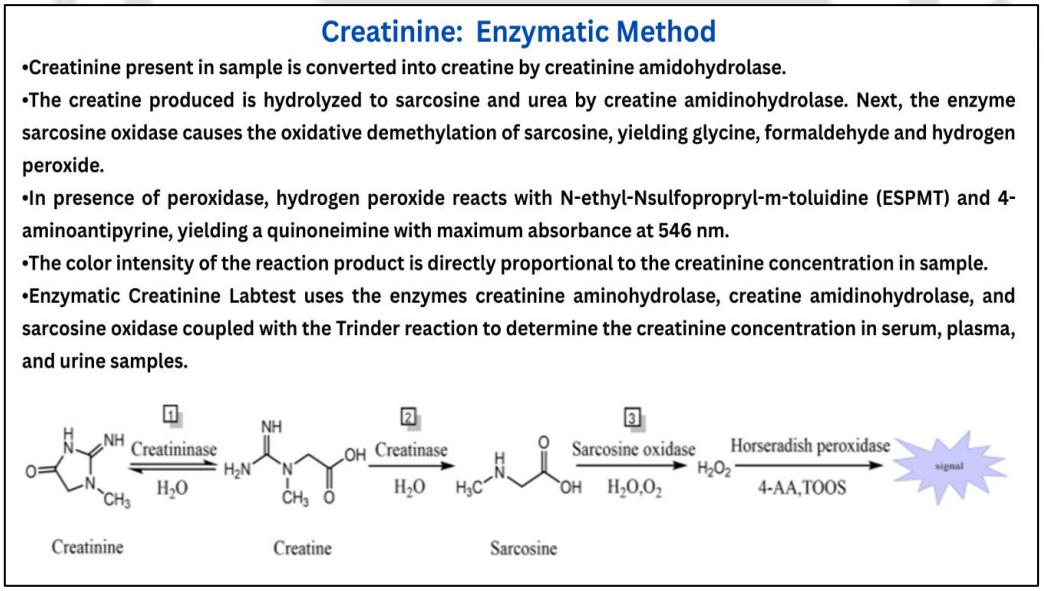

Figure 18: Principle of creatinine estimation by the enzymatic method. The scheme shows sequential enzymatic conversion of creatinine to a quinoneimine chromogen via creatininase, creatine amidinohydrolase, sarcosine oxidase, and peroxidase, with the final coloured product

measured at 546 nm. *(The method and data optimization for the triglyceride parameter were adopted from the PhD thesis study of Sahil Jagnani).*

Figure 18 illustrates the principle of the enzymatic creatinine assay. In this method, creatinine in the sample is first converted to creatine by creatininase, then hydrolysed to sarcosine and urea by creatine amidinohydrolase. Sarcosine oxidase catalyses the oxidative demethylation of sarcosine to glycine, formaldehyde and hydrogen peroxide. In the presence of peroxidase, the generated hydrogen peroxide reacts with ESPMT and 4-aminoantipyrine to form a quinoneimine dye, whose absorbance at 546 nm is directly proportional to the creatinine concentration in serum, plasma or urine. During the initial engineering optimization stage described in Chapter 2, kinetic Jaffe-based creatinine assays are evaluated primarily to study thermal regulation, optical repeatability, and reaction stability of the developed POCT platform. However, during clinical validation in Chapter 3, enzymatic end-point/Trinder-linked creatinine assays are employed to improve assay specificity, reduce analytical interference, and enhance compatibility with the Siemens Dimension EXL 200 reference analyzer. This transition reflects the progression from preliminary system optimization toward clinically robust assay implementation.

Uric Acid (Kidney & Metabolic Profile)

Uric acid is the final metabolic product of purine degradation in humans and is primarily excreted by the kidneys. Serum uric acid levels reflect the balance between purine metabolism and renal excretion and are clinically important in the evaluation of gout, renal dysfunction, metabolic syndrome, and cardiovascular risk. Persistent elevation of uric acid (hyperuricemia) is associated with crystal deposition in joints and tissues, leading to gout and urate nephropathy.

Uric acid estimation is commonly performed using the uricase–PAP (Peroxidase–Aminophenazone) enzymatic method. In this assay, uric acid is oxidized by uricase in the presence of oxygen and water to form allantoin, carbon dioxide, and hydrogen peroxide (H_2O_2). The generated hydrogen peroxide subsequently reacts with 4-aminoantipyrine and a phenolic

chromogen, such as N-ethyl-N-(2-hydroxy-3-sulfopropyl)-m-toluidine (EHSPT), in the presence of peroxidase to produce a red-colored quinoneimine complex. The intensity of the color formed is directly proportional to the uric acid concentration and is measured spectrophotometrically.

Physiologically, uric acid is eliminated mainly through renal filtration, with a smaller fraction excreted via the gastrointestinal tract. Elevated serum uric acid levels are observed in conditions such as gout, chronic kidney disease, hypertension, and metabolic disorders, whereas reduced levels may be seen in severe liver disease or enhanced renal excretion. Due to its clinical relevance and enzymatic specificity, the uricase–PAP method is widely employed in routine laboratory testing and point-of-care diagnostic platforms

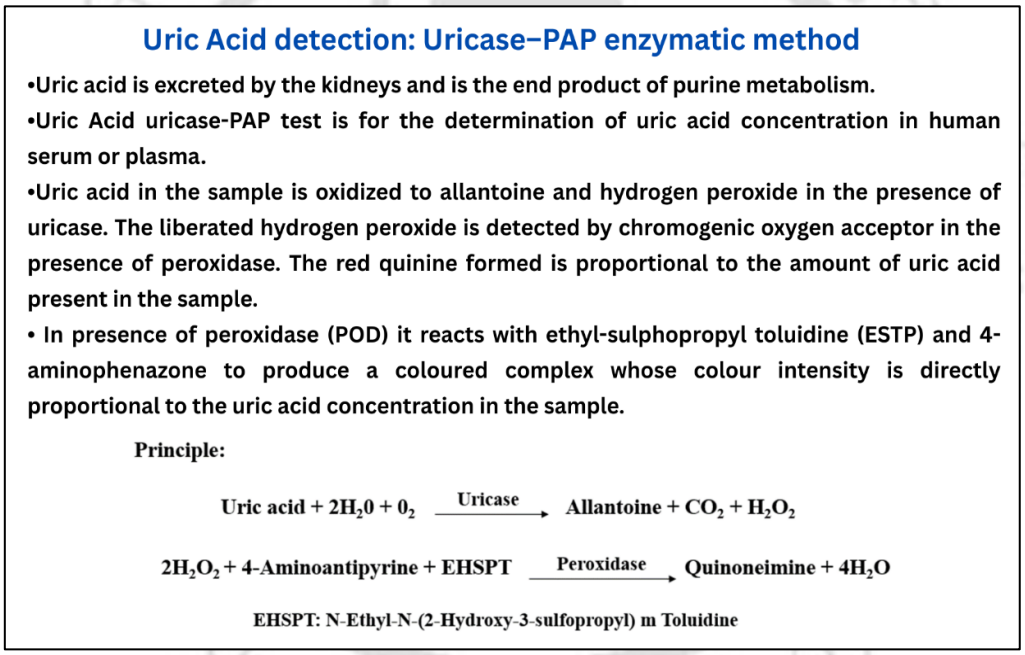

Figure 19: Uric acid detection by the Uricase–PAP enzymatic method. The figure illustrates the principle of uric acid estimation in serum or plasma using the uricase–PAP assay. Uric acid is oxidized by uricase to form allantoin, carbon dioxide, and hydrogen peroxide. The generated hydrogen peroxide participates in a peroxidase-catalyzed chromogenic reaction, producing a colored quinoneimine complex measurable spectrophotometrically.

As shown in the Figure 19, In the uricase–PAP method, uric acid is enzymatically converted to hydrogen peroxide, which reacts with 4-aminoantipyrine and EHSPT in the presence of

peroxidase to form a colored product. The color intensity is directly proportional to the uric acid concentration in the sample.

3.2 Materials & Methods

3.2.1 Materials

The purchased materials were used according to the manufacturer's protocol without any modification. The following kits used in this study were obtained from Agappe, India—a CHOL reagent kit based on the CHOD–PAP enzymatic method [226] with REF No.: 51403002; a TGL reagent kit employing the GPO–PAP method [227] with REF No.: 51410002; an LDL-C Direct kit using the selective solubilization technique with an integrated calibrator [228] and REF No.: 51415003; a CRE reagent kit utilizing the enzymatic creatinine method [229] with REF No.: 51420003; and a UA reagent kit based on the uricase–PAP method [230] with REF No.: 51413002.

The study used 4 mL polystyrene cuvettes supplied by VOLVEX, in which all experiments were conducted using the Mobilab device, a mixer device (Mobimix), an Android smartphone (Redmi 9A, Xiaomi), and a micro-USB OTG cable. Additional materials included 0.9% NaCl and BIO-RAD Liquid Assayed Multiqual control serum Level 1 (LOT NO. 45931) and Level 3 (LOT NO. 45933) to evaluate the analytical sensitivity, linearity, and precision of the test parameters on the Mobilab platform. A UV–Vis Spectrophotometer (LABMAN LCD LMSP-UV1900) was selected as the reference standard for determining linearity and validating spectrophotometric responses obtained from Mobilab.

Table 13 summarizes the analytical methods and reference ranges for the five biochemical parameters evaluated in this study, comparing GNRC Hospital's laboratory techniques with those used in the Mobilab point-of-care device. For cardiovascular markers, GNRC measures cholesterol using the Cholesterol Oxidase method, whereas Mobilab uses the CHOD–PAP method. Triglycerides are assessed using GPO–PAP in both systems. LDL-C is calculated at

GNRC using Friedewald's Formula, while Mobilab employs a direct homogeneous assay. For renal markers, GNRC quantifies creatinine via the alkaline picrate (Jaffe) method, while Mobilab uses a more specific enzymatic approach. Uric acid is measured using uricase-UV at GNRC and uricase–PAP on Mobilab. The table also lists standard adult reference ranges to facilitate clinical interpretation of results.

Table 13. Detection Methods and Reference Ranges for Parameters Used at GNRC Hospital,

Organ	Parameters	Analytical Method (GNRC)	Analytical Method (POCT device)	Reference range (Adult)
Heart	Cholesterol	Cholesterol Oxidase method	CHOD-PAP method	0-200 mg/dL
	Triglyceride	GPO – PAP method	GPO-PAP method	30-150 mg/dL
	Low Density Lipoprotein – Cholesterol	Friedewald's Formula	Direct determination method	0-100 mg/dL
Kidney	Creatinine	Alkaline picrate method	Enzymatic method	0.6-1.02 mg/dL
	Uric Acid	Uricase, UV method	Uricase PAP method	2.6-7.2 mg/dL

3.2.2. Sample collection

50-52 retained patient serum samples were considered as specimens for this clinical comparison study and were sourced from the NABL-accredited GNRC laboratory in North Guwahati, India. Prior to sample collection, ethical clearance was taken from Ethics Committee of GMRC hospital. The Siemens Dimension EXL 200 Analyzer (SDA), in GNRC are considered as the gold standards for this study. Patient identity confidentiality was ensured throughout the study, and the samples were stored at 4°C for short-term use. For long-term preservation, samples were stored frozen and subjected to no more than two freeze–thaw cycles prior to analysis before

measurement. The reference ranges for CHOL, TGL, LDL-C, UA, and CRE are aligned with the established ranges at GNRC Hospital to ensure the consistency and stringency of the study as mentioned in Table 13.

3.2.3. Methods

Mobilab has dimensions of 93.26mm in length, 56.99mm in width, 98.07mm in height, and weighs 312g as shown in the Figure 20 (a) (i-iv). To begin the quantitative measurement using Mobilab, the steps are taken as follows: a. A precise volume of reagent is pipetted into a test cuvette and inserted into the device, for the initial base reading. b. The sample is added to the cuvette and subjected to a uniform mixing in a uniform mixing device, Mobimix as shown in the Figure 20 (b) (i-iv). c. The sample-containing cuvette is then reinserted into the Mobilab device. It measures the absorbance of the products formed at the end of every reaction, or during, applying the Beer-Lambert law [206]. d. The final result is calculated, and a digital test report is generated in the Android application. This process of quantitative measurement by Mobilab is illustrated in the schematic diagram, Figure 15.

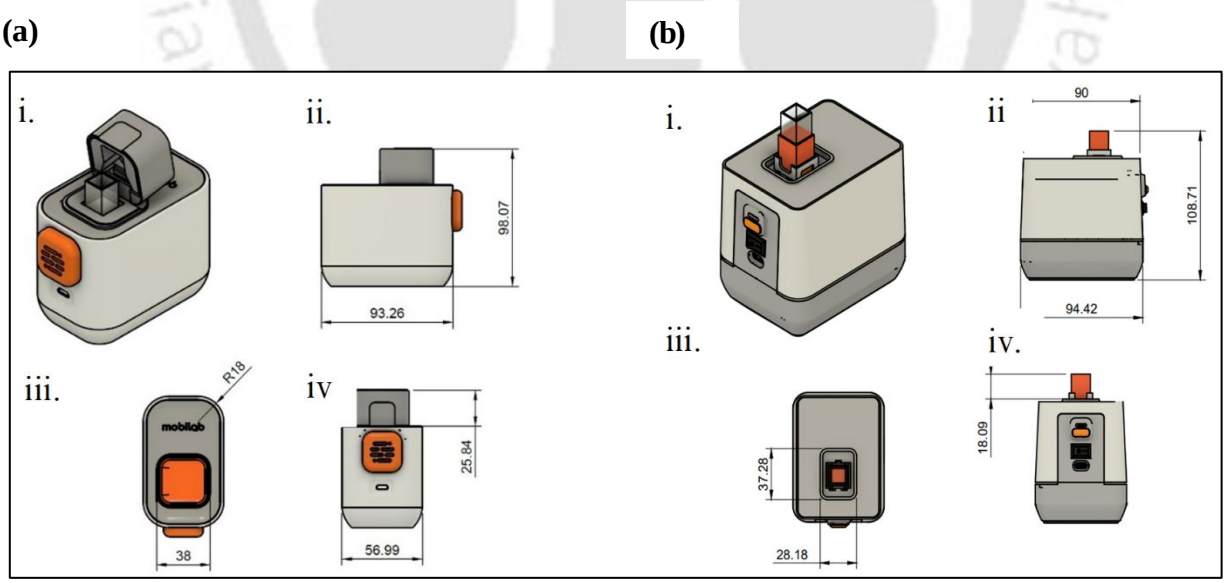

Figure 20: (a) Isometric view of the Mobilab device: (i) Overview of the device with data port for device connection to smartphone, cuvette space and its enclosure (ii) Side view with the length of Mobilab is measured to be 93.26mm, width to be 56.99mm, and the height to be 98.07mm (iii) Top view with a cap measured to be 38mm, in length and breadth and (iv) Front

view of the device with ambient sensor. (b) Isometric view of the mixer -Mobimix: (i) Overview of the Mobimix with On/ Off switch, cuvette holder, mode switch, charging port (ii) Side view with the length of Mobimix is measured to be 90 to 94.42mm, and the height to be 108.71mm (iii) Top view with a cuvette holder measured to be 37.28mm in length and 28.18mm in breadth, and (iv) Front view of the device with On/ Off switch, mode switch, and charging port.

This Figure 20 presents the detailed CAD-based dimensional layout of the Mobilab optical module developed for point-of-care biochemical testing. The images illustrate two design stages: one with the sample holder in the open configuration and the other in the closed operational mode. The isometric views (i) highlight the compact, handheld form factor engineered for portability and field usability. Side views (ii) display the vertical profile along with the overall height measurements, indicating the optimized enclosure geometry that accommodates optical components, electronics, and the heating chamber. The top and front views (iii–iv) provide accurate measurements of the cuvette slot width, enclosure curvature radius, and frontal interface, demonstrating the careful integration of mechanical, optical, and user-interaction elements. Collectively, the CAD layouts validate the ergonomic and structural considerations underlying the Mobilab device design, ensuring manufacturability, robustness, and ease of operation within resource-constrained field environments.

While the present study focuses on maintaining stable enzymatic incubation at 37°C, operation in high-temperature rural environments may pose additional challenges related to reagent stability and assay performance. Therefore, future versions of the developed POCT platform may incorporate active cooling mechanisms, thermal insulation, or adaptive temperature control strategies to ensure reliable operation under varying environmental conditions. In a way, Mobilab demonstrates acceptable analytical performance in terms of accuracy, precision, sensitivity, specificity, linearity, repeatability, reproducibility, calibration, and quality control as per the ICMR guidelines. In addition, compliance with recognized quality and regulatory frameworks, including ISO standards, CDSCO requirements, and CLSI

guidelines, have been followed to ensure the reliability, safety, and clinical acceptance of point-of-care diagnostic systems.

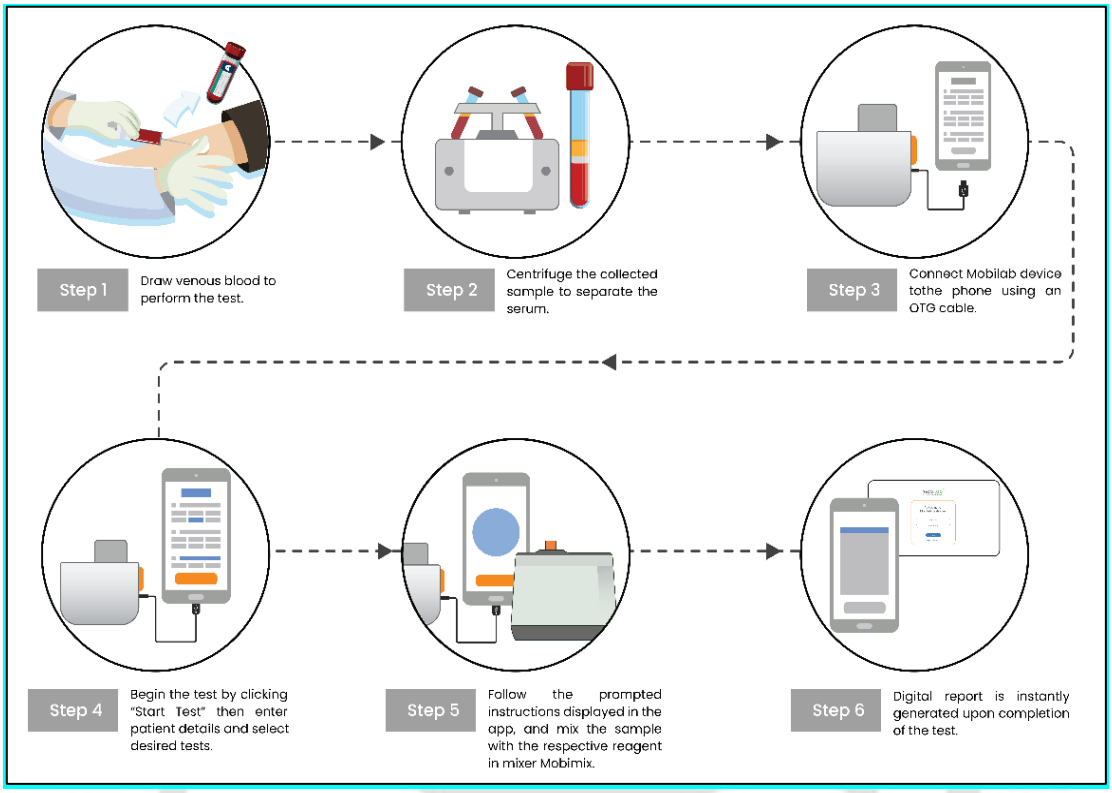

Figure 21: An elaborate breakdown of how Mobilab operates, divided into six sequential steps. Step-1: Collect venous blood for the test., Step-2: Separate the serum from the collected blood sample by centrifugation, Step-3: Connect the Mobilab device to the phone using an OTG cable, Step-4: Initiate the test by clicking on "start test," followed by inputting patient details and choosing the preferred tests, Step-5: Follow to the instructions presented in the app, and mix the sample with the corresponding reagent using the Mobimix mixer., Step 6: Immediately after completion of the test, digital report is generated.

Figure 21 illustrates the complete operational workflow of the Mobilab point-of-care diagnostic system, represented as a sequence of six interconnected steps from sample collection to report generation. The workflow begins with Step 1, where venous blood is drawn from the patient for biochemical analysis. In Step 2, the collected blood sample is centrifuged to separate serum, which serves as the analytical specimen. Step 3 shows the Mobilab device being connected to a smartphone using an OTG cable, enabling communication between the hardware and the Android application.

In Step 4, the user initiates the diagnostic process by launching the Mobilab application, selecting "Start Test," and entering the required patient information along with the desired test parameters. Step 5 depicts mixing of the serum with the appropriate reagent using the Mobimix device, following the step-by-step instructions displayed in the app. Finally, Step 6 demonstrates the automated processing of the sample within Mobilab, culminating in immediate digital report generation on the smartphone interface. The infographic provides a comprehensive and user-friendly overview of the Mobilab testing cycle, highlighting its streamlined workflow, minimal operational complexity, and suitability for use in decentralized or resource-limited healthcare environments.

3.2.4. Performance Comparison

The comparison study evaluated Mobilab's analytical methodology, sensitivity, linearity, repeatability, and overall performance against the fully automated Siemens Dimension EXL analyzer (SDA) used at GNRC Hospital. The comparison was carried out for five biochemical parameters-CHOL, TGL, LDL-C, CRE, and UA—to determine Mobilab's suitability as a reliable point-of-care diagnostic system [231]. Conventional laboratory analyzers are high-throughput centralized systems that require controlled laboratory infrastructure, uninterrupted power supply, automated fluidics, and trained personnel for operation. In contrast, Mobilab has been developed as a compact, battery-operated, and portable point-of-care testing (POCT) platform intended for decentralized healthcare settings. Unlike conventional analyzers, Mobilab utilizes simplified reagent-sample workflows, smartphone/cloud-based reporting, and modular optical detection to enable rapid near-patient biochemical testing in rural and resource-limited environments.

(i) Passing & Bablok Regression:

Passing–Bablok regression is a robust non-parametric statistical method widely used for method-comparison studies in clinical chemistry. It is resistant to the influence of outliers, assumes no distribution for measurement errors, and is appropriate when both variables contain

random error. The regression intercept signifies constant bias, while the slope reflects proportional bias between two analytical methods. The 95% Confidence Intervals (CI) for both parameters determine whether deviations from 0 (intercept) or 1 (slope) are statistically significant [232].

(ii) Bland–Altman Plot:

The Bland–Altman (B-A) plot is an established graphical method for evaluating agreement between two measurement techniques. It depicts the mean of paired measurements on the x-axis and their difference on the y-axis. The central mean difference line indicates systematic bias, while the ±2SD limits represent the boundaries of agreement. This method is extensively used in clinical validation studies to detect outliers, identify heteroscedasticity, and determine whether two analytical devices can be used interchangeably [233, 234].

(iii) Paired t-test:

The paired t-test statistically evaluates whether there is a significant difference between the means of two related measurement sets (Mobilab vs. SDA). A significance level of 0.05 was used. A p-value greater than 0.05 suggests the absence of statistically meaningful differences, supporting interchangeability; a p-value below 0.05 indicates significant deviation between methods [235, 236].

3.2.5. Analytical Sensitivity

Analytical sensitivity refers to the capability of a diagnostic system to detect low analyte concentrations with high reliability. In this study, the Limit of Blank (LOB) and Limit of Detection (LOD) were determined to assess Mobilab's ability to measure low-level analytes. LOB identifies the background signal in absence of analyte, while LOD represents the lowest analyte concentration that can be confidently distinguished from blank variability. Determination of LOB and LOD is essential in evaluating analytical systems for clinical use and follows best-practice guidelines in laboratory medicine [237].

3.2.6. Linearity

Linearity describes an analytical system's ability to generate results that are directly proportional to analyte concentration over a defined measurement interval. Mobilab was tested across a wide range of concentrations for all parameters by comparing readings against a calibrated UV-visible spectrophotometer. The resulting data were plotted with Mobilab values on the y-axis and reference values on the x-axis to construct linear regression curves. This approach follows conventional validation standards used for assessing accuracy and proportionality in biochemical assays [238, 239, 240].

3.2.7. Intra-day Precision Study

Intra-day precision reflects the repeatability of results under identical experimental conditions within a single day. Using BIO-RAD Liquid Assayed Multiqual control serum Level 1 and Level 3, each parameter was tested 20 times to compute the coefficient of variation (CV%). Precision studies are fundamental components of analytical validation, with lower CV% values indicating superior repeatability and measurement reliability [241].

3.2.8 Performance matrices

In order to estimate the accuracy of the proposed device, the sensitivity, specificity, Positive Predictive Value (PPV), Negative Predictive Value (NPV), and Diagnostic Accuracy (DA) were calculated. These were calculated using the following test results: True Positive (TP), True Negative (TN), False Negative (FN), and False Positive (FP) [242] as shown in Table 14. In the sensitivity study, Mobilab is tested to determine how often it correctly identifies the presence of the condition or disease. While, in the specificity study, the device is tested to determine how often it correctly identifies the absence of the condition. PPV analyzed the number of times Mobilab could correctly detect the amount of true positive results among all the positive results. NPV analysis described the proportion of true negative results shown by Mobilab among all the

negative instances. DA is calculated to determine the overall number of true positives and true negatives diagnosed among all the test results [242].

Table 14. The Tabular Illustration of The Performance Matrices and Their Respective Formulas to Calculate Diagnostic Accuracy for The Mobilab Device.

		Siemens Dimension EXL 200		
		Positive	**Negative**	
Mobilab	**Positive**	True Positive (TP)	False Positive (FP)	Positive Predictive Value (PPV) $\frac{TP}{(TP+FP)} \times 100$
	Negative	False Negative (FN)	True Negative (TN)	Negative Predictive Value (NPV) $\frac{TN}{(FN+TN)} \times 100$
		Sensitivity $\frac{TP}{(TP+FN)} \times 100$	Specificity $\frac{TN}{(TN+FP)} \times 100$	Diagnostic Accuracy (DA) $\frac{TP+TN}{(TP+FN+FP+TN)} \times 100$

3.3 Result and Discussion

In this study, we demonstrate the clinical comparison of the POCT device, Mobilab to determine the clinical utility and diagnostic efficacy. To conduct the study, 50-52 samples of each parameter retested separately with the help of a properly designed experimental setup for each parameter. For each parameter, the diagnostic method is validated, analytical sensitivity and linearity are determined, intra-day precision study and the performance matrices is evaluated, and the results are discussed sequentially for each parameter (CHOL, TGL, LDL-C, CRE, UA), emphasizing the device's effectiveness in early diagnosis of NCDs in individuals.

3.3.1 Cholesterol (CHOL)

(a) **Method Comparison:** To verify the outcomes of the CHOL tests carried out in Mobilab, a P-B Regression analysis Figure 22 (A) is performed, using 50 samples of different CHOL concentrations with the SDA results on the x-axis and the corresponding Mobilab results on the y-axis. The resulting slope, 1.04, and intercept, -7.51, are found to lie within the desired

confidence limit along with the R^2 value being 0.97. A mean bias of 0.33 mg/dL and a LOA between -14.77 mg/dL to 15.44 mg/dL is observed in the Bland Altman analysis (Table 15) [Figure 22 (B)] of CHOL. Some of the points outside this range could be due to experimental errors. The t-test, p-value = 0.76, supported a significant correlation between the SDA and Mobilab assays, confirming the null hypothesis (Table 15)

(b) **Analytical Sensitivity:** The LOB for CHOL is 0.34 mg/dL, whereas the LOD for CHOL is 1.4 mg/dL, which means that the lowest concentration that can be consistently and accurately detected by the Mobilab is 1.4 mg/dL (Table 15).

(c) **Linearity:** The Mobilab device concentration (y-axis) plotted against the UV-Vis Spectrophotometer concentration (x-axis) gives us a linear measurement range between 40 mg/dL to 587 mg/dL with the slope value of 1.01, intercept of -2.69 and R^2 value of 1. This signifies that the Mobilab device yields accurate results over a broad linear range of CHOL concentrations as indicated in the Table 15 and Figure 22 (C).

(d) **Intra-day precision study:** To prove the reproducibility aspect of CHOL in Mobilab, the Level 1 and Level 3 Bio-Rad control serum is used for 20 runs. For Level 1 and Level 3 serum, the CV% is around 2.00 % and 2.48 %, respectively (Table 15). This low value of precision for CV, indicating consistency and reliability of the results.

(e) **Performance Matrices:** With a sensitivity of 92.86%, the device can identify true positive cases 92.86% of the time, and a specificity of 100%, meaning it can accurately identify all true negative cases. With a remarkable PPV of 100%, CHOL indicates that the device accurately predicts all true positive values in every test. An NPV of 97.30% indicates that 97.30% of the time, the device correctly predicts true negative values. Based on calculations, the diagnostic accuracy value for CHOL is 98% as indicates in the Table 14 and Table 15.

These important findings of the comparison study for CHOL have been reported in a tabular form in Table 15, the Method comparison between Mobilab and SDA, the analytical sensitivity,

and the linearity test data report are summarized along with the intra-day precision study for CHOL.

Table 15. Summary of The Comparison Study for CHOL: Method Comparison Between Mobilab and SDA, Analytical Sensitivity, Linearity, Intra-Day Precision, and Performance Metrics

Cholesterol (CHOL)						
Method Comparison	**Passing Bablok Plot**		**Bland Altman plot**			**t-test**
	Slope	**Intercept**	**R^2**	**Bias(mg/dL)**	**LOA (mg/dL)**	**p-value**
	1.04	-7.51	0.97	0.33	-14.77 to 15.44	0.7617
Analytical Sensitivity	**LOB (mg/dL)**		**LOD (mg/dL)**			
	0.34		1.4			
Linearity Study	**Slope**	**Intercept**	**R^2**		**Linearity(mg/dL)**	
	1.01	-2.69	1		40 to 587	
Intra- Day Precision	**%CL1**		**%CL3**			
	2.00		2.48			
Sensitivity	92.86%					
Specificity	100%					
Diagnostic accuracy	98%					

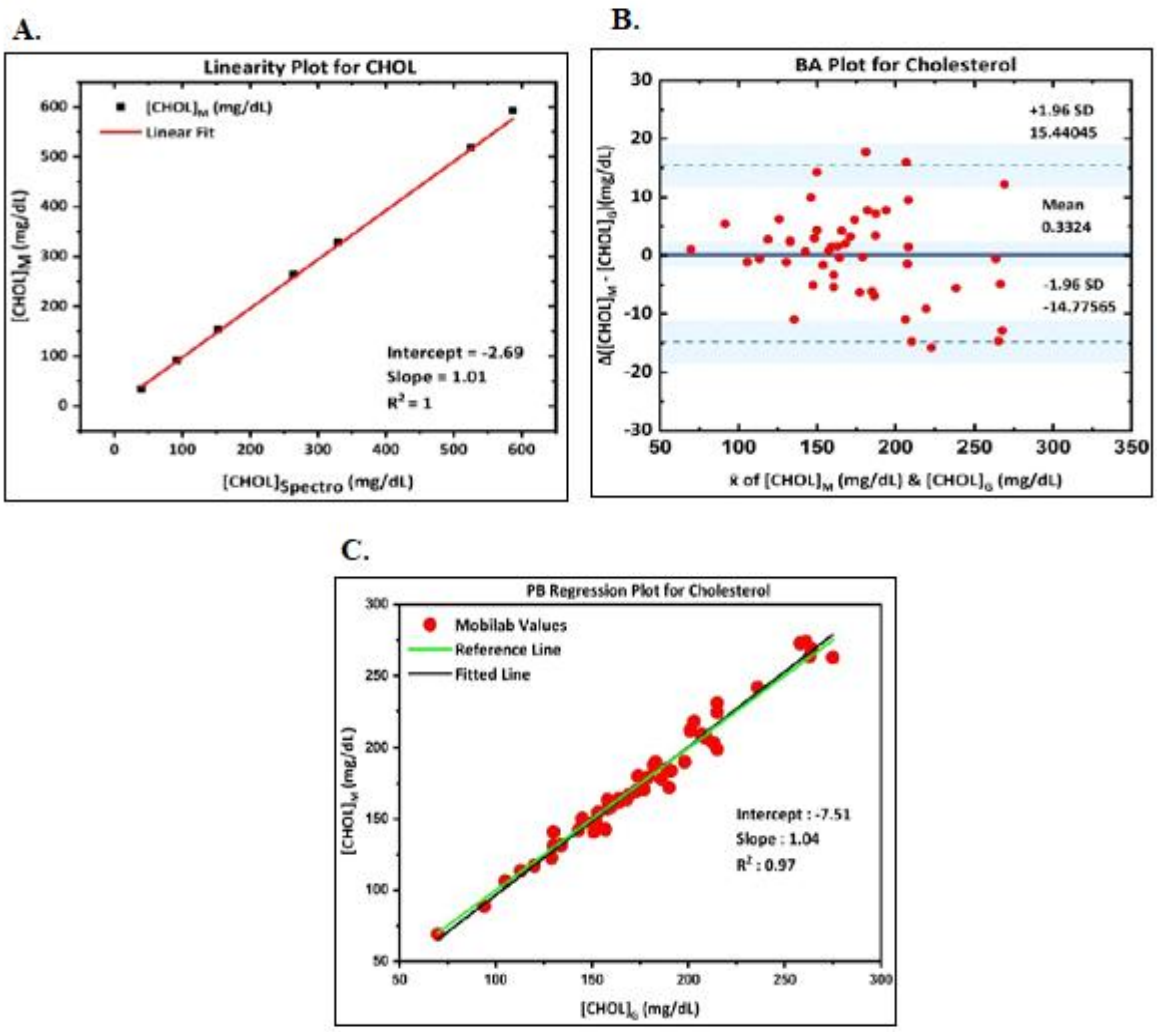

Figure 22: Method comparison between Mobilab and SDA, in terms of CHOL as a test parameter. A) Passing–Bablok regression analysis plot: The CHOL concentration measured in patient serum is plotted on the x-axis as [CHOL]G (mg/dL) from SDA and on the y-axis as [CHOL]M (mg/dL) from Mobilab. The reference line is shown in green, and the fitted line is in black. Red dots indicate the values obtained from Mobilab. The regression analysis results in intercepts = -7.51, slope=1.04, R^2 = 0.97. B) Bland–Altman plot for interrater agreement analysis: The difference in the measurement of CHOL in two devices (Mobilab and SDA) are plotted on the y axis as Δ([CHOL]M – [CHOL]G) (mg/dL) and average of measurement from both the devices are plotted on the x axis as (x of [CHOL]M (mg/dL) & [CHOL]G (mg/dL). Limits of Agreement are shown as dotted blue lines, upper limit = 15.44 and lower limit =-14.77 with 95% confidence intervals, mean of differences or bias represented as solid line with 95% confidence interval, C) Linearity plot: The plotting of concentration ranges for test parameter in Mobilab on the y-axis [CHOL]M (mg/dL) against the UV-spectrophotometer readings on the x-

axis [CHOL]Spectro (mg/dL) resulted a linear measurement with the slope value of 1.01, intercept of -2.69 and R^2 value of 1.

3.3.2. Triglyceride (TGL)

(a) Method Comparison

A slope of 1.01, an intercept of 1.25, and R^2 of 0.99 are achieved by plotting the P-B Regression plot [Table 16 and Figure 23 (A)] of TGL test results in Mobilab against the corresponding TGL concentration results from the SDA with 52 samples. These results support a high level of agreement between the two methods. Further analysis with the B-A plot displays a mean bias of -0.24 mg/dL and a LOA from -19.88 mg/dL to 19.40 mg/dL [Table 16 and Figure 23 (B)]. Most of the data points align well, though a few discrepancies observed could be due to manual errors or testing with hemolyzed samples. The paired t-test for Mobilab Device yields a p-value of 0.86, surpassing the chosen significance level of 0.05, supporting the acceptance of the null hypothesis that test results from the SDA and Mobilab are comparable (Table 16).

(b) Analytical Sensitivity

The LOB for TGL is 3.79 mg/dL. The LOD for TGL is 5.87 mg/dL, which means that the lowest concentration of TGL that can be reliably detected by Mobilab is 5.87 mg/dL (Table 16).

(c) Linearity

The Mobilab's response for TGL is in a linear range from 30 mg/dL concentrations to 759 mg/dL with a slope of 1.01, intercept of -16.1, and R^2 value of 0.99. This signifies that the Mobilab device yields accurate results over a broad linear range of TGL concentrations as indicated in the Table 16 and Figure 23 (C).

(d) Intra-day precision study

An Intra-day precision study of TGL in Mobilab is conducted for 20 runs. The CV% is 2.75% and 3.3% for Level 1 and Level 3 control serums, respectively. The considerably low Intercept of -16.1, and R^2 of 0.99. This observation underscores Mobilab's ability to deliver precise and reliable results across a broad spectrum of TGL concentrations (Table 16).

(e) Performance Matrices

In the analysis of 52 samples for TGL, a sensitivity of 96% and specificity of 100% are observed in Mobilab. Out of all genuine positive test results, the device can correctly identify 100% of true positive cases, according to its PPV of 100%. With an NPV of 96.43%, Mobilab can accurately detect approximately 96 true negative cases among all negative TGL test results. Overall, Mobilab has a diagnostic accuracy of 98.08% in the detection of TGL as indicated in the Table 16.

These important findings of the comparison study for TGL have been reported in a tabular form in Table 16, the Method comparison between Mobilab and SDA, the analytical sensitivity, and the linearity test data report are summarized along with the intra-day precision study for TGL.

Table 16. Summary of The Comparison Study For TGL: Method Comparison Between Mobilab and SDA, Analytical Sensitivity, Linearity, Intra-Day Precision and Performance Metrics

<table>
<tr><th colspan="7">Triglyceride (TGL)</th></tr>
<tr><td rowspan="2">Method Comparison</td><td colspan="3">Passing Bablok Plot</td><td colspan="2">Bland Altman plot</td><td>t-test</td></tr>
<tr><td>Slope</td><td>Intercept</td><td>R²</td><td>Bias(mg/dL)</td><td>LOA (mg/dL)</td><td>p-value</td></tr>
<tr><td></td><td>1.01</td><td>1.25</td><td>0.99</td><td>-0.24</td><td>-19.87 to 19.40</td><td>0.8642</td></tr>
<tr><td>Analytical Sensitivity</td><td colspan="3">LOB (mg/dL)</td><td colspan="3">LOD (mg/dL)</td></tr>
<tr><td></td><td colspan="3">3.79</td><td colspan="3">5.87</td></tr>
<tr><td rowspan="2">Linearity Study</td><td colspan="2">Slope</td><td>Intercept</td><td>R²</td><td colspan="2">Linearity(mg/dL)</td></tr>
<tr><td colspan="2">1.008</td><td>-16.076</td><td>0.997</td><td colspan="2">30 to 759</td></tr>
<tr><td rowspan="2">Intra-Day Precision</td><td colspan="3">%CL1</td><td colspan="3">%CL3</td></tr>
<tr><td colspan="3">2.75</td><td colspan="3">3.3</td></tr>
<tr><td>Sensitivity</td><td colspan="6">96%</td></tr>
<tr><td>Specificity</td><td colspan="6">100%</td></tr>
<tr><td>Diagnostic accuracy</td><td colspan="6">98.08%</td></tr>
</table>

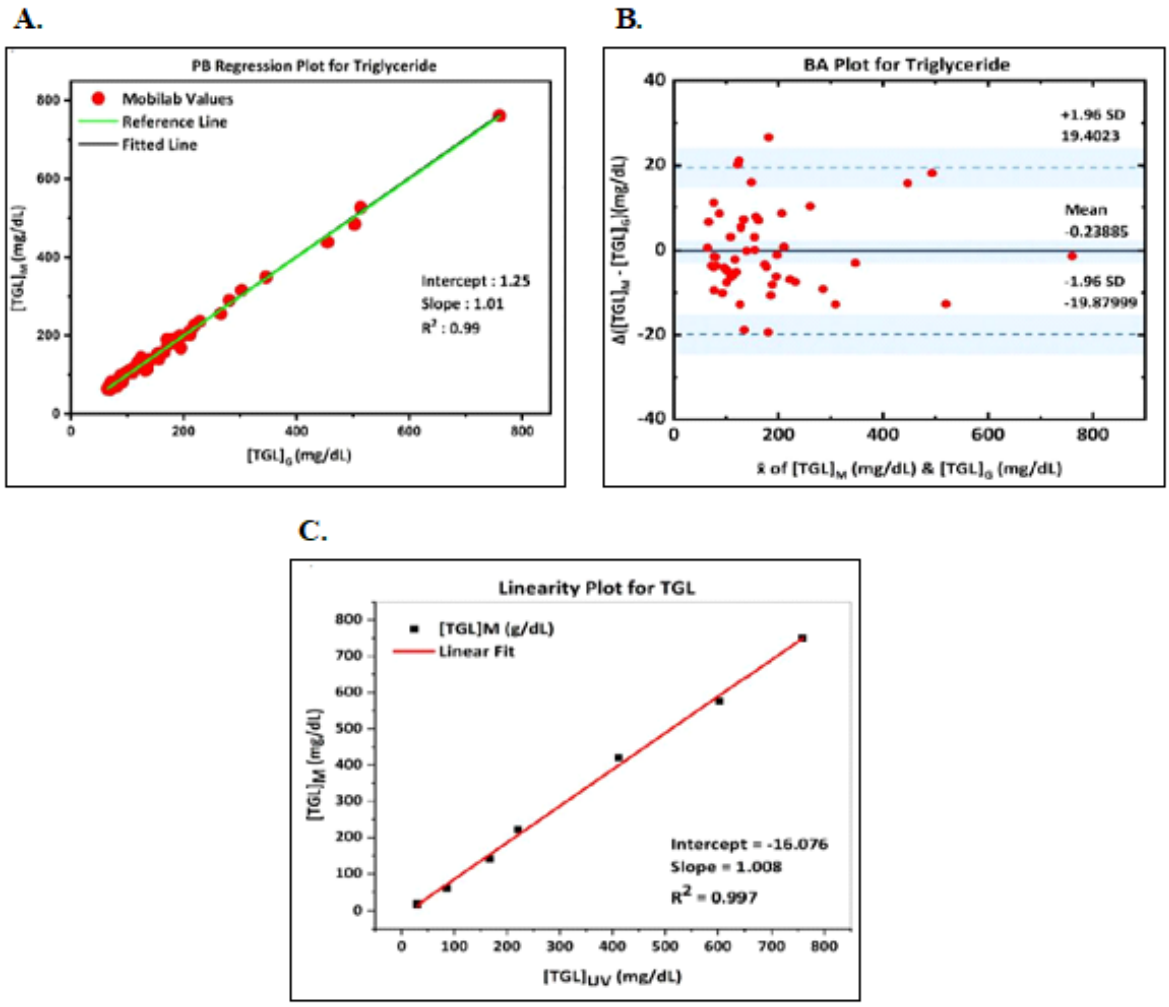

Figure 23: Method comparison between Mobilab and SDA, in terms of triglycerides as a test parameter. (A) Passing–Bablok regression analysis plot: The TGL concentration measured in patient serum is plotted on the x-axis as [TGL]G(mg/dL) from SDA and on the y-axis as [TGL]M (mg/dL) from Mobilab. The reference line is shown in green, and the fitted line is in black. Red dots indicate the values obtained from Mobilab. The regression analysis results in intercepts = 1.25, slope=1.01, R^2 = 0.99. (B) Bland–Altman plot for interrater agreement analysis: The difference in the measurement of triglycerides in two devices (Mobilab and SDA) are plotted on the y axis as Δ([TGL]M – [TGL]G) (mg/dL) and average of measurement from both the devices are plotted on the x axis as (x of [TGL]M (mg/dL) & [TGL]G (mg/dL). Limits of Agreement are shown as dotted blue lines, upper limit = 19.40 and lower limit =-19.88 with 95% confidence intervals, mean of differences or bias represented as solid line with 95% confidence interval, (C) Linearity plot: The plotting of concentration ranges for test parameter in Mobilab on the y-axis as [TGL]M (mg/dL) against the UV-spectrophotometer

readings on the x-axis as [TGL]Spectro (mg/dL) resulted a linear measurement with the slope value of 1.008, intercept of -16.07 and R^2 value of 0.997

3.3.3. Low-Density Lipoprotein-Cholesterol (LDL-C)

(a) Method Comparison

A Method comparison study is performed to evaluate the agreement between Mobilab and the SDA for LDL-C using the P-B Regression plot [Figure 24 (A)] with 50 samples. The resulting slope: 0.99, intercept: -1.27, and R^2: 0.94 values from the plot suggest a strong correlation between the two techniques (Table 17). Further comparison with B-A Plot [Figure 24 (B)] shows a low mean bias: 1.08 mg/dL with a LOA between of -13.27 mg/dL to 15.43 mg/dL, suggesting a good agreement between the results of the two methods. The p-value obtained for t-test analyzing LDL-C results is 0.307, indicating that it exceeds the predetermined significance threshold of 0.05 (Table 17). This indicates that the null hypothesis is acceptable, meaning there is no significant difference between the methods used by Mobilab and the SDA.

(b) Analytical Sensitivity

The LOB for the LDL-C test in Mobilab is measured to be 1.12 mg/dL. On the other hand, the LOD for LDL-C in Mobilab is found to be 2.09 mg/dL, signifying that Mobilab can detect 2.09 mg/dL concentrations as low as 2.09 mg/dL accurately (Table 17).

(c) Linearity

LDL-C concentrations ranging from 8.41 mg/dL to 267.41 mg/dL are plotted with values of UV-visible spectrophotometer on the X-axis and Mobilab values on the Y-axis. It is noted that the concentrations are along a straight line, with an R^2 of 0.99, a slope of 1.05, and an intercept of -2.358, indicating that the Mobilab de-vice can provide accurate results across a wide range of LDL-C concentrations as indicated in the Table 16 and Figure 24 (C).

(d) Intra-day precision study

An Intra-day precision study for LDL-C test in Mobilab is conducted over 20 runs, and the CV% is found to be approximately 2.44 % for L1 and 2.12 % for L3 control serum (Table

17). The study indicates that the device gives consistent results with high precision, reflecting consistency and reliability, which is highly advantageous for diagnostic and analytical applications.

(e) Performance Matrices

The performance matrices of LDL-C show a sensitivity and specificity of 88.89% and 96.88%, respectively. A PPV of 94.12 % implies that the likelihood of the device accurately predicting a positive value as positive is 94.12%. The negative predictive value result implies that the device predicts a true negative value as negative correctly 93.94% of the time. A diagnostic accuracy of 94% implies that 94 out of 100 times, the device accurately determines the concentration of LDL-C. Thus, from the results of the statistical measures, we confirm the overall agreement between the SDA and Mobilab test results (Table 17).

These important findings of the comparison study for LDL-C have been reported in a tabular form in Table 16, the Method comparison between Mobilab and SDA, the analytical sensitivity, and the linearity test data report are summarized along with the intra-day precision study for LDL-C.

Table 17. Summary of The Comparison Study For LDL-C: Method Comparison Between Mobilab and SDA, Analytical Sensitivity, Linearity, Intra-Day Precision, And Performance Metrics

Low Density Lipoprotein Cholesterol (LDL-C)						
Method Comparison	**Passing Bablok Plot**			**Bland Altman plot**		**t-test**
	Slope	**Intercept**	**R^2**	**Bias(mg/dL)**	**LOA (mg/dL)**	**p-value**
	0.99	-1.27	0.94	1.08	-13.37 to 15.43	0.30
Analytical Sensitivity	**LOB (mg/dL)**			**LOD (mg/dL)**		
	1.12			2.09		
Linearity Study	**Slope**		**Intercept**	**R^2**	**Linearity(mg/dL)**	
	1.05		-2.35	0.99	267.41	
	%CL1			%CL3		

Intra-Day Precision	2.44	2.12
Sensitivity	88.89%	
Specificity	96.88%	
Diagnostic accuracy	94%	

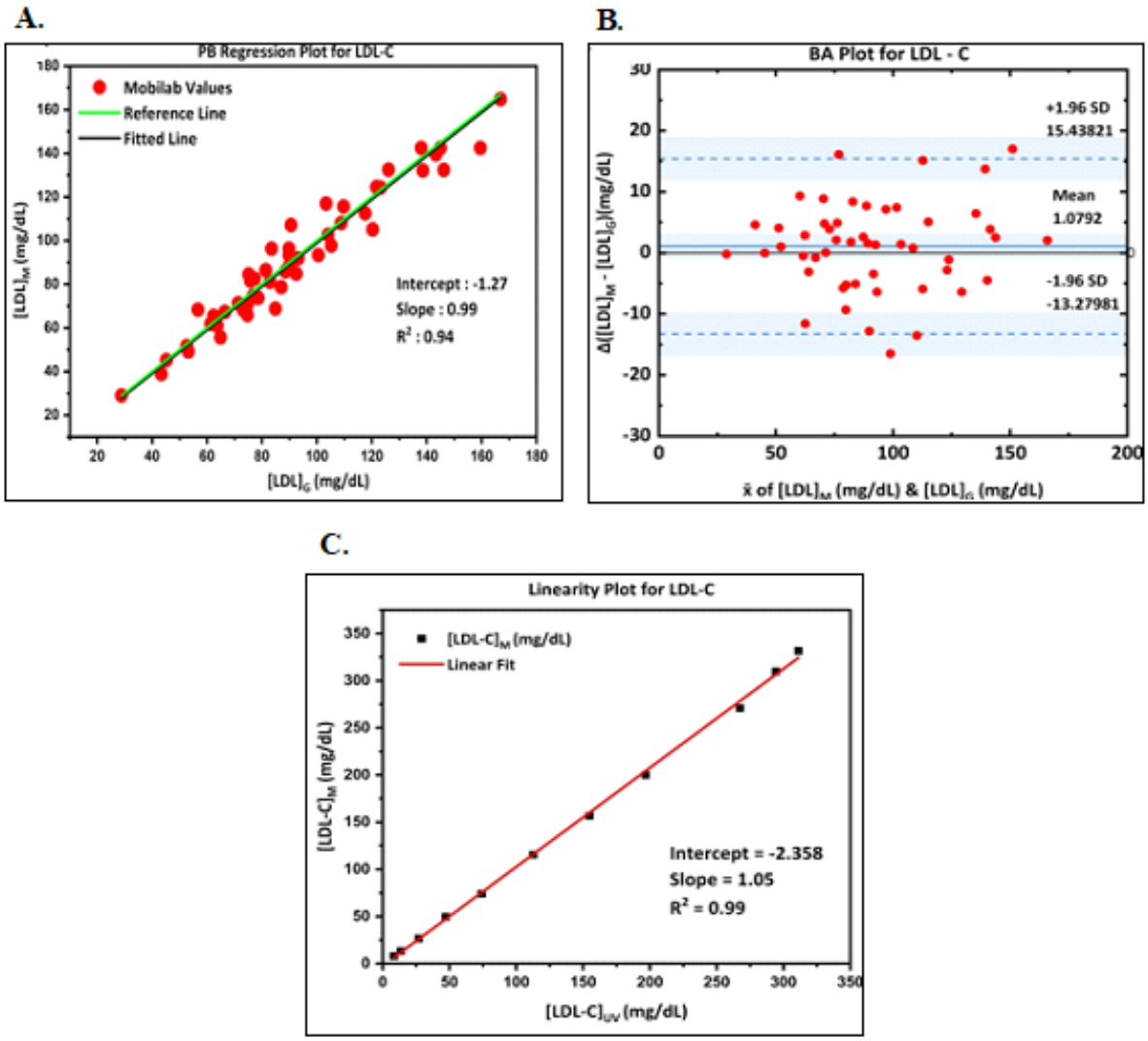

Figure 24: Method comparison between Mobilab and SDA, in terms of LDL-C as a test parameter. (A) Passing–Bablok regression analysis plot: The LDL-C concentration measured in patient serum is plotted on the x-axis as [LDL]G(mg/dL) from SDA and on the y-axis as [LDL]M (mg/dL) from Mobilab. The reference line is shown in green, and the fitted line is in black. Red dots indicate the values obtained from Mobilab. The regression analysis results in intercepts = -1.27, slope=0.99, R^2 = 0.94. (B) Bland–Altman plot for interrater agreement analysis: The difference in the measurement of LDL-C in two devices (Mobilab and SDA) are plotted on the y axis as Δ([LDL]M – [LDL]G) (mg/dL) and average of measurement from

both the devices are plotted on the x axis as (x of [LDL]M (mg/dL) & [LDL]G (mg/dL). Limits of Agreement are shown as dotted blue lines, upper limit = 15.43 and lower limit =-13.279 with 95% confidence intervals, mean of differences or bias represented as solid line with 95% confidence interval, (C) Linearity plot: The plotting of concentration ranges for test parameter in Mobilab on the y-axis as [LDL-C]M (mg/dL) against the UV-spectrophotometer readings on the x-axis as [LDL-C]Spectro (mg/dL) resulted a linear measurement with the slope value of 1.05, intercept of -2.358 and R^2 value of 0.99.

3.3.4. Uric Acid (UA)

(a) Method Comparison

For Method Comparison, we verify the UA test results from Mobilab with those from the SDA for 50 samples. Here, the x-axis represents the SDA results, while the y-axis represents the corresponding Mobilab results [Figure 25 (A)]. The resulting slope: 1.03, intercept: -0.02, and R^2: 0.92 indicate a strong linear match between the test methods (Table 18). Additional comparison is achieved by B-A Plot [Figure 25 (B)], showcasing low mean bias as -0.06 mg/dL and a narrow LOA of -1.07 mg/dL to 0.96 mg/dL. Further comparison is carried out with a t-test between the UA data obtained with the SDA and Mobilab. In this case, the p-value results are 0.45 which is greater than the chosen significance level of 0.05, suggesting strong evidence to accept our null hypothesis (Table 18).

(b) Analytical sensitivity

The LOB and LOD are measured to be 0.22 mg/dL, and 0.28 mg/dL. It makes it evident that the concentrations at which Mobilab can detect UA with good reliability range within 0.28 mg/dL and above (Table 18).

(c) Linearity

The linearity test demonstrates that the response of the Mobilab for the UA is observed to be linear in the range of 2 mg/dL to 23 mg/dL with a slope value of 0.989 and intercept value of 0.028 having a good linear fit determined by R^2 value of 1, indicating that the Mobilab

device provides accurate results or has maintained linearity across a wide range of UA concentrations as indicated in the Table 18 and Figure 25 (C).

(d) Intra-day precision study

To prove the reproducibility aspect of UA in Mobilab, the L1 and L3 Bio-Rad control serum is used, and the test is performed for 20 runs. The CV% for L1 and L3 is measured to be 1.43% and 3.29%, respectively (Table 18).

(e) Performance Matrices

In the analysis of 50 UA samples, a sensitivity of 94.44% is observed, meaning that the device can accurately detect all the positive cases. Out of all actual negative cases, the device can properly detect 96.88% of true negative cases, as indicated by its specificity of 96.88%. Out of all genuine positive test results, the device can correctly identify 94.44% of true positive cases, according to its PPV of 94.44%. Out of all the negative UA test results, Mobilab can correctly detect all the real negative instances, according to its NPV of 96.88%. Overall, Mobilab has a diagnostic accuracy of 96% in the detection of UA as indicated in the Table 18.

These important findings of the comparison study for UA have been reported in a tabular form in Table 18, the method comparison shows a good correlation between Mobilab and SDA. The data of analytical sensitivity reports low LOB (0.22mg/dL) and LOD (0.28mg/dL) values for the UA test. The Linearity test data report a broad linear range for UA. The intra-day precision study proves that the data obtained for 20 runs is consistent and repeatable. The performance matrices data proves the substantial efficiency of the device.

Table 18. Summary of The Comparison Study For UA: Method Comparison Between Mobilab and SDA, Analytical Sensitivity, Linearity, Intra-Day Precision, And Performance Metrics

Uric Acid (UA)						
Method Comparison	**Passing Bablok Plot**			**Bland Altman plot**		**t-test**
	Slope	**Intercept**	**R^2**	**Bias(mg/dL)**	**LOA (mg/dL)**	**p-value**
	1.03	-0.02	0.92	-0.058	-1.07 to 0.967	0.4535
Analytical Sensitivity	**LOB (mg/dL)**			**LOD (mg/dL)**		
	0.22			0.28		
Linearity Study	**Slope**	**Intercept**		**R^2**	**Linearity(mg/dL)**	
	0.989	0.028		1	23	
Intra-Day Precision	%CL1			%CL3		
	1.43			3.29		
Sensitivity	94.44%					
Specificity	96.88%					
Diagnostic accuracy	96%					

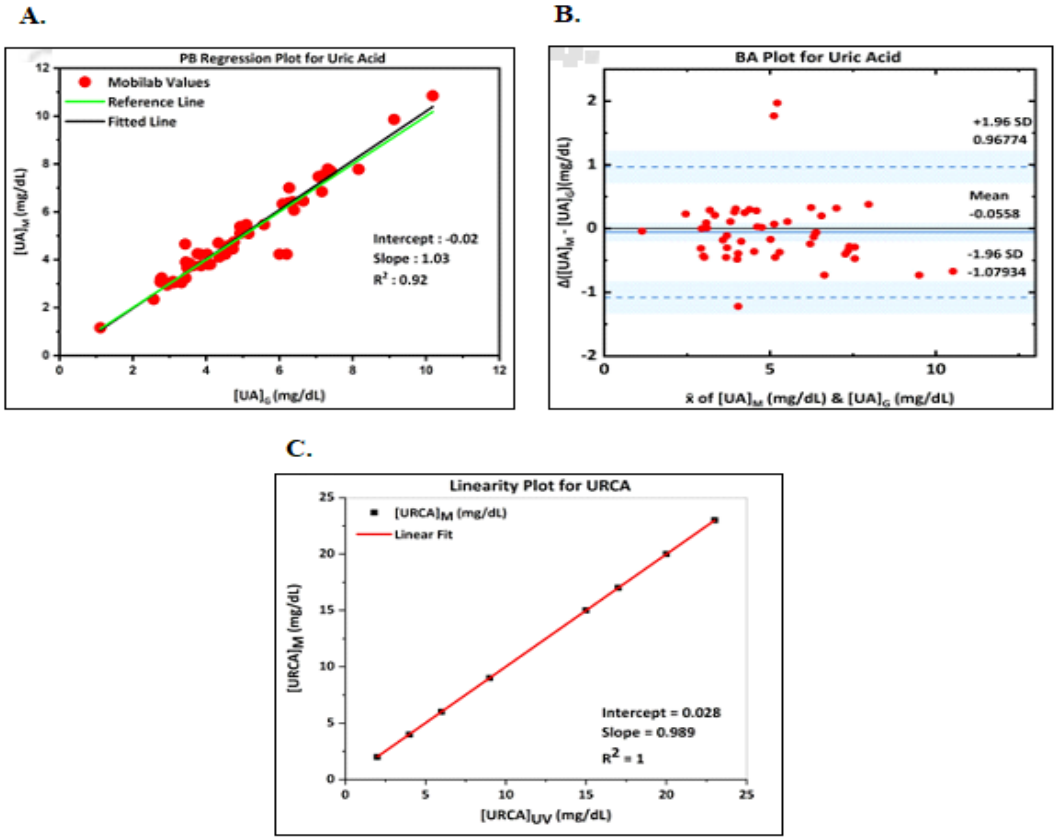

Figure 25: Method comparison between Mobilab and SDA, in terms of UA as a test parameter. (A) Passing–Bablok regression analysis plot: The UA concentration measured in

patient serum is plotted on the x-axis as [UA]G(mg/dL) from SDA and on the y-axis as [UA]M (mg/dL) from Mobilab. The reference line is shown in green, and the fitted line is in black. Red dots indicate the values obtained from Mobilab. The regression analysis results in intercepts = -0.02, slope=1.03, R^2 = 0.92. (B) Bland–Altman plot for interrater agreement analysis: The difference in the measurement of CHOL in two devices (Mobilab and SDA) are plotted on the y axis as Δ([UA]M – [UA]G) (mg/dL) and average of measurement from both the devices are plotted on the x axis as (x of [UA]M (mg/dL) & [UA]G (mg/dL). Limits of Agreement are shown as dotted blue lines, upper limit = 0.967 and lower limit =-1.079 with 95% confidence intervals, mean of differences or bias represented as solid line with 95% confidence interval, (C) Linearity plot: The plotting of concentration ranges for test parameter in Mobilab on the y-axis as [UA]M (mg/dL) against the UV-spectrophotometer readings on the x-axis as [UA]Spectro (mg/dL) resulted a linear measurement with the slope value of 0.989, intercept of 0.028 and R^2 value of 1.

3.3.5. Creatinine (CRE)

(a) Method Comparison

A method comparison study is performed to evaluate the agreement between Mobilab and the SDA for CRE using the P-B Regression plot [Figure 26 (A)] 50 samples. The resulting slope (0.96), intercept (0.02), and R^2 (0.98) values from the plot indicate a strong correlation between the two techniques. Further comparison with B-A Plot analysis Figure 26 (B)] shows a low mean bias (0.01 mg/dL) within -0.41 mg/dL to 0.44 mg/dL, which is a narrow limit of agreement (LOA), suggesting a good agreement between the results of the two methods. The t-test p-value for CRE results is 0.65, which is well above the significance level of 0.05 (Table 19). This indicates that the null hypothesis is acceptable, meaning there is no significant difference between the methods used by Mobilab and the SDA.

(b) Analytical Sensitivity

LOB for the CRE test in Mobilab is measured to be 0.24 mg/dL. On the other hand, the LOD for CRE in Mobilab is found to be 0.33 mg/dL, signifying that Mobilab can detect CRE concentration as low as 0.33 mg/dL accurately (Table 19).

(c) Linearity

CRE concentrations ranging from 0.34 mg/dL to 24.16 mg/dL are plotted with values of UV-visible spectrophotometer values on the X-axis and Mobilab values on the Y-axis. It is noted that the concentrations are along a straight line, with an R^2 of 0.99, a slope of 1.01, and an intercept of 0.02, indicating that the Mobilab device can provide accurate results across a wide range of CRE concentrations as indicated in the Table 19 and Figure 26 (C).

(d) Intra-day precision study

An Intra-day precision study for CRE test in Mobilab is conducted with 20 repetitions, and the CV% is found to be approximately 2.66% for L1 and 2.92% for L3 control serum, respectively. The study indicates that the device gives consistent results and has notably low precision (Table 19).

(e) Performance Matrices

The performance matrices for CRE show a sensitivity and specificity of 96.30% and 95.65%, respectively. A positive predicted value of 96.30% implies that the likelihood of the device accurately predicting a positive value as positive is 96.30%. The negative predictive value result implies that the device predicts a true negative value as negative correctly up to 95.65% of the time. A diagnostic accuracy of 96% implies that 96 out of 100 times, the device accurately determines the concentration of CRE. Therefore, based on the statistical measures, we confirm the overall agreement between the SDA and Mobilab test results. The data used for these calculations is provided in Table 19.

The data of analytical sensitivity reports low LOB (0.24mg/dL) and LOB (0.33mg/dL) values for the CRE test. The linearity test data report a broad linear range for CRE. The intra-day precision study proves that the data obtained for 20 runs is consistent and repeatable. The performance matrices data proves the substantial efficiency of the device (Table 19).

Table 19. Summary of The Comparison Study For CRE: Method Comparison Between Mobilab and SDA, Analytical Sensitivity, Linearity, Intra-Day Precision, And Performance Metrics

Creatinine (CRE)						
Method Comparison	**Passing Bablok Plot**			**Bland Altman plot**		**t-test**
	Slope	**Intercept**	**R^2**	**Bias(mg/dL)**	**LOA (mg/dL)**	**p-value**
	0.96	0.02	0.98	0.01	-0.41 to 0.44	0.65
Analytical Sensitivity	**LOB (mg/dL)**			**LOD (mg/dL)**		
	0.24			0.33		
Linearity Study	Slope		Intercept	R^2	Linearity (mg/dL)	
	1.01		0.02	0.99	24.16	
Intra-Day Precision	%CL1			%CL3		
	2.66			2.92		
Sensitivity	96.30%					
Specificity	95.65%					
Diagnostic accuracy	96%					

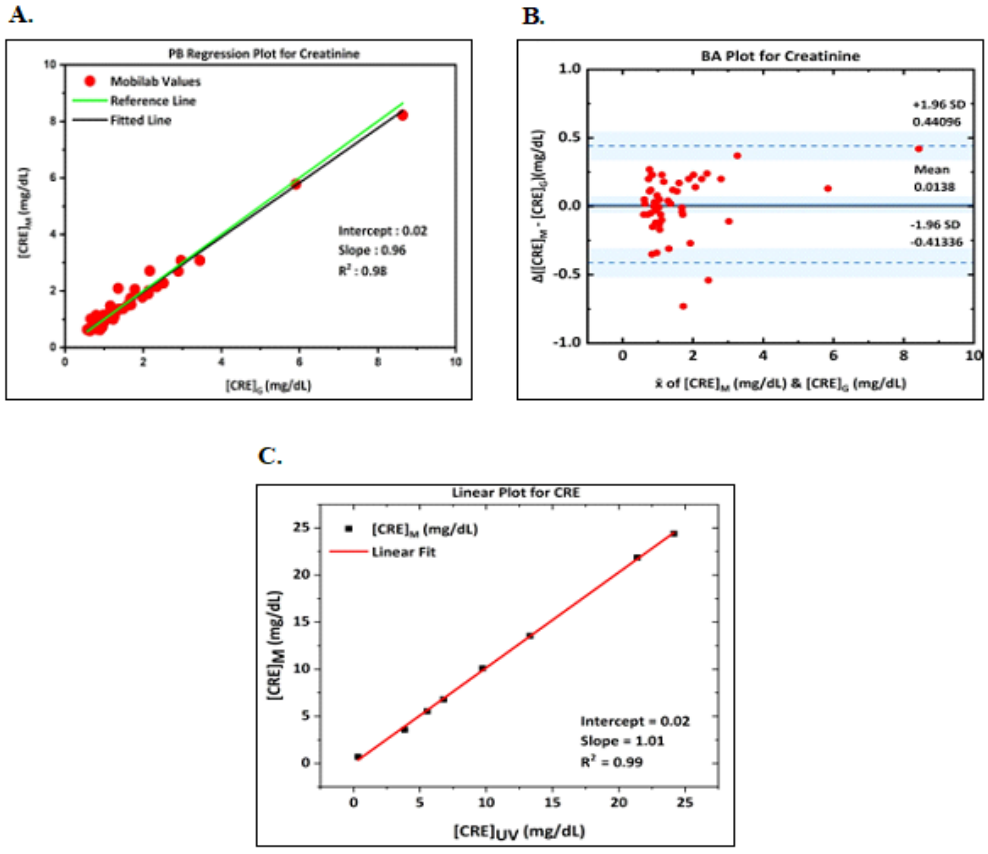

Figure 26: Method comparison between Mobilab and SDA, in terms of CRE as a test parameter**.** (A) Passing–Bablok regression analysis plot: The CRE concentration measured in

patient serum is plotted on the x-axis as [CRE]G(mg/dL) from SDA and on the y-axis as [CRE]M (mg/dL) from Mobilab. The reference line is shown in green, and the fitted line is in black. Red dots indicate the values obtained from Mobilab. The regression analysis results in intercepts = 0.02, slope=0.96, R^2 = 0.98. (B) Bland–Altman plot for interrater agreement analysis: The difference in the measurement of CRE in two devices (Mobilab and SDA) are plotted on the y axis as Δ([CRE]M – [CRE]G) (mg/dL) and average of measurement from both the devices are plotted on the x axis as (x of [CRE]M (mg/dL) & [CRE]G (mg/dL). Limits of Agreement are shown as dotted blue lines, upper limit = 0.4409 and lower limit = -0.4133 with 95% confidence intervals, mean of differences or bias represented as solid line with 95% confidence interval, (C) Linearity plot: The plotting of concentration ranges for test parameter in Mobilab on the y-axis as [CRE]M (mg/dL) against the UV-spectrophotometer readings on the x-axis as [CRE]Spectro (mg/dL) resulted a linear measurement with the slope value of 1.01, intercept of 0.02 and R^2 value of 0.99.

3.4 Conclusions

This study provides a comprehensive analytical and clinical evaluation of Mobilab, a portable blood-testing analyzer designed for point-of-care diagnostics. By comparing Mobilab's performance with that of a fully automated laboratory analyzer using retained patient samples from GNRC Hospital, the investigation establishes strong evidence supporting its diagnostic accuracy and operational reliability. The quantification of key biochemical markers, cholesterol (CHOL), triglycerides (TGL), low-density lipoprotein cholesterol (LDL-C), uric acid (UA), and creatinine (CRE), demonstrates close agreement with the reference analyzer, reflecting Mobilab's capability to produce clinically meaningful results across multiple diagnostic categories. Accurate absorbance measurement in the developed POCT platform has been achieved through constant-current LED control and PID-regulated thermal incubation. Optimization of the optical path length and maintenance of stable incubation at 37°C improve the analytical sensitivity and reproducibility, reducing creatinine assay error from approximately 19% to 1.5%.

Repeatability studies conducted over 20 consecutive runs using BIO-RAD Liquid Assayed Multiqual control serum (Levels 1 and 3) yielded coefficients of variation (CV%) consistently below 5% for all parameters, indicating high precision and minimal measurement variability. The device further exhibited robust diagnostic strength, with calculated Sensitivity, Specificity, Positive Predictive Value (PPV), Negative Predictive Value (NPV), and Diagnostic Accuracy (DA) all exceeding 90%. These findings confirm Mobilab's ability to reliably detect both normal and abnormal analyte concentrations, thereby supporting its utility in clinical decision-making.

Although occasional outliers were observed, these are likely attributable to factors such as sample degradation, pre-analytical variability, or mishandling during transport or processing. Importantly, such occurrences did not significantly impact overall performance metrics, underscoring the stability and robustness of the system. The clinical validation of the Mobilab platform is associated with challenges such as delays in obtaining ethical approvals and dependence on the availability and proper storage of retained clinical samples. Despite these limitations, successful analytical and clinical evaluations demonstrate the feasibility of the platform for decentralized point-of-care testing applications.

Overall, this investigation highlights Mobilab's potential as a dependable diagnostic tool for a broad spectrum of biochemical parameters associated with non-communicable diseases (NCDs). Its portability, affordability, rapid turnaround time, and compatibility with minimally resourced environments position it as a transformative solution for remote and resource-constrained areas (RCAs). By enabling accessible, reliable, and real-time biochemical testing at the point of care, Mobilab has the capacity to strengthen community health systems, facilitate early disease detection, and support timely interventions—thereby contributing meaningfully to improved public health outcomes.

CHAPTER 4

DESIGN AND DEVELOPMENT OF CENTRIFUGAL MULTIPLEXER FOR TARGETING FRUGAL POCT

Abstract

This study reports the development and validation of a low-cost, 3D-printed centrifugal multiplexer (CM) for point-of-care biochemical analysis. The CM integrates interconnected microchambers and microchannels to enable precise volume dispensing, centrifugal transport, in-situ mixing, and reagent–analyte reactions within a single platform. The device is compatible with a portable centrifuge and smartphone-based optical detection, allowing multiple analytical steps to be performed in one unit.

The analytical performance of the CM is demonstrated through colorimetric estimation of total protein using Biuret's reagent and albumin using the bromocresol green method. Calibration was performed using known analyte concentrations, and optimized centrifugation facilitated controlled fluid handling and reaction within sensing chambers. An LED-based illumination system and smartphone imaging were used to capture color variations corresponding to analyte concentrations.

The CM exhibited an average intra-device variability of 1.56%, with variation as low as 0.42%, and showed strong linearity across clinically relevant concentration ranges for both analytes. The results confirm the feasibility of combining 3D printing, centrifugal microfluidics, and smartphone imaging for quantitative biochemical testing. The proposed platform offers a scalable and cost-effective approach for multi-analyte point-of-care diagnostics, particularly suited for resource-limited settings.

This chapter is published in ***IEEE Journal on Flexible Electronics (J-FLEX),*** *vol. 2, no. 5, pp. Sept. 2023, doi: 10.1109/JFLEX.2023.3291332.*

4.1 Introduction

The modern therapeutic practices in healthcare demand accurate and real-time diagnosis of various biomarkers to mitigate life-threatening diseases at their early stage and at the patient's site [243-245]. Presently, centralized laboratories equipped gold standard instruments like the automated or semi-automated analyzers or ELISA/RTPCR kits have been serving such purposes in a localized manner. These high-end automated systems in general facilitate a large-scale estimation of diverse health parameters ranging from molecular diagnostics to the detection of disease specific biomarkers. However, these instruments are in general bulky and integrated with complex parts and electronic control systems, which needs trained technicians for the operations as well as analysis [246, 247]. Even the simpler and widely employed semi-automated biochemistry analyzers require multi-step sample preparation and analyses methodologies using test tubes, cuvettes, micro pipettes, among others. Such requirements not only make these devices more prone to pre-analytical errors [248, 249] but also enforces the system to be more skill dependent, resource intensive, costly and isolated. In order to address such issues, in the recent years, integrated microfluidic platforms have emerged targeting in-vitro diagnostics. These platforms enable point-of-care (POC) volume metering, collection of samples, in-situ separation and mixing of reagents with the samples, analysis and finally displaying the test results.

For example, prior-art indicates the presence of such platforms for plasma separation, DNA extraction, immunoassays, and analyte detection [250-253]. Further, the centrifugal disc based POC platforms like Abaxis Piccolo, Skyla HB1, ed Elisa systems from Samsung are already available at the commercial levels [254]. However, such systems are also facing major challenges due to the complex design issues of the discs, automated driving and analysis processes, which eventually increases the cost and skill requirement for any resource constraint setting [255-257]. In one way or other, these factors limit the accessibility of

healthcare diagnostics to remote corners of the world especially to the primary or subsidiary health centers (PHCs or SHCs).

The recent advent of the point-of-care-testing (POCT) platforms are directed towards mitigating such problems owing to their ease of use, frugality and simplicity [258–260].

These kits are majorly employing simple or gold standard colorimetry, electrochemistry, fluorimetry, microfluidics lab-on-a-chip techniques for the early detection various chronic diseases at the patient's site [264-268]. In particular, most of these POCT devices are meant for single parameter with either two to three step operating procedures. Again, training and adoption, maintenance of the health protocols, standardization of sample collection method, and real-time data aggregation remain some of the major challenges for the modern day POCT devices [269-271]. Importantly, in the recent years, the advent of 3D printing, smartphones, integrated circuits, system on chips, and internet of things (IoT) have opened up the possibility to overcome of some of these challenges related to the POCT devices. Integration of such newer technological paradigms in the POCT devices is expected to promote a wider connectivity alongside real-time data collection and analysis, which will not only reduce human interventions and related errors but also may enable instant delivery of more accurate test results at the patient's site. In a way, such advancements in at the POCT levels are envisioned to provide evidence backed disease control in a more efficient and inexpensive manner even at resource constraint environments [272]. In view of the background, we report an economic, 3D printed centrifugal multiplexer (CM) for POCT of non-communicable diseases (NCDs). The platform is inexpensive to fabricate, easy to operate, mitigate pre-analytical errors like reagent handling, mixing and manual data logging. The reusable CM, a centrifuge, and a smartphone enabled detection module together constitute the system for diagnosis of liquid reagent-based biomarker analysis. In particular we focus on two markers, albumin and total protein, to show the efficacy of the CM in handling multiple markers inside a single platform. It is well known that abnormality of human serum albumin is an important

marker for liver, coronary heart disease, diabetes, liver cirrhosis, nephrotic syndrome, CKD and other diseases [273]. Similarly, proteinuria is a condition that resembles high protein concentration in human urine and an essential indicator for early chronic kidney disease (CKD) [274,275]. Thus, we consider these parameters as tests cases to demonstrate the effectiveness of the CM.

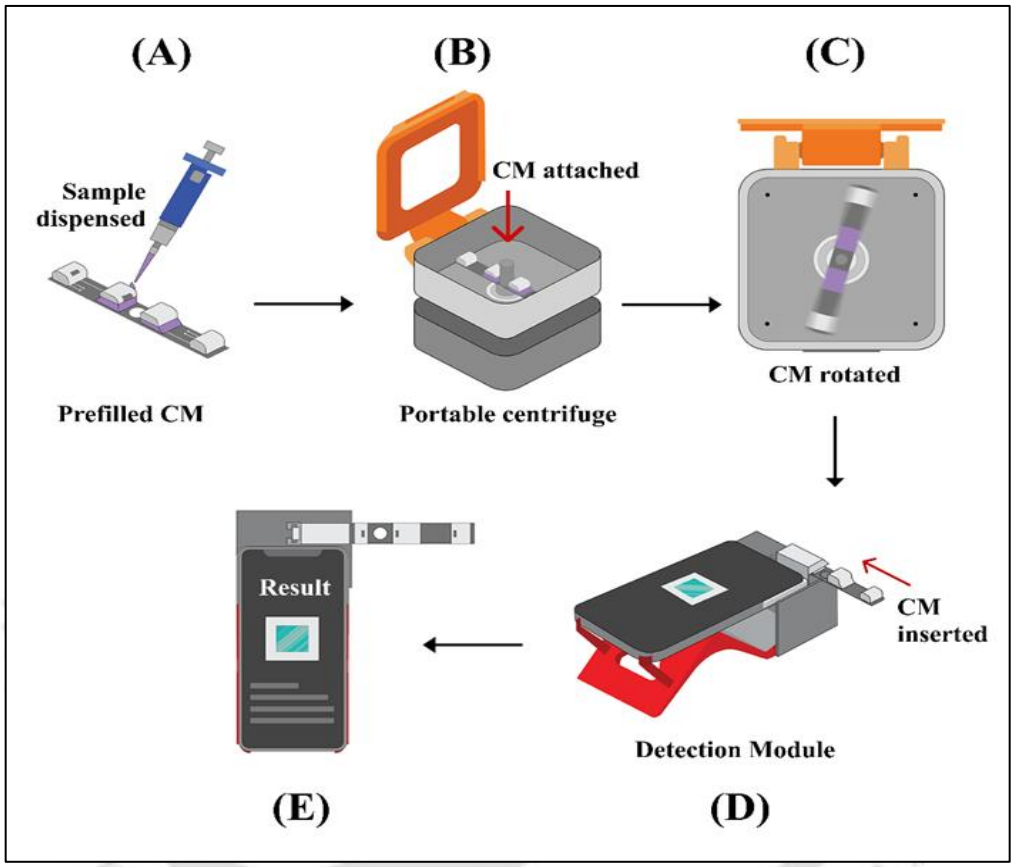

Figure 27: Workflow of the centrifugal multiplexer (CM)–based point-of-care diagnostic platform. (A) Dispensing of a defined volume of biological sample into a prefilled centrifugal multiplexer (CM) containing the required liquid reagents. (B) Insertion of the CM into a portable centrifuge, enabling secure attachment and alignment. (C) Centrifugal rotation of the CM, facilitating controlled reagent–sample mixing and transfer into the sensing microchamber. (D) Insertion of the CM into a smartphone-enabled optical detection module for colorimetric analysis. (E) Image acquisition and digital processing via a mobile application to generate quantitative test results in real time.

The schematic illustrations in Figure 27 images (A) to (G) shows the overall process proposed. In (A), the sample is pipetted in the collection microchamber of definite volume, which is prefilled with another reagent to be mixed before placing in the centrifuge to spin the CM, as shown in images (B) and (C), and supporting video 1. With the centrifugation the sensing microchamber gets filled and develops the color, then the CM is detached from the centrifuge and inserted into the detection module (D). The detection module is composed of a light source (e.g. light emitting diode – LED) to illuminate the chamber while the transmitted light passing through the CM is diverted to the smartphone camera. Thereafter, the image is captured and analysed to calculate the respective absorbance equivalent (Ae) values, as shown in figure (E). The variations in intensity of the color at the sensing microchamber is found to have direct correlation with the concentration of the total protein and albumin. The images are analysed in the mobile phone wherein the variation in the color intensity has been further correlated with the specific concentration of the analyte. The integrated system allows the dispensation of a definite volume of reagent, instant mixing and reaction, accurate image analysis, and real-time reporting of the results at the patient's site.

The Chapter 4 extends the central theme of this thesis on frugal, decentralized, and digitally connected point-of-care testing (POCT) systems by addressing limitations associated with manual fluid handling and multiplexed biochemical analysis. While Chapter 2 focuses on the development of the portable spectrophotometric detection system and Chapter 3 demonstrates its clinical validation using selected biomarkers, Chapter 4 introduces a centrifugal microfluidic multiplexer as a complementary module for future Mobilab-type platforms. The proposed system supports automated sample-reagent transport, reduced manual pipetting, controlled volume metering, multiplexed detection, and smartphone-based optical analysis, thereby improving workflow automation and reducing pre-analytical variability in portable POCT applications.

4.2 Materials and Methods

4.2.1 Materials

All the chemicals used in this experiment were received in their original form and were not modified or processed further. This included bovine serum albumin (BSA) (HiMedia, India), bromocresol green (BCG) (Sigma Aldrich, USA), and total protein (Agappe, India). The chemicals were of analytical grade and were used as received. Deionized water used in the experiment was obtained from a MilliQ Millipore system with 18.2 MΩcm resistivity (Millipore, Burlington, USA). The smartphones Redmi 9A (Xiaomi India), Poco C3 (Xiaomi, India) and Realme Narzo 20 (Realme, India) were procured from Amazon.in. DC Motor, LED, DC Driver Circuit, Esun PLA filament were procured from Robu.in.

4.2.2 Microfluidic CM Design and fabrication

The centrifugal CM was fabricated using 3D Printing, the designs were done in Fusion 360 (Autodesk, San Rafael, USA). The CM consisted of two pairs of collection and sensing microchambers, each capable of holding a maximum volume of 500 µL. The respective collection and sensing microchamber were coupled with microchannel network of width and depth of 500 × 500 µm and two air outlets. The design was exported to '.stl' format and then imported to Ultimaker Cura 5.0 (Ultimaker, Netherlands) for slicing and convert it into '.gcode' . This was further fed to a fusion deposition modeling-based 3D printer, Ender 3 V2 (Creality, Shenzhen, China). The CM was fabricated on a glass bed with a nozzle temperature of 200ºC and at a bed temperature of 65ºC, using a transparent poly-lactic acid (PLA) filament from ESun (ESun, China). The use of a glass bed resulted in a clearer bottom surface on the CM, making resolution of the acquired image better. Once the 3D Printing was complete, the adhesion brim was removed and CM was ready for experimentation. Further, we compared the centrifugal force in radial direction to the transversal Coriolis force with the characteristics of water in a microchannel of width 500 µm [71], using the formula:

$$F_c/F_\omega = (\rho \Delta x^2 \omega)/4\eta. \quad (1)$$

where, F_c, F_ω, ρ, Δx^2, ω, and η are Coriolis force, centrifugal force, density of water, channel width, angular velocity, and viscosity, respectively. The calculation shows that the ratio is $6.25\times10^{-4}\,\omega$, which indicates that, theoretically, for angular frequencies above ~16 rad/s (~152 rpm), Fc will be dominant.

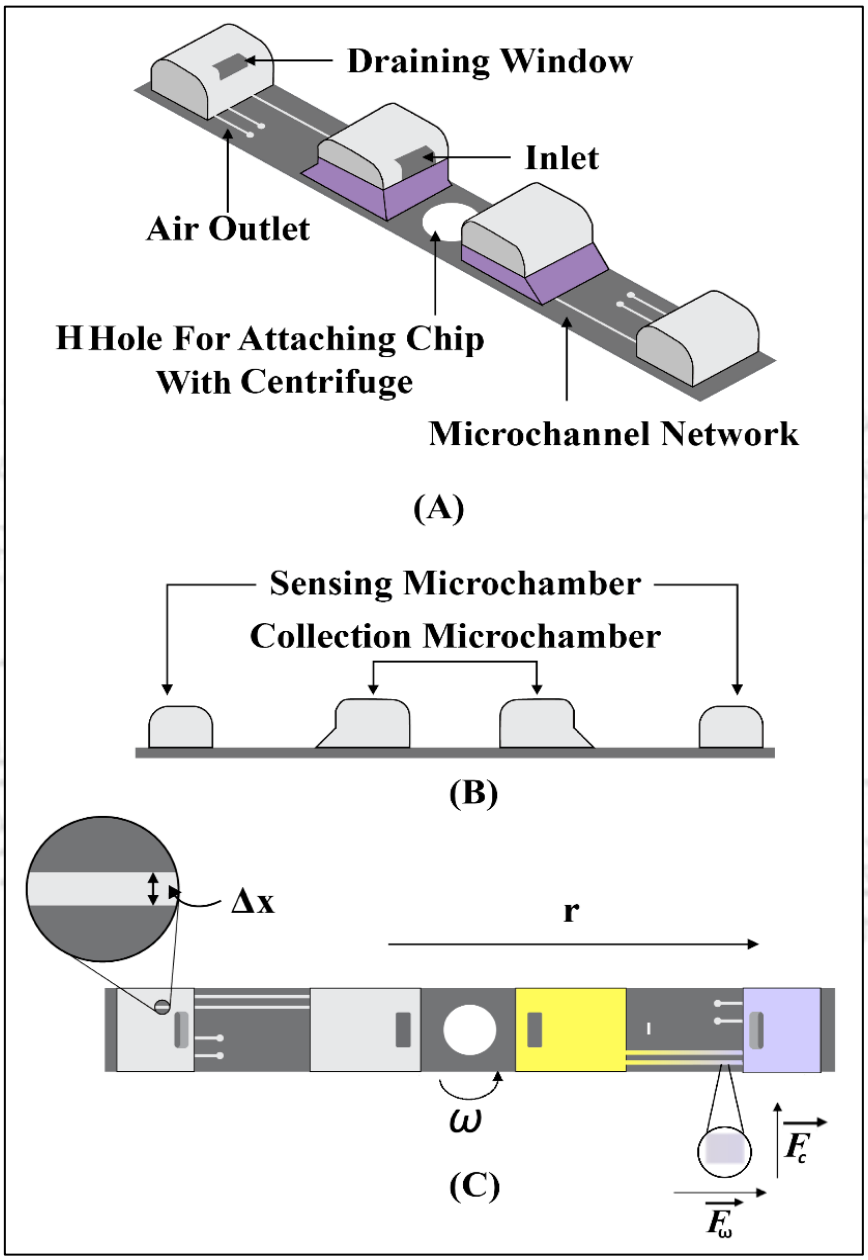

Figure 28: Structural design and operating principles of the centrifugal multiplexer (CM). (A) Isometric view of the centrifugal multiplexer highlighting key structural features, including the sample inlet, microchannel network, air outlet, draining window, and attachment hole for secure mounting onto the centrifuge. (B) Cross-sectional view of the CM illustrating the arrangement of paired collection microchambers and sensing microchambers along the device length. (C) Schematic representation of the forces acting on the CM during centrifugal

operation, indicating angular velocity (ω), radial distance (r), fluid displacement (Δx), and the resulting centrifugal force (Fc) acting on the fluid elements.

Figure 28 presents the design architecture and fluidic operation of the centrifugal multiplexer (CM). The isometric representation (A) details the integrated microfluidic features that enable controlled sample handling, reagent transport, air venting, and fluid drainage under centrifugal actuation. The attachment hole ensures stable positioning of the CM within the centrifuge during rotation. Panel (B) depicts the internal layout of the CM, comprising paired collection and sensing microchambers designed to facilitate precise volume metering, reagent mixing, and analyte detection. Panel (C) illustrates the physical forces governing fluid motion during centrifugation, where rotation at angular velocity ω generates a centrifugal force proportional to the radial distance r, driving fluid displacement (Δx) from the collection chamber toward the sensing chamber. This centrifugal-force-driven transport enables passive, pump-free fluid manipulation and reliable assay execution within the CM.

2.2.3 Portable centrifuge

The portable centrifuge was designed using Fusion 360 (Autodesk, San Rafael, USA) and 3D printed with Ender 3 V2 (Creality, Shenzhen, China). The system included a DC motor that rotated the CM at 1000 RPM, along with a control PCB, and a power unit that could power the device for two days on a single charge. The bottom portion of the housing contained the electronics components and control circuit, while the top portion was used to attach the CM, as shown in Figure 28. The system had a mass about 500 g and dimensions of 120 mm × 120 mm × 100 mm.

Figure 29 presents the internal configuration of the portable centrifuge used for operating the centrifugal multiplexer (CM). The upper section accommodates the CM and ensures secure positioning during rotation, while the protective lid provides mechanical stability and user safety. The lower section contains the electronic subsystems, comprising a DC motor

responsible for rotating the CM at controlled speeds (up to ~1000 RPM), a control printed circuit board (PCB) for speed regulation and system control, and a rechargeable battery-based power unit. The centrifuge operation is wirelessly controlled through a smartphone interface, enabling precise and repeatable centrifugal actuation for microfluidic assays.

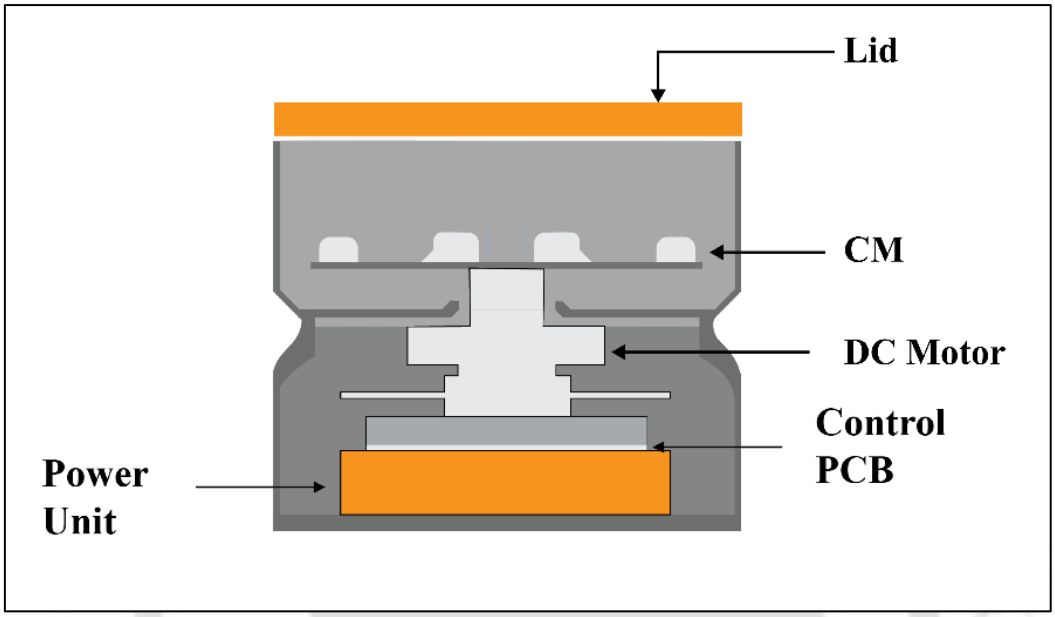

Figure 29: Cross-sectional architecture of the portable centrifuge for CM operation. Cross-sectional schematic of the portable centrifuge illustrating the placement of the centrifugal multiplexer (CM) in the upper compartment beneath a protective lid, while the lower compartment houses the electronic components, including the DC motor, control PCB, and power unit.

2.2.4. Detection Module

The detection module [Figure 30 (A)] is attached with the smartphone (Redmi 9A Sport), in order to acquire the image of the sensing microchamber. This module was designed in Fusion 360 (Autodesk, San Rafael, USA) and 3D printed with Ender 3 V2 (Creality, Shenzhen, China). It consists of a phone holder and a periscopic mirror arrangement wherein two mirrors kept perpendicular to each other. The transmitted light passing through the sensing window it directed towards the smartphone camera that acquired the image of the sensing microchamber, as shown in Figure 30 (B). In most of the image analysis based POCT devices the major issue is the image quality. The light arrangement eliminates the possibility of the errors that may arise due to the adequacy or inadequacy of light on the chamber during

the image capturing. This image is further processed and segmented using K-Means-Clustering technique, then a summarization of the dominant color is done in order to obtain

the RGB channel images, the color intensities are obtained for calculating the Ae of the sample with respect to reagent color intensity value (blank reading), for a specific channel e.g., R channel for albumin as shown in Figure 23 (C).

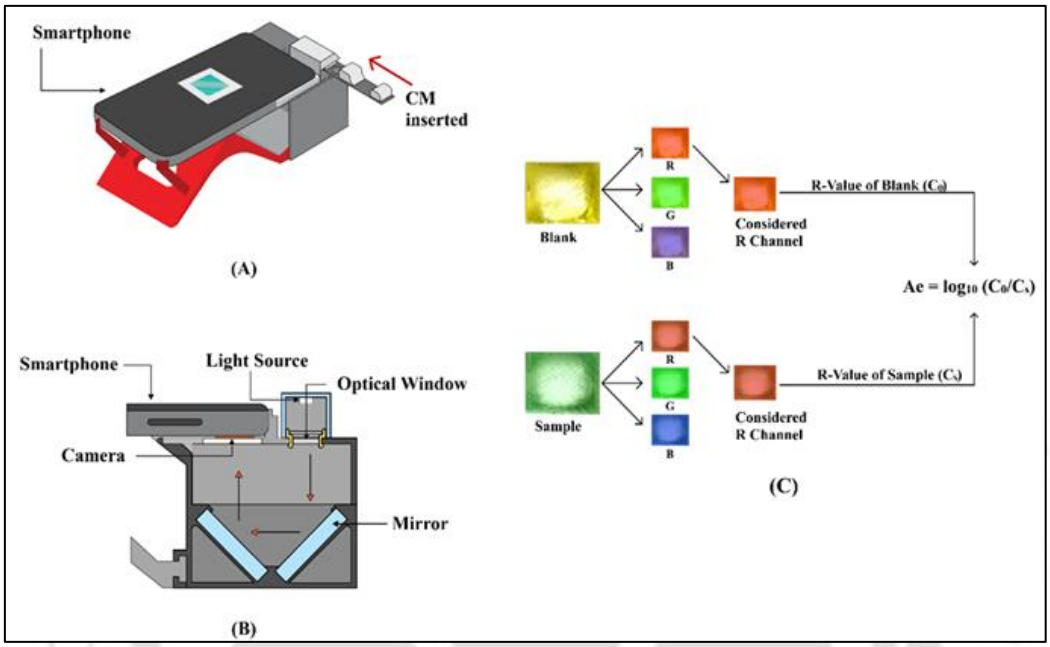

Figure 29: Smartphone-enabled optical detection module and image-based quantification workflow. (A) Isometric view of the smartphone-integrated optical detection module with the centrifugal multiplexer (CM) inserted into the sensing slot. (B) Cross-sectional schematic illustrating the optical working principle, where an LED light source illuminates the sensing microchamber and the transmitted light is redirected via two mirrors oriented at 90° toward the smartphone camera through an optical window. (C) Image analysis workflow showing extraction of RGB channel intensities from blank and sample images, with the red (R) channel selected for quantification and absorbance-equivalent (Ae) calculation.

Figure 30 illustrates the design and operational principle of the smartphone-enabled optical detection module used for colorimetric analysis. As shown in (A), the CM is inserted into the detection module, which aligns the sensing microchamber with the smartphone camera. In (B), an integrated LED provides uniform illumination across the sensing chamber, while transmitted light is reflected by two 90° mirrors and directed to the camera, enabling a

compact optical path. Panel (C) describes the digital image analysis process, wherein RGB channel values are extracted from both blank and sample images. The red channel intensity is selected for analysis, and absorbance-equivalent values ($Ae = \log_{10}(C_o/C_s)$) are computed, allowing quantitative determination of analyte concentration. This configuration enables portable, low-cost, and real-time diagnostics at the point of care.

2.2.5 Experimentation methodology

Once the CMs were 3D printed, the adhesion brim was removed and the CMs were used for testing immediately. During the experiment, we used one of the microchamber pair (named as CA) for the base reading and another microchamber pair (named as CB) for the analyte reading. The collection microchambers CA and CB were pre-filled with 350 µl of respective reagents. For albumin and total protein, a stock solution was prepared from about 10 g/L solution Bovine Serum Albumin (BSA) in 1% sodium chloride solution, further diluted to obtain 9 known concentrations of the sample. 3.5 µl from the prepared sample solution of BSA were dispensed in the pre-loaded collection microchambers of the CM. After centrifugation 1000 RPM for 10 seconds as shown in Figure 27, the sensor microchamber showed purple coloration from the initial bluish coloration for total protein and from yellowish coloration to bluish green coloration for albumin. The intensity of the coloration for both the proteins found be increasing, with increase in their concentration. This increase of intensity was further quantified in terms of, Ae with the smartphone enabled detection module. The CM was inserted into the detection module, where the sensor microchamber was illuminated from above with a white LED, the transmitted light was then diverted 180º by the periscopic mirror arrangement as schematically illustrated in Figure 30. The resulting image was captured using the primary camera of the smartphone in "Pro" mode, with an exposure value of -0.3 and other default settings. Finally, after processing RGB channel color intensity values for both the base reagent and the sample from the respective sensing microchamber were obtained. In case of total protein quantification, the G channel color intensity value (G-

value) of the base reagent was considered as C_0 and G-value of the sample image was considered as Cs, Ae was calculated using the formula below:

$$\mathbf{Ae = log10\ (C_0/C_S)} \qquad \textbf{(Equation 2)}$$

Similarly, for albumin the R channel color intensity value (R-value) of the base and the sample were obtained in order to calculate the corresponding Ae of the dispensed sample.

4.3 Results and Discussion

In the present study, we have fabricated a 3D platform of centrifugable microchambers embedded with microchannels, centrifuge and a smartphone enabled detection module for quantification of biomarkers for disease diagnosis. The CMs are fabricated using FDM technique, where in molten polymeric material here, poly lactic acid (PLA) is deposited layer-by-layer. Since the CMs are 3D printed using FDM methodology, there are, always a degree of variation in the layers formed, as shown in Figure 31 (A). Such variation interferes the optical transmittance of sensing microchamber, creating noise in the acquired image data. Hence, a critical aspect of the CM is that the variation in intensity of light transmitted by the base reagent (I0) from the sensing microchamber should be as minimum as possible, or in other words coefficient of variation (CV), of the sensing microchambers should be as minimum as possible.

Figure 31 (B) shows the average intra-CM variation of 1.56% obtained from CVs of each CM, for which 6 CMs are considered. Collection micro chambers of each of these CM is filled with de-ionized water and centrifuged to fill the sensing microchambers. Then 10 images are acquired from the detection module utilizing a smartphone' (Redmi 9A) camera, for each microchamber. 'G values' are considered for determining the CV, variations were as low as 0.42% with an average of 1.56%. This indicates, that a significant consistency in the CM fabrication is achieved. In the centrifugal multiplexer, rough channel surfaces may therefore influence the reproducibility of fluid transfer from the loading chamber to the sensing chamber. This is particularly relevant for FDM-printed devices because layer-by-layer

printing creates visible ridges and micro-irregularities. These roughness-related limitations have been discussed in Chapter 4, along with future improvements such as SLA printing, surface polishing, solvent vapor smoothing, hydrophilic coating, or injection molding. Interestingly, the surface roughness is an important parameter influencing fluid flow behavior in microfluidic channels, particularly in FDM-based 3D-printed devices. Increased surface roughness can disturb smooth liquid movement, affect capillary pressure, promote air bubble entrapment, and introduce variability in reagent-sample transport and mixing. In the developed centrifugal multiplexer, layer-by-layer fabrication produced micro-irregularities that could influence flow reproducibility and burst behavior. Future improvements such as SLA printing, surface polishing, and hydrophilic surface modification may help reduce these flow-related variations and improve microfluidic performance.

4.3.1. Sensing methodology

The detection of albumin and total protein are based on the principles of colorimetry, where initially the collection microchambers of the CM is pre-loaded with respective reagents, then centrifuged to fill the sensing microchamber for the base reading (Blank), as indicated in Figure 31 (A). The detection of albumin and total protein are based on the principles of colorimetry, where initially the collection microchambers of the CM is pre-loaded with respective reagents, then centrifuged to fill the sensing microchamber for the base reading (Blank), as indicated in Figure 31 (A). In the next step, another CM is prefilled with reagent and sample is dispensed in the same chamber and after centrifugation of the CM the color change is observed in the sensing microchamber which is further quantified with the smartphone enabled detection module. The reaction between Biuret's reagent that contains copper II sulphate and peptide bonds of total protein led to the formation of purple colored complex. The CMs are then centrifuged at 1000 rpm for 10 s that led to flow of the fluid along with to in-situ mixing within the microchannels, to the sensing microchamber. It is then

inserted in the smartphone enabled detection module with an embedded white LED that illuminates above the sensing microchamber of the CM. Image is captured by the smartphone camera for quantification of the intensity of the color and to provide the final result. The acquired images indicate a gradual increase in intensity of the purple coloration with concentration of the reagent, as shown in Figure 32 (A).

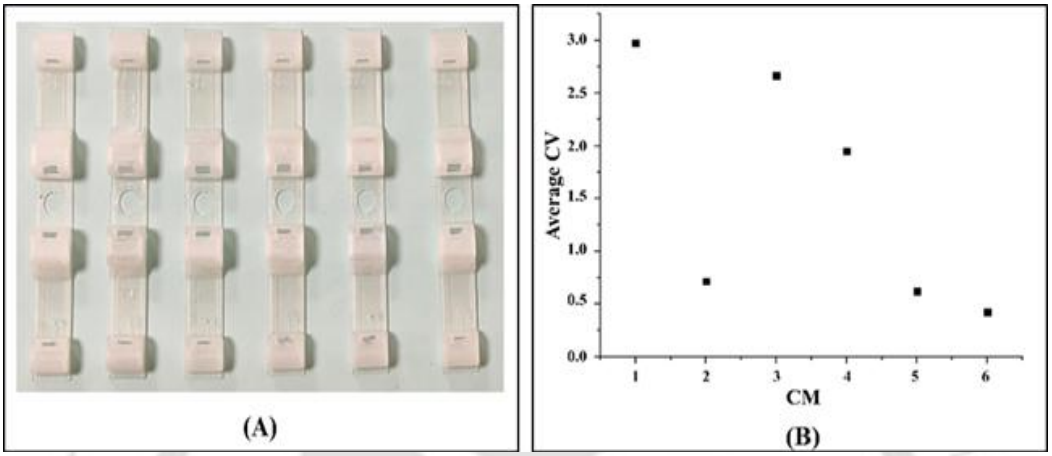

Figure 30: Fabrication consistency and intra-device variability of the 3D-printed centrifugal multiplexer (CM). (A) Photograph of multiple 3D-printed centrifugal multiplexers prefilled with reagents, showing clearly identifiable collection microchamber inlet, sensing microchamber, and outlet regions. (B) Plot showing average intra-CM coefficient of variation (CV) obtained from six independently fabricated CMs.

Figure 30 demonstrates the fabrication reproducibility and performance consistency of the 3D-printed centrifugal multiplexer (CM). Panel (A) shows six representative CMs fabricated using the same printing protocol and prefilled with reagents, highlighting uniformity in structural features such as the collection microchamber inlet, sensing microchamber, and outlet. Panel (B) presents the average intra-CM variability measured across the six devices, expressed as coefficient of variation (CV). The mean intra-CM variation was 1.56%, with values as low as 0.42%, indicating high fabrication consistency and reliable assay performance across independently manufactured CMs.

Following this, with K-Means-Clustering, the specific sensing area is segmented from the overall image and further summarized for extracting the dominant coloration. From the acquired RGB channel images and the respective color intensities are obtained, a gradual

decrement in the G-value is observed with respect to the increase in concentration of the analyte.

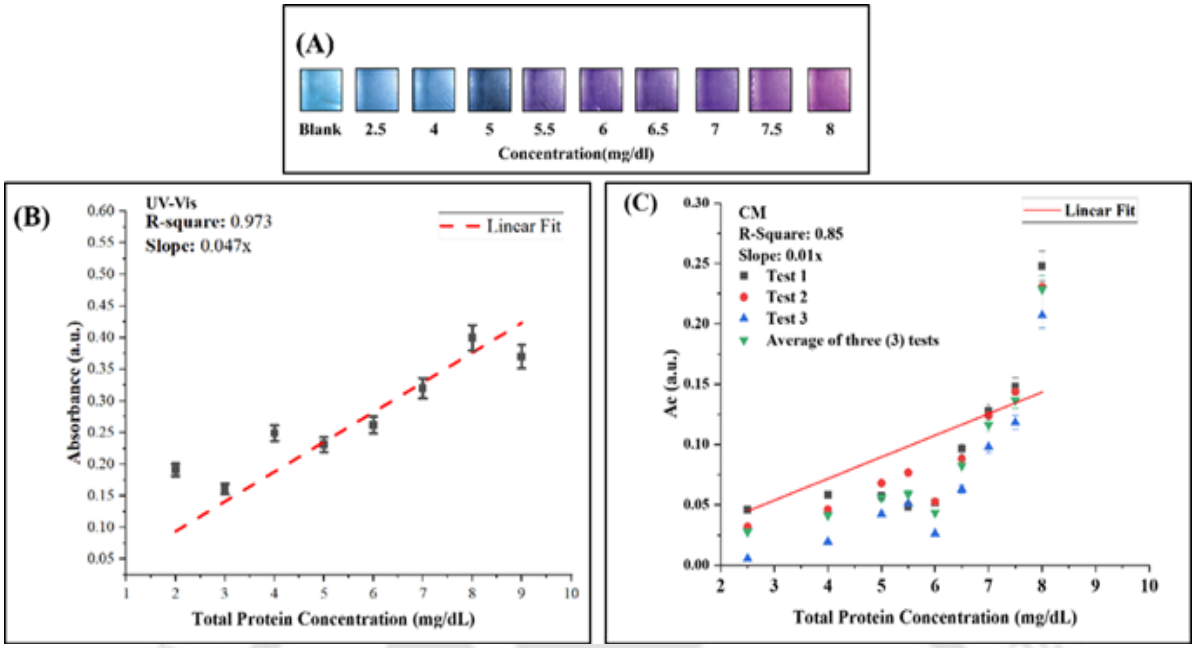

Figure 31: Colorimetric response and analytical performance of the CM for total protein estimation. (A) Representative colorimetric images showing progressive color change in the sensing microchamber of the CM with increasing total protein concentration (2.5–8 mg/dL), including a blank. (B) Calibration plot obtained using a standard UV–Visible spectrophotometer showing absorbance as a function of total protein concentration with linear regression. (C) Calibration plot generated using the CM-based smartphone detection system, showing absorbance-equivalent (Ae) values obtained from three independent tests and their average with linear fitting.

Figure 31 illustrates the colorimetric response and quantitative performance of the centrifugal multiplexer (CM) for total protein analysis. Panel (A) demonstrates a visible and progressive change in color intensity within the sensing microchamber as the concentration of total protein increases, confirming concentration-dependent signal generation. Panel (B) presents the reference calibration obtained using a conventional UV–Visible spectrophotometer, showing a strong linear relationship between absorbance and total protein concentration ($R^2 = 0.973$). Panel (C) shows the corresponding calibration obtained using the CM-based smartphone detection module, where absorbance-equivalent (Ae) values derived from image analysis exhibit good linearity ($R^2 \approx 0.85$) across three independent measurements. The agreement between the benchtop and CM-based results validates the

analytical capability of the proposed platform for quantitative point-of-care total protein estimation.

Initially, G-value acquired from image of the reagent filled sensing chamber is considered as transmitted blank intensity C_0, whereas the G-value of the sample after reaction is considered as the transmitted sample intensity C_S. The *Ae* calculated for each concentration of the total protein sample from equation (2), that is found to reflect an increasing trend with concentration. These experiments are conducted three time for each CM. Another set of experiments with same concentrations, are done with UV-Visible Spectrophotometer (Shimadzu, Japan) to obtain the absorbance value at 600 nm. An apparent linear correlation is observed with $R^2 = 0.85$ and slope 0.01 as indicated in Figure 31 (C), wherein each test is conducted three times. In the following sections, a detailed explanation is presented to shed light on the factors contributing to the observed linearity. Additionally, the result is compared with UV-Visible Spectrophotometer of = 0.97 and slope = 0.047, as indicated in Figure 31 (B). However, there are no definitive conclusions, while conducting experiments using unknown samples at this stage as further optimizations are required for CM fabrication.

Further, CMs are washed with distilled water and isopropyl alcohol and kept overnight for drying. To conduct the albumin test, the CMs are reused with operations similar to total protein. The collection chambers of all the CMs are prefilled with the albumin reagent that consisted BCG, after centrifugation the base color at the sensing microchamber appeared yellowish, as shown in Figure 32 (A). Subsequently, different concentrations of the protein are dispensed, BCG reacted with albumin and resulted in formation of bluish-green coloration in the sensing microchamber with a gradual increasing trend in intensity of the color with the concentration of the protein as shown in the image sets of Figure 32 (A). Quantification of this color change is done from the acquired 'R-value' using equation 2. The obtained values plotted against the concentration which shows an apparent linear correlation with the albumin concentration as indicated in Figure 32 (B) with $R^2 = 0.98$ and slope = 0.17 for UV-Visible

Spectrophotometer and R^2 = 0.90 and slope = 0.06 for CM Figure 32 (C). The comparative results of both the tests, indicates that with the introduction of a factor may improve the accuracy of both the test (e.g., total protein and albumin). Also, it should be taken into consideration that this system will be capable of conducting tests solely with human serum as the sample in the future. Figure 32 demonstrates the colorimetric behaviour and quantitative performance of the centrifugal multiplexer (CM) for albumin estimation. Panel (A) shows a clear and concentration-dependent color transition within the sensing microchamber as albumin levels increase, confirming effective reagent–analyte interaction. Panel (B) presents the reference calibration obtained using a UV–Visible spectrophotometer, exhibiting strong linearity between absorbance and albumin concentration (R^2 = 0.983). Panel (C) shows the corresponding calibration obtained using the CM-based smartphone detection module, where absorbance-equivalent (Ae) values derived from image analysis demonstrate good linearity ($R^2 \approx 0.909$) across three independent measurements. These results validate the capability of the proposed CM platform for reliable, quantitative albumin detection at the point of care.

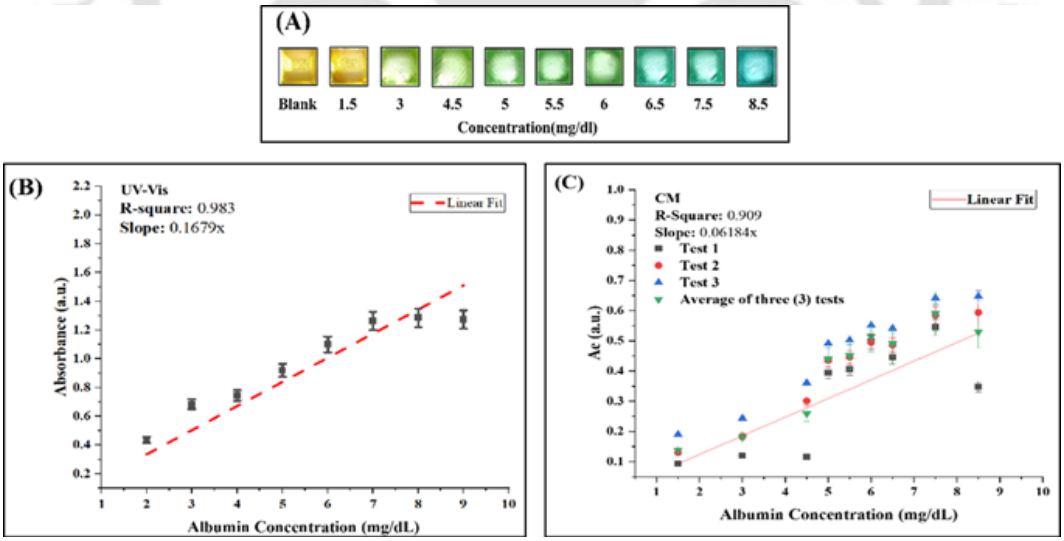

Figure 32: Colorimetric response and analytical validation of the CM for albumin detection (A) Representative colorimetric images showing progressive color change in the albumin sensing microchamber of the CM with increasing albumin concentration (1.5–8.5 mg/dL), including a blank. (B) Calibration curve obtained using a standard UV–Visible spectrophotometer, showing absorbance as a function of albumin concentration with linear regression. (C) Calibration curve generated using the CM-based smartphone detection system,

showing absorbance-equivalent (Ae) values from three independent tests and their average with linear fitting.

Figure 33 presents the experimental validation of the proposed centrifugal multiplexer-based point-of-care diagnostic platform. Panel (A) shows the complete proof-of-concept setup comprising a portable centrifuge for centrifugal actuation, a smartphone-enabled optical detection module, and reusable 3D-printed CMs. Panel (B) highlights the CM design, which allows preloading of analyte-specific reagents into the microchambers, enabling minimal sample handling.

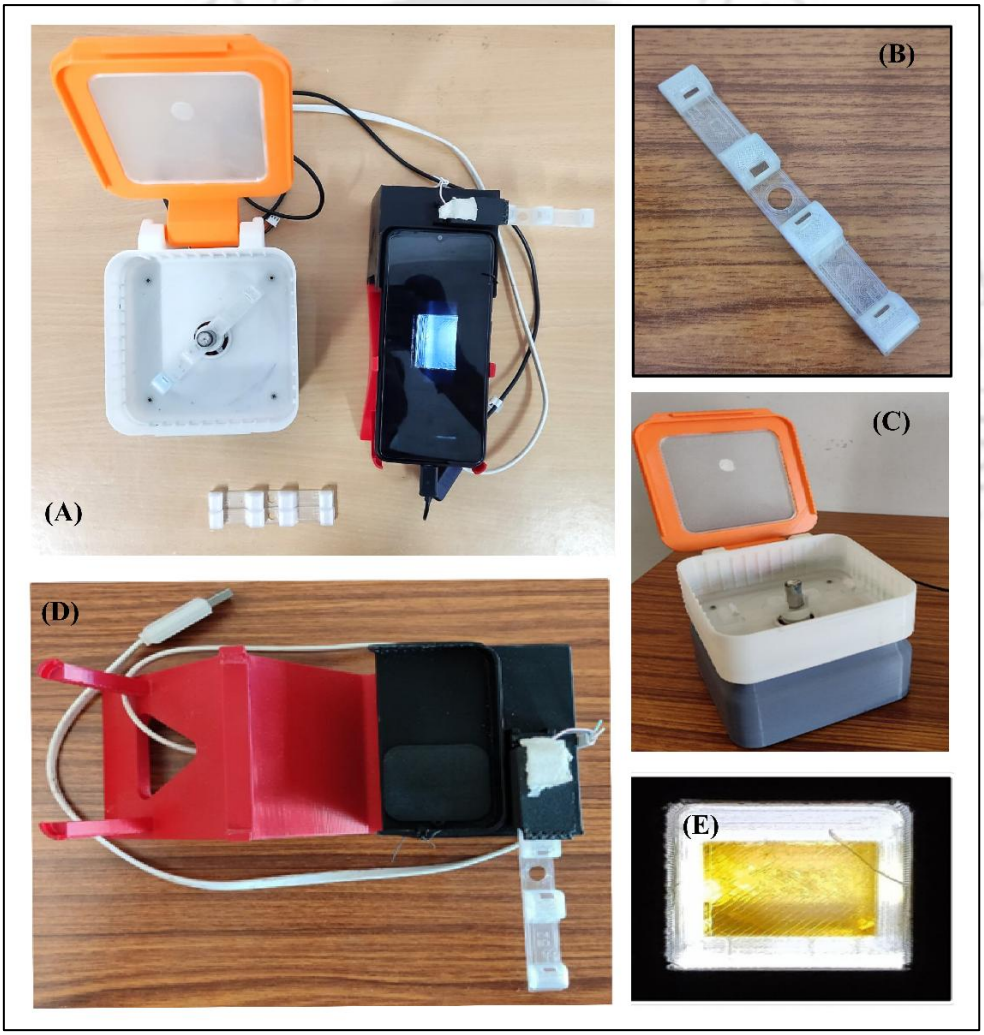

Figure 33: Experimental proof-of-concept setup of the 3D-printed centrifugal multiplexer (CM) platform. (A) Photograph of the complete proof-of-concept experimental setup, including the portable centrifuge, smartphone-based detection module, and multiple reusable centrifugal multiplexers. (B) 3D-printed centrifugal multiplexer showing the collection and sensing microchambers, designed for preloading with liquid reagents. (C) Portable centrifuge

used to rotate the CM during assay execution. (D) Smartphone-integrated optical detection module incorporating a white LED illumination source for colorimetric measurements. (E) Captured image of the sensing microchamber containing albumin reagent after reaction.

Panel (C) depicts the compact centrifuge employed to drive controlled fluid transport within the CM. Panel (D) shows the detection module integrated with a white LED to provide uniform illumination for image-based analysis. Panel (E) illustrates a representative image of the sensing microchamber after reaction with albumin reagent, demonstrating effective color development suitable for quantitative analysis. Together, these components validate the feasibility, portability, and usability of the proposed POCT system. Figure 33 (A), shows the image of the overall setup of the developed proof-of-concept for the proposed CM, which can quantitatively measure albumin and total protein for resource constraint areas. The data can be further transferred to the cloud server for real-time analysis. Figure 33 (B), shows the CM fabricated using 3D printing. Figure 33 (C), is the portable centrifuge that can be wirelessly operated with the smartphone with Bluetooth where one can put the input parameters. The smartphone enabled detection module is shown in Figure 27 (D), that integrated with the smartphone to acquire the image [Figure 33 (E)] and quantify.

4.3.2 Variability of Data Acquisition

In this section, we discuss the variability of data acquisition from the CMs and the factors that influence it. To begin with the CMs are fabricated using FDM 3D printing. The pattern formed at the bottom of the microchambers is a mesh, which varies from CM to CM depending on multiple non-linear factors such as flow rate of the polymer, cooling down and solidification of the polymer and so on. Another factor that affects the results is the smartphone camera system, which consists of the hardware and the image processing algorithm. Different smartphones may have different camera systems, leading to variation in the output images. The images are processed by a standard K-Means-Clustering algorithm that assigns pixels to different color clusters based on their intensity to calculate the values from the images. To investigate the variabilities further, three entry level smartphones: Poco

C3 (Xiaomi, China), Realme Narzo 20 (BBK Electronics, China) and Redmi 9A (Xiaomi, China), are used. To measure the variability of data acquisition from the CMs, we performed an experiment using four CMs and obtained their blank readings. Then, the average coefficient of variation (CV) is calculated for each CM. The results as indicated in Figure 28, shows that the average CV is between 14% and 19%, indicating a low to moderate level of variability among the CMs. Lastly, another factor that has a correlation with the variability in CMs data is that we have used K-Means-Clustering to segment the images and extract the color values of the CMs. However, this method may not be the most suitable or reliable for this task, as it can be affected by noise, outliers, or initialization parameters [72]. Therefore, in future iteration, we plan to explore other image analysis algorithm along with a dedicated CMOS camera instead of the smartphone camera for capturing the images. This would enhance the image quality, consistency and resolution, and reduce the variability in the data. Then, the smartphone will serve as a display and operating device for the user.

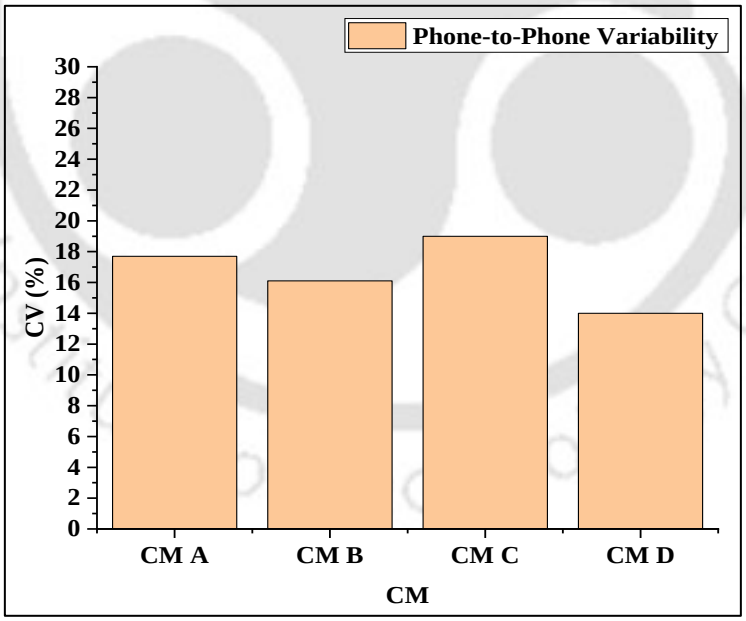

Figure 34: Phone-to-phone variability in CM-based smartphone detection. Bar graph showing the coefficient of variation (CV, %) obtained for four centrifugal multiplexers (CM A, CM B, CM C, and CM D) measured using three different smartphone devices, highlighting phone-to-phone variability in the optical detection system.

Figure 34 illustrates the variability introduced by different smartphone cameras in the CM-based detection platform. The coefficient of variation (CV) was calculated for four independent CMs (CM A–D) across three smartphones. The observed CV values ranged from approximately 14% to 19%, indicating moderate phone-to-phone variability. Among the tested devices, CM C exhibited the highest variability, while CM D showed the lowest. These results underscore the importance of device-specific calibration or normalization strategies to minimize inter-phone variability in smartphone-based point-of-care diagnostics.

4.3.3 Analysis of the linearity of the CM data

Linearity of the data is an essential aspect of its reliability as it gauges the extent to which the device's response varies linearly with the concentration of the analyte under consideration. This section aims to investigate the linearity trend in the dataset acquired from the CM device. By doing so, we can gain valuable insights into the device's accuracy and precision, which will help assess its suitability for clinical applications. To begin with, the data presented in Figure 31 (C) and 32 (C) has been acquired from the proof-of-concept device. At this stage the data is scattered with R^2 value of 0.85 with slope 0.01 for total protein and R^2 value of 0.90 with slope 0.06 for albumin. Thus, highlighting the need for further investigation to improve the accuracy and reliability of the system. In the previous section, we discussed how the CMs used in this experiment are printed using FDM 3D printing, this method of manufacturing introduces multiple inconsistencies during experimentation. A smartphone camera system was used to acquire the images for analysis, which varies from smartphone to smartphone, although within considerable range, as shown in Figure 27. In this experiment, the smartphone is placed on the detection module which is a periscopic system, to acquire the mirror image of the CM's bottom surface. However, this approach has limitations, including the possibility of image distortion and dust on the mirrors, which could lead to measurement errors. Moreover, the algorithm is optimized for specific parameters and may not perform well under different conditions. It is crucial to consider and control all these factors to ensure

accurate and dependable results. The dataset acquired from the CM proof-of-concept exhibits variability at this stage. Further, to improve the system, we plan to fabricate the CMs using SLA 3D printing to improve the surface finish. In addition, using industrial techniques such as injection molding, we can greatly reduce the variables introduced during manufacturing. Also, integrating a CMOS camera inside the centrifuge will eliminate the reliance on smartphone camera and the variabilities associated with it. This will result in greater control over the image being acquired and the processing that goes behind it. Further, other alternatives of the K-Means-Clustering need to be employed for better analysis of the CM. We believe these improvements will result in better fitting of the data and a clearer linear trend.

Finally, it needs to be considered that the results presented in the study are at the stage of proof- of-concept. A significant amount of work needs to be done in order to improve the precision, accuracy in detection, optimizing the 3D printing with different materials for the CM fabrication, prefilling of reagent, improving the transparency of the CM, robust quantification algorithms, fine tuning of the portable centrifuge and the detection module to name a few. It is also important to note that the CM can be tailored in terms of material, reagent, volume, mixing, detection method etc. for quantification of a broader variety of human biomarkers for which individual studied needs to be conducted. The versatility of the system provides the opportunity for quality, simple, adaptable POC real-time diagnostics at resource constraint areas making healthcare affordable and accessible. For now, the aforementioned remains a scope for future work.

4.4 Conclusions

In this chapter, we have presented the successful design, fabrication, and proof-of-concept validation of a centrifugal multiplexer (CM)–based frugal point-of-care testing (POCT) platform aimed at enabling affordable, rapid, and near-patient biomarker quantification. The proposed system integrates a 3D-printed centrifugal microfluidic chip, a portable battery-

operated centrifuge, and a smartphone-enabled optical detection module, thereby demonstrating a compact, reusable, and digitally connected diagnostic solution suitable for resource-constrained healthcare settings.

The centrifugal multiplexer was fabricated using FDM-based 3D printing, incorporating paired collection and sensing microchambers interconnected through microchannel networks. The design enables passive fluid transport, in-situ reagent–sample mixing, and controlled volume metering solely through centrifugal actuation, eliminating the need for external pumps, valves, or complex user intervention. Importantly, the intra-CM fabrication variability was found to be low, with an average coefficient of variation of approximately 1.56%, indicating acceptable reproducibility despite the inherent limitations of FDM printing. This consistency underscores the feasibility of additive manufacturing for rapid prototyping and low-cost deployment of centrifugal microfluidic devices.

To validate the analytical capability of the platform, albumin and total protein were selected as representative biomarkers due to their clinical relevance in liver and kidney disease diagnostics. Colorimetric assays based on bromocresol green for albumin and biuret reaction for total protein were successfully implemented within the CM. The observed concentration-dependent color changes in the sensing microchambers were quantified using a smartphone camera, where absorbance-equivalent (Ae) values were extracted through image processing. The results demonstrated a clear and monotonic relationship between analyte concentration and Ae, with good agreement when compared to conventional UV–Visible spectrophotometry. These findings confirm the platform's ability to perform quantitative biochemical assays using minimal sample volumes and simplified workflows.

The smartphone-enabled detection module played a crucial role in enabling portable optical readout and real-time data processing. The use of a controlled illumination source and a periscopic mirror arrangement ensured uniform lighting and compact optical path geometry. While moderate phone-to-phone variability (CV ~14–19%) was observed, the results

remained within an acceptable range for proof-of-concept validation. This variability highlights the importance of future device-specific calibration strategies, improved image analysis algorithms, or dedicated imaging hardware to further enhance measurement robustness and clinical reliability.

The phone-to-phone variability observed during smartphone-based colorimetric detection is primarily attributed to differences in camera sensors, exposure settings, white balance, and internal image-processing algorithms across different smartphone models. This variability may be reduced through the use of fixed imaging enclosures, standardized illumination conditions, calibration-based image normalization, and dedicated image acquisition software with controlled camera settings. Future versions of the platform may incorporate fixed CMOS-based optical detection to further improve reproducibility and analytical reliability.

Overall, the proposed CM-based platform addresses several key challenges associated with conventional diagnostic systems, including high cost, operational complexity, dependence on skilled personnel, and limited accessibility in primary healthcare settings. By integrating centrifugal microfluidics with low-cost fabrication, portable actuation, and smartphone-based detection, the system significantly reduces pre-analytical errors related to reagent handling, mixing, and manual data recording. Moreover, its modular architecture allows adaptability in terms of assay chemistry, detection modality, and degree of multiplexing. In the developed centrifugal microfluidic system, burst frequency has been governed by the balance between centrifugal pressure and capillary pressure, which is influenced by channel geometry, chamber volume, rotational speed, surface wettability, and microchannel dimensions. The channel and chamber design are optimized to ensure reproducible fluid transfer, proper reagent-sample mixing, and compatibility with smartphone-based optical detection. Clinical samples are not used in this proof-of-concept

study to minimize biological variability and focus on evaluating the fabrication consistency, fluid handling performance, and analytical feasibility of the centrifugal multiplexer platform.

While the present work demonstrates feasibility at the proof-of-concept level, several opportunities exist for further refinement. These include improving surface finish through alternative fabrication methods such as SLA printing or injection molding, enhancing optical consistency through integrated CMOS sensors, implementing more robust image-processing algorithms, and extending validation to clinically relevant human serum samples. Importantly, the CM architecture supports scalable multiplexing, enabling simultaneous estimation of multiple biomarkers, which opens the possibility of developing comprehensive liver or kidney function panels on a single disposable platform.

In conclusion, this study establishes a versatile, economical, and scalable centrifugal POCT platform that has strong potential for early disease screening and longitudinal monitoring in resource-limited environments. The integration of microfluidics, additive manufacturing, and digital health tools demonstrated here represents a meaningful step toward democratizing access to diagnostic healthcare and lays a strong foundation for future translational and clinical deployment.

CHAPTER 5

CONCLUSIONS

5.1 Overall Summary of the Research

Non-communicable diseases (NCDs) such as diabetes mellitus, cardiovascular disorders, chronic kidney disease (CKD), and liver dysfunctions continue to impose a substantial clinical and economic burden on healthcare systems worldwide. Early diagnosis, periodic biochemical screening, and longitudinal monitoring are central to effective disease management and prevention. However, conventional diagnostic infrastructures—characterized by centralized laboratories, high-cost automated analyzers, and dependence on skilled personnel—remain largely inaccessible to primary healthcare centers (PHCs), sub-centers, and rural clinics, particularly in low- and middle-income countries.

This doctoral research was undertaken to bridge this critical gap by developing affordable, portable, and clinically reliable point-of-care testing (POCT) platforms capable of delivering laboratory-comparable biochemical diagnostics at or near the patient's site. The thesis integrates multidisciplinary approaches spanning microfluidics, optical engineering, embedded electronics, additive manufacturing, and clinical validation. Two complementary diagnostic paradigms were realized: (i) a portable optical multi-parameter analyzer (Mobilab) for serum-based biochemistry, and (ii) a centrifugal multiplexer (CM)–based frugal microfluidic platform coupled with smartphone-enabled optical detection. Together, these systems demonstrate a scalable technological framework for decentralized diagnostics, addressing cost, accessibility, and operational simplicity without compromising analytical performance.

Non-communicable diseases (NCDs) represent one of the most pressing global healthcare challenges, particularly in low- and middle-income countries where access to centralized diagnostic infrastructure remains limited. Early diagnosis, routine biochemical screening, and continuous monitoring are essential for effective prevention and management of chronic conditions such as diabetes mellitus, cardiovascular diseases, chronic kidney disease (CKD), and liver disorders. However, conventional laboratory-based diagnostic systems are often inaccessible at the primary healthcare level due to high costs, infrastructural complexity, skilled

manpower requirements, and delayed turnaround times. This doctoral research was conceived to address these gaps through the development of frugal, portable, and digitally enabled point-of-care testing (POCT) platforms capable of delivering laboratory-comparable biochemical analysis in decentralized and resource-constrained settings.

The work presented in this thesis systematically integrates engineering design, microfluidics, optics, electronics, and clinical validation to realize two complementary POCT solutions: (i) a portable spectrophotometric multi-parameter analyzer (Mobilab) for serum-based biochemical profiling, and (ii) a centrifugal multiplexer (CM)-based microfluidic platform coupled with smartphone-enabled optical detection for frugal and multiplexed biomarker estimation. Together, these systems demonstrate a scalable technological pathway toward democratizing access to essential diagnostic testing at the patient's site.

5.2 Summary of Chapter-wise Contributions

5.2.1 Chapter 1: Introduction

Chapter 1 established the clinical and societal motivation underpinning this research by highlighting the rising global burden of non-communicable diseases and the limitations of existing diagnostic paradigms. The chapter emphasized the central role of biochemical markers in early disease detection and long-term monitoring, while critically examining the constraints faced by primary healthcare centres (PHCs) in delivering timely diagnostics.

The research objectives were defined to focus on the development of portable, accurate, and multi-parameter diagnostic platforms that bridge the performance gap between laboratory analyzers and field-deployable devices.

5.2.2 Chapter 2: Design & development of a portable optical system for multi-parameter serum analysis for early diagnosis of NCDs

Chapter 2 detailed the design, development, and validation of a compact spectrophotometric point-of-care analyzer optimized for quantitative serum biochemistry. The system architecture

was built around a modular optical core incorporating LED-based illumination, CMOS sensing, and robust electronic control circuits. Extensive iterative CAD-based optimization was undertaken to minimize optical misalignment, stray light interference, and illumination drift. A closed-loop constant-current LED driver ensured illumination stability, achieving blank and water coefficients of variation below 0.1%.

A major contribution of this chapter was the integration of a CNC-machined incubation and thermal control subsystem with PID regulation, addressing the temperature sensitivity of enzymatic assays. Experimental results demonstrated that creatinine estimation without incubation exhibited errors approaching 19%, whereas implementation of controlled incubation reduced analytical error to approximately 1.5%, representing a more than twelve-fold improvement. The device architecture was designed to be battery-operated, smartphone-connected, and cloud-enabled, enabling real-time data acquisition, digital reporting, and remote consultation. Collectively, Chapter 2 established the feasibility of achieving laboratory-comparable analytical precision within a portable and field-ready spectrophotometric POCT platform.

5.2.3 Chapter 3: Clinical Evaluation of Heart and Kidney Profiles

Chapter 3 focused on the clinical validation of the Mobilab POCT device through comparative studies with a fully automated laboratory analyzer (Siemens Dimension EXL 200). Five clinically relevant biochemical parameters—cholesterol, triglycerides, LDL-cholesterol, creatinine, and uric acid—were selected to represent cardiovascular and renal function profiles. The study involved analysis of over fifty retained human serum samples sourced from a NABL-accredited clinical laboratory.

Comprehensive method-comparison statistics, including Passing–Bablok regression, Bland–Altman analysis, paired t-tests, and performance matrices (sensitivity, specificity, PPV, NPV, and diagnostic accuracy), were employed to assess agreement between Mobilab and the reference analyzer. The results demonstrated strong correlation, minimal systematic bias, and

high diagnostic accuracy across all tested parameters, confirming the clinical reliability of Mobilab as a POCT device. This chapter provided critical translational evidence supporting the deployment of portable spectrophotometric analyzers in real-world primary healthcare settings.

5.2.4 Chapter 4: Design and Development of centrifugal multiplexer for targeting frugal POCT

Chapter 4 introduced a complementary frugal diagnostic approach through the development of a 3D-printed centrifugal multiplexer (CM) integrated with a portable centrifuge and smartphone-based optical detection module. The CM design incorporated paired collection and sensing microchambers connected via microchannel networks, enabling passive, pump-free fluid handling driven solely by centrifugal forces. Fabrication using fused deposition modeling (FDM) demonstrated acceptable reproducibility, with intra-CM coefficient of variation values averaging approximately 1.56%.

The platform was validated using albumin and total protein assays as representative biomarkers relevant to liver and kidney function. Colorimetric reactions were successfully quantified using image-based absorbance-equivalent (Ae) analysis on smartphones. Comparative studies with UV–Visible spectrophotometry demonstrated good linearity and agreement, confirming the feasibility of smartphone-enabled quantitative analysis. Although moderate phone-to-phone variability was observed, the results remained acceptable for proof-of-concept validation and highlighted clear pathways for future calibration and algorithmic correction. Chapter 4 thus demonstrated a low-cost, reusable, and multiplexable POCT architecture capable of minimizing pre-analytical errors and operational complexity.

In the centrifugal multiplexer, rough channel surfaces may influence the reproducibility of fluid transfer from the loading chamber to the sensing chamber. The roughness-related limitations have been discussed in Chapter 4, along with future improvements such as SLA printing, surface polishing, solvent vapor smoothing, hydrophilic coating, or injection molding. Thus, in the developed centrifugal multiplexer, layer-by-layer fabrication produced

micro-irregularities that could influence flow reproducibility and burst behavior. Future improvements such as SLA printing, surface polishing, and hydrophilic surface modification may help reduce these flow-related variations and improve microfluidic performance.

5.3 Key Scientific and Technological Contributions

The major scientific and technological contributions of this thesis are summarized in Table 20, highlighting how the proposed work advances the state of the art in point-of-care diagnostics.

Table 20. Key contributions of the present research.

Contribution Area	Description	Impact
Portable spectrophotometry	Development of a compact, LED–CMOS based optical analyzer with thermal control	Enables laboratory-grade accuracy in field settings
Temperature-controlled incubation	Integration of PID-controlled incubation to stabilize enzymatic assays	Reduced analytical error from ~19% to ~1.5%
Smartphone-enabled diagnostics	Cloud-connected, mobile-based data acquisition and reporting	Facilitates real-time digital health integration
Centrifugal microfluidics	Design of a reusable 3D-printed centrifugal multiplexer	Eliminates pumps/valves, reduces pre-analytical errors
Frugal manufacturing	Use of additive manufacturing for rapid prototyping	Enables low-cost, scalable POCT deployment

These contributions collectively demonstrate that carefully engineered portable systems can approach the analytical rigor of centralized laboratories while maintaining affordability and usability for decentralized healthcare. This thesis makes several important contributions to the field of point-of-care diagnostics:

(a) Demonstration of laboratory-comparable spectrophotometric accuracy in a portable, battery-operated POCT device through robust optical, electronic, and thermal design.

(b) Development of a modular, smartphone-connected diagnostic ecosystem enabling real-time digital reporting and cloud-based data integration.

(c) Clinical validation of a portable POCT analyzer against a gold-standard laboratory system across multiple cardiovascular and renal biomarkers.

(d) Design and fabrication of a frugal centrifugal microfluidic platform enabling passive fluid handling, multiplexing, and image-based quantitative analysis.

(e) Establishment of additive manufacturing and smartphone imaging as viable tools for scalable and affordable POCT development.

5.4 Limitations of the Present Work

Despite the encouraging outcomes, certain limitations of the present work must be acknowledged to provide a balanced and critical assessment. These limitations, along with corresponding mitigation pathways, are summarized in Table 21.

Table 21. Limitations of the study and future mitigation strategies.

Limitation	Observed Issue	Potential Mitigation
Smartphone variability	Phone-to-phone CV of 14–19%	Device-specific calibration, dedicated imaging hardware
Fabrication resolution	FDM printing limits microchannel precision	Transition to SLA or injection molding
Clinical sample size	Limited clinical validation for CM platform	Large-scale multi-center trials
Environmental sensitivity	Lighting and temperature effects	Improved enclosure, adaptive algorithms

Recognizing these limitations provides a roadmap for further optimization and translational readiness of the proposed systems.

While the results presented in this thesis are promising, certain limitations must be acknowledged. The centrifugal multiplexer platform was validated using prepared standards

rather than large-scale clinical samples, necessitating further clinical trials to establish diagnostic accuracy under real-world conditions. Phone-to-phone variability in smartphone-based detection highlights the need for standardized imaging hardware or advanced normalization algorithms. Additionally, FDM-based fabrication, while cost-effective, imposes constraints on microchannel resolution and surface finish that may affect long-term assay robustness.

5.5 Future Scope and Research Directions

The platforms developed in this thesis provide a strong foundation for continued research, optimization, and real-world deployment. Key future directions are summarized in Table 21.

Table 21. Future research and translational opportunities.

Domain	Proposed Direction	Expected Outcome
Biomarker expansion	Liver enzymes, electrolytes, inflammatory markers	Comprehensive diagnostic panels
AI integration	Anomaly detection, decision support	Improved diagnostic reliability
Manufacturing scale-up	Injection molding, standardized cartridges	Reduced cost and higher throughput
Clinical validation	Multi-site, longitudinal studies	Regulatory and clinical acceptance
Digital health	ABDM/ABHA integration	National health data interoperability

Collectively, these directions position the proposed technologies for large-scale impact in both public health systems and private diagnostic markets. The work presented in this thesis opens several avenues for future research and translational development. These include expansion of biomarker panels to include liver enzymes, electrolytes, inflammatory markers, and infectious disease assays; integration of automated calibration and AI-driven anomaly detection; transition from FDM printing to injection moulding for large-scale manufacturing;

and extensive multi-centre clinical validation studies. Integration with national digital health frameworks such as ABDM/ABHA can further enhance interoperability and impact.

5.6 Concluding Remarks

In conclusion, this thesis demonstrates that carefully engineered portable diagnostic systems can achieve analytical performance approaching that of centralized laboratories while retaining the affordability, simplicity, and portability required for decentralized healthcare delivery. By combining spectrophotometric POCT, centrifugal microfluidics, smartphone-enabled detection, and digital health integration, this work contributes meaningfully to the advancement of accessible diagnostics. The proposed platforms have strong potential to strengthen primary healthcare systems, enable early disease detection, and ultimately reduce the burden of non-communicable diseases in resource-limited environments.

Publications, Patents and Conferences

Publications:

1. **Ankit Chowdhury**, Bimalendu Deka, Sahil Jagnani, and Dipankar. Bandyopadhyay, "Centrifugable Multiplexer Targeting Frugal Point-of-Care-Testing," IEEE Journal on Flexible Electronics (J-FLEX), vol. 2, no. 5, pp. Sept. 2023, doi: 10.1109/JFLEX.2023.3291332.

2. **Ankit Chowdhury**, Sahil Jagnani, Nilanjana Medhi, Saurabh Dubey, Shweta Tiwari, Suchita Markan, Rajesh Sagar, Pankaj Upadhyay, Madhumita Das, Dipankar Bandyopadhyay Clinical Diagnostic Efficacy of a Point-of-Care Testing Device for Non- Non-Communicable Diseases. IEEE Sensors, 2024 (Under review)

Patents:

1. Smartphone-Based Portable Optical System for Spectrophotometric Analysis of Chemical Compounds. Patent Granted – Patent No. 5262992.
2. Portable mixing device for low Volume Vials. Patent Granted – Patent No. 568325.
3. Portable Mini Chemistry Analysis System (Mobicase). Patent Applied – Application No. 202431072182.
4. Lens-free optical system for spectrophotometric analysis. Patent Applied – Application No. 202431079962.
5. Standalone multi-cavity incubation system for low volume vials. Patent Applied – Application No. 202431008115.
6. Low cost Electrochemical Sensor for Serum Ions. Patent Applied – Application No. 202331009162.

Bibliography

Bibliography

1. World Health Organization. Global Status Report on Noncommunicable Diseases 2014. WHO, 2014.
2. International Diabetes Federation. IDF Diabetes Atlas. 10th ed., International Diabetes Federation, 2021.
3. Lippi, Giuseppe, and Mario Plebani. "Continuous Evolution of Laboratory Medicine." Clinical Chemistry and Laboratory Medicine, vol. 48, no. 7, 2010, pp. 911–917.
4. World Health Organization. ASSURED Criteria for Point-of-Care Diagnostics. WHO Special Programme for Research and Training in Tropical Diseases (TDR), 2017.
5. Luppa, P. B., et al. "Point-of-Care Testing (POCT): Current Techniques and Future Perspectives." Trends in Analytical Chemistry, vol. 30, no. 6, 2011, pp. 887–898.
6. Shaw, J. L. V. "Practical Challenges Related to Point-of-Care Testing." Practical Laboratory Medicine, vol. 4, 2016, pp. 22–29.
7. Kimani, F. W., et al. "Rethinking the Design of Low-Cost Point-of-Care Diagnostic Devices." Micromachines, vol. 8, no. 11, 2017, article 317.
8. Speers, D. J. "Spectrophotometry for Clinical Applications." Clinical Biochemist Reviews, vol. 27, no. 3, 2006, pp. 99–111.
9. Toora, B. D., and G. Rajagopal. "Measurement of Creatinine by Jaffe's Reaction—Determination of Concentration of Sodium Hydroxide Required for Maximum Color Development." Indian Journal of Experimental Biology, vol. 40, no. 3, 2002, pp. 352–354.
10. Plebani, Mario. "Does POCT Reduce the Risk of Error in Laboratory Testing?" Clinica Chimica Acta, vol. 404, no. 1, 2009, pp. 59–64.
11. Clinical and Laboratory Standards Institute (CLSI). EP09-A3: Measurement Procedure Comparison and Bias Estimation Using Patient Samples. Clinical and Laboratory Standards Institute, 2018.
12. Passing, H., and W. Bablok. "A New Biometrical Procedure for Testing the Equality of Measurements from Two Different Analytical Methods." Journal of Clinical Chemistry and Clinical Biochemistry, vol. 21, no. 11, 1983, pp. 709–720.
13. Bland, J. M., and D. G. Altman. "Statistical Methods for Assessing Agreement Between Two Methods of Clinical Measurement." The Lancet, vol. 327, no. 8476, 1986, pp. 307–310.

14. Dincer, Can, et al. "Multiplexed Point-of-Care Testing (xPOCT): Recent Advances in Rapid Diagnosis." Trends in Biotechnology, vol. 35, no. 8, 2017, pp. 728–742.
15. World Health Organization. Noncommunicable Diseases: Key Facts. WHO, 2023.
16. GBD 2019 Diseases and Injuries Collaborators. "Global Burden of 369 Diseases and Injuries." The Lancet, vol. 396, no. 10258, 2020, pp. 1204–22.
17. Beaglehole, Robert, et al. "Priority Actions for the Non-Communicable Disease Crisis." The Lancet, vol. 377, no. 9775, 2011, pp. 1438–47.
18. Bloom, David E., et al. "The Global Economic Burden of NCDs." World Economic Forum, 2011.
19. Ministry of Health and Family Welfare, Government of India. National Health Mission: Framework for Implementation, 2022.
20. Rao, K. Sujatha, et al. "Human Resources for Health in India." The Lancet, vol. 377, 2011, pp. 587–98.
21. Allen, Luke N., et al. "Addressing the Global NCD Burden." BMJ Global Health, vol. 2, no. 2, 2017.
22. Pai, Nitika P., et al. "Point-of-Care Testing for Infectious Diseases." PLoS Medicine, vol. 9, no. 9, 2012.
23. Wilding, Peter. "The Diagnostic Utility of Automated Analyzers." Clinical Chemistry, vol. 51, 2005, pp. 24–27.
24. Luppa, Peter B., et al. "Point-of-Care Testing (POCT)." Clinical Chimica Acta, vol. 412, 2011, pp. 1–7.
25. Yadav, Santosh, et al. "Healthcare Access in Rural India." Indian Journal of Community Medicine, vol. 45, 2020, pp. 123–28.
26. Prabhakaran, Dorairaj, et al. "Cardiovascular Diseases in India." The Lancet, vol. 397, 2021, pp. 70–78.
27. Jameson, J. Larry, et al. Harrison's Principles of Internal Medicine. 21st ed., McGraw-Hill, 2022.
28. Drain, Paul K., et al. "Point-of-Care Diagnostics." New England Journal of Medicine, vol. 368, 2014, pp. 2319–31.
29. Mills, Katherine T., et al. "Global Disparities of NCD Detection." The Lancet, vol. 388, 2016, pp. 37–55.
30. Nichols, James H. "POCT Challenges." Clinical Chemistry, vol. 64, 2018, pp. 143–50.
31. Grundy, Scott M., et al. "Cardiovascular Risk Assessment." Circulation, vol. 139, 2019.
32. Yetisen, Ali K., et al. "Paper-Based and Microfluidic Diagnostics." Lab on a Chip, vol. 13, 2013, pp. 2210–51.

33. Wang, Xiaoming, et al. "Portable Diagnostic Systems." Biosensors and Bioelectronics, vol. 165, 2020.

34. Cullum, Brian M., et al. "Optical Sensing in Diagnostics." Applied Spectroscopy, vol. 68, 2014.

35. Skoog, Douglas A., et al. Principles of Instrumental Analysis. 6th ed., Cengage Learning, 2014.

36. Horowitz, Paul, and Winfield Hill. The Art of Electronics. 3rd ed., Cambridge UP, 2015.

37. Åström, Karl J., and Tore Hägglund. PID Controllers: Theory, Design, and Tuning. ISA, 2006.

38. Strohmeier, Oliver, et al. "Centrifugal Microfluidics." Lab on a Chip, vol. 15, 2015.

39. Shen, Linda, et al. "Smartphone-Based Diagnostics." Analytical Chemistry, vol. 87, 2015.

40. Topol, Eric. "High-Performance Medicine." Nature Medicine, vol. 25, 2019.

41. Whitesides, George M. "Frugal Science." Nature, vol. 502, 2013, pp. 201–03.

42. Mehl, Gerd, and Alain Labrique. "Digital Health for NCDs." Bulletin of the WHO, vol. 96, 2018.

43. Kost, Gerald J. Principles and Practice of Point-of-Care Testing. AACC Press, 2002.

44. World Health Organization. ASSURED Criteria for Diagnostics. WHO, 2012.

45. Drain, Paul K., et al. "Diagnostic Point-of-Care Tests in Resource-Limited Settings." New England Journal of Medicine, vol. 368, 2014, pp. 2319–31.

46. Nichols, James H. "Point-of-Care Testing." Clinical Chemistry, vol. 64, no. 1, 2018, pp. 143–50.

47. Luppa, Peter B., et al. "POCT—Current Techniques and Future Perspectives." Clinical Chimica Acta, vol. 412, 2011, pp. 1–7.

48. American Diabetes Association. "Standards of Medical Care in Diabetes." Diabetes Care, vol. 46, 2023.

49. Grundy, Scott M., et al. "2019 ACC/AHA Guideline on the Primary Prevention of CVD." Circulation, vol. 139, 2019.

50. Pai, Nitika P., et al. "Impact of POCT on Decentralized Diagnostics." PLoS Medicine, vol. 9, no. 9, 2012.

51. Whitesides, George M. "Point-of-Care Diagnostics." Nature, vol. 502, 2013, pp. 201–03.

52. Yager, Paul, et al. "Microfluidic Diagnostics." Nature, vol. 442, 2006, pp. 412–18.

53. Yetisen, Ali K., et al. "Paper-Based Microfluidic Diagnostic Devices." Lab on a Chip, vol. 13, 2013, pp. 2210–51.

54. Wang, Xiaoming, et al. "Multiplexed POCT Systems." Biosensors and Bioelectronics, vol. 165, 2020.

55. Chin, Curtis D., et al. "Commercialization Challenges of POCT." Lab on a Chip, vol. 12, 2012.

56. Burtis, Carl A., et al. Tietz Textbook of Clinical Chemistry. 6th ed., Elsevier, 2018.

57. Sacks, David B., et al. "Guidelines for POCT Quality." Clinical Chemistry, vol. 54, 2008.

58. Kost, Gerald J., et al. "POCT System Design." Point of Care, vol. 15, 2016.

59. Wilding, Peter. "The Challenge of Point-of-Care Testing." Clinical Chemistry, vol. 51, 2005.

60. Aebersold, Ruedi, and Matthias Mann. Nature, vol. 422, 2003.

61. Dettmer, Katja, et al. Mass Spectrometry Reviews, vol. 26, 2007.

62. Cullum, Brian M., et al. "Portable Spectroscopic Diagnostics." Applied Spectroscopy, vol. 68, 2014.

63. Skoog, Douglas A., et al. Principles of Instrumental Analysis. Cengage, 2014.

64. Burns, David A., and Emil W. Ciurczak. Handbook of Near-Infrared Analysis. CRC Press, 2007.

65. Bergmeyer, Hans-Ulrich. Methods of Enzymatic Analysis. Academic Press, 1974.

66. Strohmeier, Oliver, et al. "Centrifugal Microfluidics." Lab on a Chip, vol. 15, 2015.

67. Mark, Daniel, et al. Chemical Reviews, vol. 110, 2010.

68. Ducrée, Jens, et al. Microsystems & Nanoengineering, 2020.

69. Madou, Marc, et al. Annual Review of Biomedical Engineering, 2006.

70. Gorkin, R., et al. Lab on a Chip, vol. 10, 2010.

71. Topol, Eric. Nature Medicine, vol. 25, 2019.

72. Mehl, Gerd, and Alain Labrique. Bulletin of the WHO, vol. 96, 2018.

73. Ozcan, Aydogan. Lab on a Chip, vol. 14, 2014.

74. Adler-Milstein, Julia, et al. Health Affairs, vol. 36, 2017.

75. Kruse, Clemens S., et al. JMIR Medical Informatics, vol. 5, 2017.

76. WHO. Digital Health Guidelines, 2019.

77. Yetisen, Ali K., et al. Advanced Materials, 2018.

78. Chin, Curtis D., et al. Nature Medicine, vol. 17, 2011.

79. Wang, Yu, et al. Biosensors and Bioelectronics, vol. 148, 2020.

80. Whitesides, George M., et al. Annual Review of Biomedical Engineering, 2017.

81. Jameson, J. Larry, et al. Harrison's Principles of Internal Medicine. 21st ed., McGraw-Hill, 2022.

82. Ronco, Claudio, et al. "Cardiorenal Syndrome." Journal of the American College of Cardiology, vol. 52, no. 19, 2008, pp. 1527–39.

83. Nichols, James H. "Point-of-Care Testing." Clinical Chemistry, vol. 64, no. 1, 2018, pp. 143–50.

84. Yusuf, Salim, et al. "Global Burden of Cardiovascular Diseases." Circulation, vol. 134, 2016, pp. 112–29.

85. Grundy, Scott M. "Lipid Metabolism and Cardiovascular Risk." Circulation, vol. 139, 2019.

86. Ference, Brian A., et al. "Low-Density Lipoproteins and ASCVD." European Heart Journal, vol. 38, 2017, pp. 2459–72.

87. Libby, Peter. "Inflammation in Atherosclerosis." Nature, vol. 420, 2002, pp. 868–74.

88. Kost, Gerald J. Principles and Practice of Point-of-Care Testing. AACC Press, 2002.

89. Grundy, Scott M., et al. "2018 Cholesterol Clinical Practice Guidelines." Circulation, vol. 139, 2019.

90. Brown, Michael S., and Joseph L. Goldstein. "A Receptor-Mediated Pathway for Cholesterol Homeostasis." Science, vol. 232, 1986, pp. 34–47.

91. Lewington, Sarah, et al. "Blood Cholesterol and Vascular Mortality." The Lancet, vol. 370, 2007, pp. 1829–39.

92. Nelson, David L., and Michael M. Cox. Lehninger Principles of Biochemistry. 8th ed., W.H. Freeman, 2021.

93. Steinberg, Daniel. "Low Density Lipoprotein Oxidation." Journal of Biological Chemistry, vol. 272, 1997.

94. Ross, Russell. "Atherosclerosis—An Inflammatory Disease." New England Journal of Medicine, vol. 340, 1999, pp. 115–26.

95. Schatz, Ian J., et al. "Low Serum Cholesterol and Mortality." The Lancet, vol. 352, 1998.

96. Miller, Michael, et al. "Triglycerides and Cardiovascular Disease." Circulation, vol. 123, 2011.

97. Nordestgaard, Børge G., et al. "Hypertriglyceridaemia." The Lancet, vol. 384, 2014, pp. 626–35.

98. Toth, Peter P. "Triglyceride-Rich Lipoproteins." Journal of the American College of Cardiology, vol. 68, 2016.

99. Scherer, Julia, et al. "Hypertriglyceridemia and Pancreatitis." Gastroenterology, vol. 149, 2015.

100. Varbo, Anette, et al. "Remnant Cholesterol and ASCVD." Journal of the American College of Cardiology, vol. 72, 2018.

101. Eckel, Robert H., et al. "Metabolic Syndrome." The Lancet, vol. 375, 2010.

102. Grundy, Scott M., et al. "2018 Cholesterol Clinical Practice Guidelines." Circulation, vol. 139, 2019, pp. e1082–e1143.

103. Libby, Peter. "Inflammation in Atherosclerosis." Nature, vol. 420, 2002, pp. 868–74.

104. Ference, Brian A., et al. "Low-Density Lipoproteins and ASCVD." European Heart Journal, vol. 38, 2017, pp. 2459–72.

105. Miller, Michael, et al. "Triglycerides and Cardiovascular Disease." Circulation, vol. 123, 2011, pp. 2292–2333.

106. Nordestgaard, Børge G., et al. "Hypertriglyceridaemia." The Lancet, vol. 384, 2014, pp. 626–35.

107. Scherer, Julia, et al. "Hypertriglyceridemia and Pancreatitis." Gastroenterology, vol. 149, 2015, pp. 1210–1214.

108. Levey, Andrew S., et al. "Definition and Classification of Chronic Kidney Disease." Kidney International, vol. 61, 2003, pp. 2089–2100.

109. Coresh, Josef, et al. "Prevalence of Chronic Kidney Disease." JAMA, vol. 298, 2007, pp. 2038–47.

110. Ronco, Claudio, et al. "Cardiorenal Syndrome." Journal of the American College of Cardiology, vol. 52, 2008, pp. 1527–39.

111. Johnson, Richard J., et al. "Hyperuricemia, Kidney Disease, and Cardiovascular Risk." Nature Reviews Nephrology, vol. 9, 2013, pp. 13–23.

112. Kanbay, Mehmet, et al. "Uric Acid and Cardiovascular Disease." Journal of the American Heart Association, vol. 2, 2013.

113. Ndrepepa, Gjin. "Uric Acid and Cardiovascular Disease." Clinica Chimica Acta, vol. 484, 2018, pp. 150–163.

114. Coresh, Josef, et al. "Chronic Kidney Disease Awareness, Prevalence, and Trends." Journal of the American Society of Nephrology, vol. 18, no. 4, 2007, pp. 129–136.

115. Ronco, Claudio, et al. "Cardiorenal Syndrome." Journal of the American College of Cardiology, vol. 52, no. 19, 2008, pp. 1527–1539.

116. Levey, Andrew S., et al. "Chronic Kidney Disease." The Lancet, vol. 379, no. 9811, 2012, pp. 165–180.

117. Nichols, James H. "Point-of-Care Testing in Nephrology." Clinical Chemistry, vol. 64, no. 1, 2018, pp. 143–150.

118. Levey, Andrew S., et al. "Definition and Classification of Chronic Kidney Disease." Kidney International, vol. 61, no. 1, 2002, pp. 2089–2100.

119. Stevens, Lesley A., and Andrew S. Levey. "Measurement of Kidney Function." Medical Clinics of North America, vol. 89, no. 3, 2005, pp. 457–473.

120. Perrone, Ronald D., et al. "Serum Creatinine as an Index of Renal Function." Clinical Chemistry, vol. 38, no. 10, 1992, pp. 1933–1953.

121. Go, Alan S., et al. "Chronic Kidney Disease and Cardiovascular Risk." New England Journal of Medicine, vol. 351, 2004, pp. 1296–1305.

122. Matsushita, Kunihiro, et al. "Estimated GFR and Cardiovascular Disease." The Lancet, vol. 375, 2010, pp. 2073–2081.

123. Johnson, Richard J., et al. "Hyperuricemia, Acute and Chronic Kidney Disease." Nature Reviews Nephrology, vol. 9, 2013, pp. 13–23.

124. Dalbeth, Nicola, et al. "Uric Acid and Cardiovascular Disease." The Lancet, vol. 388, 2016, pp. 2039–2052.

125. Kanbay, Mehmet, et al. "Uric Acid and Endothelial Dysfunction." Journal of Hypertension, vol. 34, 2016, pp. 226–233.

126. Feig, Daniel I., et al. "Uric Acid and the Origins of Hypertension." Journal of Clinical Investigation, vol. 118, 2008, pp. 158–165.

127. Ndrepepa, Gjin. "Uric Acid and Cardiovascular Disease." Clinica Chimica Acta, vol. 484, 2018, pp. 150–163.

128. Kuwabara, Masanari, et al. "Hyperuricemia Is an Independent Risk Factor for CKD." Kidney International, vol. 93, no. 2, 2018, pp. 460–469.

129. Grundy, Scott M., et al. "2018 Guideline on the Management of Blood Cholesterol." Journal of the American College of Cardiology, vol. 73, no. 24, 2019, pp. e285–e350.

130. Stone, Neil J., et al. "ACC/AHA Guideline on the Treatment of Blood Cholesterol." Circulation, vol. 129, no. 25, 2014, pp. S1–S45.

131. Libby, Peter. "Inflammation in Atherosclerosis." Nature, vol. 420, 2002, pp. 868–74.

132. Ference, Brian A., et al. "LDL Causally Contributes to Atherosclerotic Cardiovascular Disease." European Heart Journal, vol. 38, no. 32, 2017, pp. 2459–72.

133. Yusuf, Salim, et al. "Effect of Lipids on Cardiovascular Risk." The Lancet, vol. 375, no. 9655, 2010, pp. 1830–40.

134. Baigent, Colin, et al. "Efficacy of Cholesterol-Lowering Therapy." Lancet, vol. 366, no. 9493, 2005, pp. 1267–78.

135. Jacobs, David, et al. "Low Serum Cholesterol and Mortality." BMJ, vol. 296, 1988, pp. 882–84.

136. Miller, Michael, et al. "Triglycerides and Cardiovascular Disease." Circulation, vol. 123, 2011, pp. 2292–2333.

137. Nordestgaard, Børge G., et al. "Fasting vs Nonfasting Triglycerides." JAMA, vol. 298, no. 3, 2007, pp. 299–308.

138. Scherer, Julia, et al. "Hypertriglyceridemia-Induced Pancreatitis." Gastroenterology, vol. 149, no. 3, 2015, pp. 604–06.

139. Musunuru, Kiran. "Atherogenic Dyslipidemia." Arteriosclerosis, Thrombosis, and Vascular Biology, vol. 30, 2010, pp. 235–43.

140. Targher, Giovanni, et al. "NAFLD and Metabolic Syndrome." Diabetes Care, vol. 33, 2010, pp. 244–49.

141. Krauss, Ronald M. "Low Triglycerides and Clinical Significance." Metabolism, vol. 49, no. 3, 2000, pp. 16–19.

142. Levey, Andrew S., et al. "Definition and Classification of Chronic Kidney Disease." Kidney International, vol. 61, no. 1, 2002, pp. 2089–2100.

143. Perrone, Ronald D., et al. "Serum Creatinine as an Index of Renal Function." Clinical Chemistry, vol. 38, 1992, pp. 1933–1953.

144. Matsushita, Kunihiro, et al. "Association of eGFR with Cardiovascular Disease." The Lancet, vol. 375, 2010, pp. 2073–2081.

145. Go, Alan S., et al. "Chronic Kidney Disease and Cardiovascular Risk." New England Journal of Medicine, vol. 351, 2004, pp. 1296–1305.

146. Sarnak, Mark J., et al. "Kidney Disease and Hypertension." Circulation, vol. 108, 2003, pp. 2154–69.

147. Rule, Andrew D., et al. "Serum Creatinine and Muscle Mass." CJASN, vol. 1, no. 5, 2006, pp. 1004–09.

148. Johnson, Richard J., et al. "Hyperuricemia, CKD, and Cardiovascular Risk." Nature Reviews Nephrology, vol. 9, 2013, pp. 13–23.

149. Richette, Pascal, and Thomas Bardin. "Gout." The Lancet, vol. 375, 2010, pp. 318–28.

150. Feig, Daniel I., et al. "Uric Acid and Hypertension." Journal of Clinical Investigation, vol. 118, no. 4, 2008, pp. 1456–65.

151. Kanbay, Mehmet, et al. "Uric Acid and Endothelial Dysfunction." Hypertension, vol. 54, no. 6, 2009, pp. 1101–06.

152. Ndrepepa, Gjin. "Uric Acid and Cardiovascular Disease." Clinica Chimica Acta, vol. 484, 2018, pp. 150–163.

153. Kuwabara, Masanari, et al. "Uric Acid as an Independent Risk Factor for CKD." Kidney International, vol. 93, 2018, pp. 460–69.

154. Choi, Hyon K., et al. "Purine Intake and Risk of Gout." NEJM, vol. 350, 2004, pp. 1093–1103.

155. World Health Organization. Global Status Report on Noncommunicable Diseases 2014. WHO, 2014.

156. GBD 2019 Diseases and Injuries Collaborators. "Global Burden of 369 Diseases and Injuries." The Lancet, vol. 396, no. 10258, 2020, pp. 1204–1222.

157. Bloom, David E., et al. "The Global Economic Burden of Noncommunicable Diseases." World Economic Forum, 2011.

158. Beaglehole, Robert, et al. "Priority Actions for the Non-Communicable Disease Crisis." The Lancet, vol. 377, no. 9775, 2011, pp. 1438–1447.

159. Nugent, Rachel. "Chronic Diseases in Developing Countries." Annals of the New York Academy of Sciences, vol. 1136, 2008, pp. 70–79.

160. Mayeux, Richard. "Biomarkers: Potential Uses and Limitations." NeuroRx, vol. 1, no. 2, 2004, pp. 182–188.

161. Rifai, Nader, et al. "Biomarkers in Clinical Medicine." Clinical Chemistry, vol. 52, no. 4, 2006, pp. 663–672.

162. Pai, Nitika Pant, et al. "Point-of-Care Testing for Infectious Diseases." PLoS Medicine, vol. 9, no. 2, 2012, e1001306.

163. Nichols, James H. "Point-of-Care Testing." Clinical Chemistry, vol. 64, no. 1, 2018, pp. 1–2.

164. Price, Christopher P. "Point of Care Testing." BMJ, vol. 336, 2008, pp. 1022–1024.

165. Peeling, Rosanna W., et al. "Diagnostics in a Digital Age." Nature, vol. 544, 2017, pp. 247–249.

166. Luppa, Peter B., et al. "Point-of-Care Testing (POCT): Current Techniques and Future Perspectives." Trends in Analytical Chemistry, vol. 30, no. 6, 2011, pp. 887–898.

167. St John, Andrew, and Christopher P. Price. "Existing and Emerging Technologies for Point-of-Care Testing." Clinica Chimica Acta, vol. 411, 2010, pp. 1739–1744.

168. Burtis, Carl A., and Edward R. Ashwood. Tietz Textbook of Clinical Chemistry and Molecular Diagnostics. Elsevier, 2012.

169. Higgins, Chris. "Glucose Oxidase–Peroxidase Method." Biomedical Scientist, 2012. PubMed PMID: 22725968.

170. Myers, Gary L., et al. "Calibration of Serum Creatinine." Clinical Chemistry, vol. 52, no. 1, 2006, pp. 5–18.

171. Phetsang, W., et al. "LED-Based Spectrophotometry for Clinical Diagnostics." Sensors and Actuators B, vol. 273, 2018, pp. 1070–1077.

172. Arnold, M. A., and D. L. Small. "Optical Determination in Clinical Chemistry." Analytical Chemistry, vol. 43, no. 1, 1971, pp. 69–76.

173. Saha, S., et al. "Photodiode Detection Systems for Biomedical Applications." IEEE Sensors Journal, vol. 20, no. 5, 2020, pp. 2541–2550.

174. Luppa, Peter B., et al. "Point-of-Care Testing (POCT): Current Techniques and Future Perspectives." Trends in Analytical Chemistry, vol. 30, no. 6, 2011, pp. 887–898.

175. Wong, Y. M., et al. "Miniaturized Optical Spectrometers: Performance Challenges." Applied Optics, vol. 54, no. 4, 2015, pp. 785–793.

176. Liu, H., et al. "LED Stability in Analytical Devices: Temperature Effects." Sensors and Actuators A, vol. 236, 2015, pp. 259–266.

177. Kahn, S. E., et al. "Temperature Dependence of Enzymatic Clinical Assays." Clinical Chemistry, vol. 44, no. 6, 1998, pp. 1233–1239.

178. Villegas, M., et al. "Microfluidic Integration of Colorimetric Detection." Lab on a Chip, vol. 16, 2016, pp. 3756–3765.

179. Skoog, Douglas A., F. James Holler, and Stanley R. Crouch. Principles of Instrumental Analysis. 6th ed., Cengage Learning, 2007.

180. Harris, Daniel C. Quantitative Chemical Analysis. 9th ed., W. H. Freeman and Company, 2016.

181. Burns, Donald A., and Emil W. Ciurczak. Handbook of Near-Infrared Analysis. 3rd ed., CRC Press, 2007.

182. Ingle, James D., and Stanley R. Crouch. Spectrochemical Analysis. Prentice Hall, 1988.

183. Kaplan, Lawrence A., and Amadeo J. Pesce. Clinical Chemistry: Theory, Analysis, and Correlation. 4th ed., Mosby, 2003.

184. Burtis, Carl A., Edward R. Ashwood, and David E. Bruns. Tietz Textbook of Clinical Chemistry and Molecular Diagnostics. 5th ed., Elsevier Saunders, 2012.

185. Doumas, Basil T., et al. "Candidate Reference Method for Determination of Total Bilirubin in Serum." Clinical Chemistry, vol. 31, no. 11, 1985, pp. 1779–1789.

186. Chen, Yihong, et al. "Limitations of the Beer–Lambert Law in Biological Systems." Analytical Chemistry, vol. 86, no. 10, 2014, pp. 4621–4626.

187. Luppa, Peter B., et al. "Point-of-Care Testing (POCT): Current Techniques and Future Perspectives." Trends in Analytical Chemistry, vol. 30, no. 6, 2011, pp. 887–898.

188. St John, Andrew, and Christopher P. Price. "Existing and Emerging Technologies for Point-of-Care Testing." Clinical Chemistry and Laboratory Medicine, vol. 52, no. 5, 2014, pp. 635–640.

189. Büttner, Johannes, and Walter Hubl. "Spectrophotometry in Clinical Chemistry: Principles and Applications." Clinical Chemistry and Laboratory Medicine, vol. 57, no. 3, 2019, pp. 300–312.

190. Lott, John A., and Kenneth K. Turner. "Evaluation of Colorimetric and Enzymatic Methods in Clinical Chemistry." Clinical Biochemistry, vol. 72, 2019, pp. 18–28.

191. Moss, David W., and Robert J. Henderson. "Kinetic Spectrophotometric Assays in Diagnostic Enzymology." Annals of Clinical Biochemistry, vol. 54, no. 2, 2017, pp. 121–139.

192. Doumas, Basil T., et al. "A Review of Bilirubin Spectrophotometric Methods in Clinical Laboratories." Clinical Chemistry, vol. 57, no. 3, 2011, pp. 32–45.

193. Zhang, Yang, et al. "Miniaturized UV–Visible Spectrophotometric Systems for Point-of-Care Diagnostics." Biosensors and Bioelectronics, vol. 152, 2020, 112008.

194. Yadav, Jyoti, et al. "Optical Biosensing Techniques for Rapid and Portable Clinical Diagnostics." Sensors, vol. 20, no. 14, 2020, p. 3982.

195. Fossum, Eric R. "CMOS Image Sensors: Electronic Camera-on-a-Chip." IEEE Transactions on Electron Devices, vol. 44, no. 10, 1997, pp. 1689–1698.

196. Saha, Sudip, et al. "High-Performance Photodiodes for Biomedical Sensing Applications." IEEE Sensors Journal, vol. 20, no. 5, 2020, pp. 2541–2550.

197. Zhang, Yang, et al. "Miniaturized Spectrometers for Point-of-Care Optical Diagnostics." Biosensors and Bioelectronics, vol. 152, 2020, 112008.

198. Esposito, Fabio, et al. "Portable and Low-Cost Spectrometers: Design Challenges and Clinical Application Potential." Sensors, vol. 20, no. 16, 2020, p. 4532.

199. Kaufmann, Arnold. "The Current Role of Mass Spectrometry in Clinical Diagnostics." Clinical Chemistry and Laboratory Medicine, vol. 49, no. 5, 2011, pp. 623–635.

200. Cate, David M., et al. "Recent Developments in Paper-Based Microfluidic Devices." Analytical Chemistry, vol. 87, no. 1, 2015, pp. 19–41.

201. Bahadir, Elif Burcu, and Melek K. Sezgintürk. "Electrochemical Biosensors for Medical Applications." Biosensors and Bioelectronics, vol. 68, 2015, pp. 1–14.

202. Wang, Joseph, and Aaron H. Turner. "Electrochemical Biosensors for Clinical Diagnostics." Chemical Reviews, vol. 116, no. 19, 2016, pp. 123–161.

203. Rodriguez-Mozaz, Sara, et al. "Advances in Optical Biosensors for Point-of-Care Diagnostics." Trends in Analytical Chemistry, vol. 79, 2016, pp. 134–150.

204. Myers, Gary L., et al. "Recommendations for Improving Serum Creatinine Measurement: A Report from the Laboratory Working Group of the National Kidney Disease Education Program." Clinical Chemistry, vol. 52, no. 1, 2006, pp. 5–18.

205. Lamb, Edmund J., et al. "Accuracy of Point-of-Care Creatinine Measurement in Clinical Practice." Critical Care Medicine, vol. 43, no. 8, 2015, pp. 1621–1627.

206. Scholz, Friedrich. "Beer–Lambert Law and Its Application in Modern UV–Visible Spectrophotometry." Journal of Analytical Chemistry, vol. 70, no. 3, 2015, pp. 257–265.

207. St John, Andrew, and Christopher P. Price. "Existing and Emerging Technologies for Point-of-Care Testing." Clinical Biochemistry Review, vol. 35, no. 3, 2014, pp. 155–167.

208. St. John, Andrew, and Christopher P. Price. "Existing and Emerging Technologies for Point-of-Care Testing." Clinical Biochemistry Review, vol. 35, no. 3, 2014, pp. 155–167.

209. Kruk, M. E., et al. "Building resilient health systems: A proposal for a resilience index." BMJ, vol. 357, 2017, j2323.

210. Bitton, A., et al. "Primary health care as a foundation for strengthening health systems in low- and middle-income countries." J Gen Intern Med, vol. 32, no. 5, 2017, pp. 566–571.

211. Rohland, E., et al. "Primary healthcare and public health: Foundations of universal health coverage." The Lancet, vol. 392, 2018, pp. 1371–1372.

212. Peeling, R. W., and Mabey, D. "Point-of-care tests for diagnosing infections in resource-limited settings." Clin Microbiol Infect, vol. 16, no. 8, 2010, pp. 1062–1069.

213. Hawkins, R. "Laboratory turnaround time." Clin Biochem Rev, vol. 28, no. 4, 2007, pp. 179–194.

214. Drain, P. K., et al. "Point-of-care diagnostics for global health." Lancet Infect Dis, vol. 14, no. 3, 2014, pp. 239–249.

215. Kosack, C. S., et al. "ASSURED criteria: A useful framework for developing and evaluating point-of-care tests." Lancet Infect Dis, vol. 17, no. 11, 2017, pp. e1–e8.

216. Nugent, R. "A perspective on the global burden of noncommunicable diseases." Sci Transl Med, vol. 4, no. 152, 2012, pp. 152–154.

217. Oni, T., et al. "The burden of NCDs in developing countries." Lancet Global Health, vol. 3, 2015, pp. S15–S16.

218. Yetisen, A. K., et al. "Paper-based microfluidic point-of-care diagnostic devices." Lab Chip, vol. 13, no. 12, 2013, pp. 2210–2251.

219. Levey, A. S., et al. "Serum creatinine as a marker of kidney function." Ann Intern Med, vol. 139, no. 12, 2003, pp. 929–937.

220. Hovind, P., et al. "Serum uric acid and kidney disease progression." Kidney Int, vol. 78, no. 5, 2010, pp. 493–498.

221. Feig, D. I., et al. "Uric acid and cardiovascular risk." N Engl J Med, vol. 359, 2008, pp. 1811–1821.

222. Ference, B. A., et al. "Low-density lipoproteins cause atherosclerotic cardiovascular disease." Eur Heart J, vol. 38, no. 32, 2017, pp. 2459–2472.

223. Miller, M., et al. "Triglycerides and cardiovascular disease." J Am Coll Cardiol, vol. 61, no. 4, 2013, pp. 498–507.

224. Goldstein, J. L., and Brown, M. S. "Familial hypercholesterolemia and LDL metabolism." Science, vol. 292, 2001, pp. 1310–1314.

225. Stone, N. J., et al. "Lipid management and cardiovascular risk." Circulation, vol. 129, 2014, pp. S1–S45.

226. Allain, C. C., et al. "Enzymatic determination of total serum cholesterol." Clinical Chemistry, vol. 20, no. 4, 1974, pp. 470–475.

227. Fossati, P., and Prencipe, L. "Serum triglycerides determined colorimetrically with an enzyme that produces hydrogen peroxide." Clinical Chemistry, vol. 28, no. 10, 1982, pp. 2077–2080.

228. Sjoblom, L., et al. "Homogeneous assay for LDL cholesterol using selective solubilization: Evaluation and comparison with ultracentrifugation and Friedewald equation." Clinical Chemistry, vol. 43, no. 4, 1997, pp. 617–623.

229. Spencer, K. "Analytical reviews in clinical biochemistry: The estimation of creatinine." Annals of Clinical Biochemistry, vol. 23, 1986, pp. 1–25.

230. Fossati, P., et al. "Uric acid production and enzymatic measurement: Uricase-based methodologies revisited." Clinical Chemistry, vol. 26, no. 2, 1980, pp. 227–231.

231. Armbruster, David A., and Thomas Pry. "Limitations of method comparison studies." Clinical Biochemistry Review, vol. 29, 2008, pp. S47–S52.

232. Passing, H., and W. Bablok. "A new biometrical procedure for testing the equality of measurements from two different analytical methods." Journal of Clinical Chemistry and Clinical Biochemistry, vol. 21, 1983, pp. 709–720.

233. Bland, J. Martin, and Douglas G. Altman. "Statistical methods for assessing agreement between two methods of clinical measurement." The Lancet, vol. 327, no. 8476, 1986, pp. 307–310.

234. Giavarina, Davide. "Understanding Bland–Altman analysis." Biochemia Medica, vol. 25, no. 2, 2015, pp. 141–151.

235. Ruxton, Graeme D. "The unequal variance t-test is an underused alternative to Student's t-test and the Mann–Whitney U test." Behavioral Ecology, vol. 17, no. 4, 2006, pp. 688–690.

236. de Vet, Henrica C. W., et al. "When to use agreement versus reliability measures." Journal of Clinical Epidemiology, vol. 59, 2006, pp. 1033–1039.

237. Clinical and Laboratory Standards Institute (CLSI). Protocols for Determination of Limits of Detection and Limits of Quantitation. CLSI EP17-A2, 2012.

238. Bonini, Paola, et al. "Quality specifications for analytic linearity." Clinical Chemistry, vol. 48, no. 6, 2002, pp. 999–1007.

239. Krouwer, Jan S. "Calibration and linearity assessment in clinical chemistry." Clinical Chemistry, vol. 41, no. 8, 1995, pp. 1054–1056.

240. Miller, W. Greg. "Regression methods in method-comparison studies." Clinical Chemistry, vol. 60, no. 1, 2014, pp. 227–234.

241. Westgard, James O., et al. "Basic method validation: Precision, accuracy, and analytical performance." Clinical Chemistry, vol. 40, no. 7, 1994, pp. 1233–1238.

242. Altman, Douglas G., and Martin J. Bland. "Diagnostic tests 1: Sensitivity and specificity." BMJ, vol. 308, 1994, p. 1552.

243. P. B. Luppa, C. Müller, A. Schlichtiger, and H. Schlebusch, "Point-of-care testing (POCT): Current techniques and future perspectives," TrAC - Trends in Analytical Chemistry, vol. 30, no. 6. pp. 887–898, Jun. 2011. doi: 10.1016/j.trac.2011.01.019.

244. G. Abel, "Current status and future prospects of point-of-care testing around the globe," Expert Review of Molecular Diagnostics, vol. 15, no. 7, pp. 853–855, Jul. 01, 2015. doi: 10.1586/14737159.2015.1060126.

245. Kapoor, S., & Goel, V. "Modular Design of Automated Biochemistry Analyzer," International Journal of Computer Applications, vol. 71, no.18. pp. 0975 – 8887, Jun. 2013.

246. Taneja, S. R., Gupta, R. C., Kumar, J., Thariyan, K. K., & Verma, S. "Design and Development of Microcontroller-Based Clinical Chemistry Analyser for Measurement of Various Blood Biochemistry Parameters." Journal of Automated Methods & Management in Chemistry, vol. 4, pp. 223-229, Feb. 2005. doi: 10.1155/JAMMC.2005.223

247. W. Newman and E. Behling-Kelly, "Quality Assurance and Quality Control in Point-of-Care Testing," Topics in Companion Animal Medicine, vol. 31, no. 1. W.B. Saunders, pp. 2–10, Mar. 01, 2016. doi: 10.1053/j.tcam.2016.05.003.

248. R. Haeckel, "General principles for the classification of analysers."

249. J. Steigert, T. Brenner, M. Grumann, L. Riegger, R. Zengerle and J. Ducree, "Design and Fabrication of a Centrifugally Driven Microfluidic Disk for Fully Integrated Metabolic Assays on Whole Blood," 19th IEEE International Conference on Micro Electro Mechanical Systems, Istanbul, Turkey, 2006, pp. 418-421, doi: 10.1109/MEMSYS.2006.1627825.

250. Y. K. Cho, J. G. Lee, J. M. Park, B. S. Lee, Y. Lee, and C. Ko, "One-step pathogen specific DNA extraction from whole blood on a centrifugal microfluidic device," Lab Chip, vol. 7, no. 5, pp. 565–573, May 2007, doi: 10.1039/B616115D.

251. H. C. Wu, Y. H. Chen, and C. H. Shih, "Disk-based enzyme-linked immunosorbent assays using the liquid-aliquoting and siphoning-evacuation technique," Biomicrofluidics, vol. 12, no. 5, p. 054101, Sep. 2018, doi: 10.1063/1.5047281.

252. R. Gorkin et al., "Centrifugal microfluidics for biomedical applications," Lab on a Chip, vol. 10, no. 14, pp. 1758–1773, 2010. doi: 10.1039/b924109d.

253. R. Burger et al., "Centrifugal microfluidics for cell analysis," Current Opinion in Chemical Biology, vol. 16, no. 3–4. pp. 409–414, Aug. 2012. doi: 10.1016/j.cbpa.2012.06.002.

254. Maguire, R. O'Kennedy, J. Ducrée, and F. Regan, "A review of centrifugal microfluidics in environmental monitoring," Analytical Methods, vol. 10, no. 13, pp. 1497–1515, Apr. 07, 2018. doi: 10.1039/c8ay00361k.

255. O. Strohmeier et al., "Centrifugal microfluidic platforms: advanced unit operations and applications," Chem Soc Rev, vol. 44, no. 17, pp. 6187–6229, Sep. 2015, doi: 10.1039/c4cs00371c.

256. C. M. Miyazaki, E. Carthy, and D. J. Kinahan, "Biosensing on the centrifugal microfluidic lab-on-a-disc platform," Processes, vol. 8, no. 11. MDPI AG, pp. 1–44, Nov. 01, 2020. doi: 10.3390/pr8111360.

257. P. K. Drain et al., "Diagnostic point-of-care tests in resource-limited settings," Lancet Infect Dis, vol. 14, no. 3, pp. 239–249, Mar. 2014, doi: 10.1016/S1473-3099(13)70250-0.

258. Stranieri et al., "Emerging point of care devices and artificial intelligence: Prospects and challenges for public health," Smart Health, vol. 24, Jun. 2022, doi: 10.1016/j.smhl.2022.100279.

259. V. Rinkoo et al., "Getting on the Bandwagon of Innovative Point-of-Care Diagnostic Devices to Boost Primary Healthcare in India: A Short Critique and Way Forward," Health Care Curr Rev, vol. 7, no. 2, pp. 1–4, May 2019, doi: 10.35248/2375-4273.19.07.243.

260. S. Choudhary, G. Pandey, R. Mukherjee, and A. Joshi, "Biomedical instrumentation: Focus toward point-of-care devices," Biomedical Engineering and its Applications in Healthcare, pp. 297–326, Jan. 2019, doi: 10.1007/978-981-13-3705-5_13/COVER.

261. Briggs, S. Kimber, and L. Green, "Where are we at with point-of-care testing in haematology?", doi: 10.1111/j.1365-2141.2012.09207.x.

262. N. Engel et al., "Point-of-care testing in India: Missed opportunities to realize the true potential of point-of-care testing programs," BMC Health Serv Res, vol. 15, no. 1, Dec. 2015, doi: 10.1186/s12913-015-1223-3.

263. S. K. Vashist, "Point-of-care diagnostics: Recent advances and trends," Biosensors, vol. 7, no. 4. MDPI, Dec. 18, 2017. doi: 10.3390/bios7040062.

264. N. Konwar and V. Borse, "Current status of point-of-care diagnostic devices in the Indian healthcare system with an update on COVID-19 pandemic," Sensors International, vol. 1. KeAi Communications Co., Jan. 01, 2020. doi: 10.1016/j.sintl.2020.100015.

265. W. Zhang, S. Guo, W. S. Pereira Carvalho, Y. Jiang, and M. J. Serpe, "Portable point-of-care diagnostic devices," Analytical Methods, vol. 8, no. 44. Royal Society of Chemistry, pp. 7847–7867, Nov. 28, 2016. doi: 10.1039/c6ay02158a.

266. T. Shu et al., "Portable point-of-care diagnostic devices: An updated review," Analytical Methods, vol. 13, no. 45. Royal Society of Chemistry, pp. 5418–5435, Dec. 07, 2021. doi: 10.1039/d1ay01643a.

267. L. V. Shaw, "Practical challenges related to point of care testing," Practical Laboratory Medicine, vol. 4. Elsevier B.V., pp. 22–29, Apr. 01, 2016. doi: 10.1016/j.plabm.2015.12.002.

268. M. Biehl and T. Velten, "Gaps and challenges of point-of-care technology," IEEE Sens J, vol. 8, no. 5, pp. 593–600, May 2008, doi: 10.1109/JSEN.2008.918919.

269. F. W. Kimani et al., "Rethinking the design of low-cost point-of-care diagnostic devices," Micromachines (Basel), vol. 8, no. 11, Oct. 2017, doi: 10.3390/mi8110317.

270. N. Engel et al., "Barriers to point-of-care testing in India: Results from qualitative research across different settings, users and major diseases," PLoS One, vol. 10, no. 8, Aug. 2015, doi: 10.1371/journal.pone.0135112.

271. P. J. Garcia, P. You, G. Fridley, D. Mabey, and R. Peeling, "Point-of-care diagnostic tests for low-resource settings," The Lancet Global Health, vol. 3, no. 5. Elsevier Ltd, pp. e257–e258, May 01, 2015. doi: 10.1016/S2214-109X(15)70089-6.

272. S. Sang et al., "A Portable Device for Rapid Detection of Human Serum Albumin using an immunoglobulin-coating-based Magnetoelastic Biosensor," Biosens Bioelectron, vol. 141, Sep. 2019, doi: 10.1016/j.bios.2019.111399.

273. S. Aitekenov, A. Gaipov, and R. Bukasov, "Review: Detection and quantification of proteins in human urine," Talanta, vol. 223. Elsevier B.V., Feb. 01, 2021. doi: 10.1016/j.talanta.2020.121718.

274. F. Xu, Y. S. Yang, A. Q. Jiang, and H. L. Zhu, "Detection Methods and Research Progress of Human Serum Albumin," Critical Reviews in Analytical Chemistry, vol. 52, no. 1, pp. 72–92, 2022. doi: 10.1080/10408347.2020.1789835.

275. Brenner, T., Glatzel, T., Zengerle, R., and Ducree, J., 2003, "A Flow-Switch Based on Coriolis Force," Proceedings of the 7th Int. Conf on μTAS, Squaw Valley, Callfornla USA, 2003, pp. 5-9.

Appendix

List of abbreviations

Abbreviation	Full Form
Ae	Absorbance Equivalent
ALP	Alkaline Phosphatase
ASSURED	Affordable, Sensitive, Specific, User-friendly, Rapid and Robust, Equipment-free, Deliverable to End User
B-A	Bland–Altman
BCG	Bromocresol Green
BSA	Bovine Serum Albumin
CAD	Computer-Aided Design
CHC	Community Health Centre
CHOD–PAP	Cholesterol Oxidase–Phenol Aminophenazone
CKD	Chronic Kidney Disease
CMOS	Complementary Metal–Oxide–Semiconductor
CM	Centrifugal Multiplexer
CRE	Creatinine
CV	Coefficient of Variation
DC	Direct Current
ELISA	Enzyme-Linked Immunosorbent Assay
EMR	Electronic Medical Record
FDM	Fused Deposition Modeling
Fc	Centrifugal Force
GFR	Glomerular Filtration Rate
GNRC	Gauhati Neuro Research Centre
GOD–POD	Glucose Oxidase–Peroxidase
GPO–PAP	Glycerol Phosphate Oxidase–Phenol Aminophenazone
HDL	High-Density Lipoprotein
HPLC	High-Performance Liquid Chromatography
IoT	Internet of Things

Abbreviation	Full Form
LED	Light Emitting Diode
LDL-C	Low-Density Lipoprotein Cholesterol
LOB	Limit of Blank
LOD	Limit of Detection
LMIC	Low- and Middle-Income Country
NCD	Non-Communicable Disease
NABL	National Accreditation Board for Testing and Calibration Laboratories
PCB	Printed Circuit Board
PHC	Primary Health Centre
PID	Proportional–Integral–Derivative
POCT	Point-of-Care Testing
PPV	Positive Predictive Value
RCA	Resource-Constrained Area
RPM	Revolutions Per Minute
RT-PCR	Reverse Transcription Polymerase Chain Reaction
SDA	Siemens Dimension Analyzer
SHC	Sub Health Centre
TGL	Triglycerides
UA	Uric Acid
UV–Vis	Ultraviolet–Visible
WHO	World Health Organization
ω	Angular Velocity